UNIVERSITEIT VAN PRETORIA
UNIVERSITY OF PRETORIA
YUNIBESITHI YA PRETORIA

In vitro cell signaling events of 2-methoxyestradiol-bis-sulphamate in a breast adenocarcinoma- and a non-tumorigenic breast epithelial cell line

by

Michelle Helen Visagie

(24065766)

Submitted in fulfilment of the requirements for the degree

Masters of Science (Physiology)

in the Faculty of Health Sciences

University of Pretoria

Pretoria

25 November 2010

Declaration

I declare that the dissertation, which I hereby submit for the degree MSc: Human Physiology at the University of Pretoria, is my own work and has not previously been submitted by me for a degree at this or any other tertiary institution.

Table of contents

Summary

2-Methoxyestradiol, an endogenous metabolite of 17-β-estradiol exerts antipropliferative, antiangiogenic and antitumor effects *in vitro* and *in vivo* and is currently in clinical trials phase II for various types of cancers including breast cancer. Due to low oral bioavailability and rapid metabolic degradation, several analogues have been developed in recent years. 2-Methoxyestradiol-bis-sulphamate (2-MeOE2bisMATE), a novel bis-sulphamoylated derivative of 2-methoxyestradiol exerts *in vitro* antipropliferative effects. Although 2-MeOE2bisMATE holds therapeutic potential as an anticancer agent, several questions remain regarding the signal transduction and exact mechanism of action used by 2-MeOE2bisMATE.

In vitro effects of 2-MeOE2bisMATE were investigated in a breast adenocarcinoma cell line (MCF-7) and a non-tumorigenic epithelial breast cell line (MCF-12A) by analysing its influence on cell growth, cytotoxicity, morphology, cell cycle progression, mitochondrial membrane potential, reactive oxygen species production and induction of apoptosis and autophagy.

Spectrophotometrical studies indicated that 2-MeOE2bisMATE decreased cell numbers to 47% in MCF-7 cells and to 79% in MCF-12A cells after 48h of exposure. Haematoxylin and eosin staining revealed several 2-MeOE2bisMATE-treated cells with the presence of apoptotic bodies. Transmission electron microscopy demonstrated membrane blebbing, nuclear fragmentation and chromatin condensation indicating the occurrence of apoptosis. Increased lysosomal staining was revealed by fluorescent microscopy using propidium iodide, Hoechst 33342 and acridine orange; suggesting cell death via autophagy. Data obtained employing flow cytometry using rabbit polyclonal anti-LC3B conjugated to DyLight 488 verified the induction of autophagy in 2-MeOE2bisMATE-treated cells. In addition, cell cycle progression revealed an apoptotic sub-G_1 peak, confirming the induction of apoptosis by 2-MeOE2bisMATE. Reactive oxygen species generation increased when cells were exposed to 2-MeOE2bisMATE. Annexin V-FITC and the investigation of a possible reduction in the mitochondrial membrane potential verified induction of apoptosis by 2-MeOE2bisMATE. All of the above-mentioned results were observed more prominently in the tumorigenic MCF-7 cell line when compared to the non-tumorigenic MCF-12A cell line.

Data obtained from this *in vitro* study contributes to the embedded scientific knowledge regarding the signaling transduction mechanism exerted by 2-MeOE2bisMATE.

Key words: 2-MeOE2bisMATE, MCF-7, MCF-12A, apoptosis, autophagy

Acknowledgements

- Professor AM Joubert (associate professor from Department of Physiology) as my study leader for this project. Her assistance, insight, motivation, support and positive attitude made this project possible. It has been an honour to have Professor AM Joubert as my supervisor.
- Professor D van Papendorp (head of the Department of Physiology) for allowing me the opportunity to study under the Department and allowing me to use the facilities and apparatuses at the department.
- Cancer Association of South Africa, the Struwig Germeshuysen Trust, RESCOM (Research Council of the University of Pretoria), National Research Foundation and The Medical Research Council for providing financial support.
- Professor Vleggaar (Department of Chemistry, University of Pretoria, Pretoria, South Africa) who especially synthesized 2-MeOE2bisMATE to the amount of R30 000.
- The Electron Microscopy Unit (University of Pretoria' Hatfield campus, Pretoria, South Africa) for the use of the transmission electron microscopy.
- The Flow Cytometry Unit (Department of Pharmacology, University of Pretoria, Pretoria, South Africa) for the availability of the flow cytometer for use during the research project.
- Colleagues, friends and relatives for motivation, support and insight.
- Francina and Ezekiel for maintenance of the lab and sterilization of glassware.
- God Almighty for without him none of this would have been possible.

List of Figures

List of Tables

Abbreviations

2ME2	2-Methoxyestradiol
2-MeOE2bisMATE	2-Methoxyestradiol-Bis-Sulphamate
APAF-1	Apoptosis Activating Factor 1
Adiol	Androstenediol
AIF	Apoptosis Inducing Factor
AMP	Adenosine Monophosphate
AMPK	AMP-Activated Protein Kinase
APC	Anaphase Promoting Complex
APC/C	Promoting Complex/Cyclosome
Apo-2L	Apo-2 Ligand
ADP	Adenosine Diphosphate
ANG-1	Angiopoietins 1
ANG-2	Angiopoietins 2
Apo1	NF Receptor Superfamily, Member 6
ARGs	Autophagy-Related Genes
ASK1	Apoptosis Signal-Regulated Kinase 1
Atg	Autophagy-Related Proteins
Atg6	Autophagy-Related Protein 6
Atg8p	Autophagy-Related Protein 8 Precursor
ATM	Ataxia Telangiectasia Mutated
ATP	Adenosine Triphosphate

ATR	Rad3-Related Kinase
BAD	Bcl-2 Antagonist Of Cell Death
BAK	Bcl-2 Homologous Antagonist/Killer
BAX	Bcl-2-Associated X Protein
BCL-2	B-Cell Lymphoma-2 Family Members
BFP	Back Focal Plane
BH3	Bcl-2 Homology Region 3
BID	BH3-Interacting Domain Death Agonist
BIK	Bcl-2-Interacting Killer
BIM	Bcl2-Interacting Mediator Of Cell Death
BRCA 1	Breast Cancer Gene 1
BRCA 2	Breast Cancer Gene 2
BSA	Bovine Serum Albumin
BUB1	Budding Inhibited Benzimidazole 1
BUB2	Budding Inhibited Benzimidazole 2
BUB3	Budding Inhibited Benzimidazole 3
Ca^{2+}	Calcium
CARD	Caspase-Recruiting Domain
CAK	Cyclin Activated Kinase
CBP	CREB-Binding Protein
CD95	Clonal Deletion 95
CD95L	CD95 Ligand

Cdc	Cell Division Cycle
Cdc14	Cell Division Cycle 14
Cdc20	Cell Division Cycle 20
Cdc25A	Cell Division Cycle 25A
Cdc25B	Cell Division Cycle 25B
Cdc25C	Cell Division Cycle 25C
Cdc6	Cell Division Cycle 6
Cdh1	Cadherin 1
CDK	Cyclin Dependent Kinases
CDK1	Cyclin Dependent Kinase 1
CDK2	Cyclin Dependent Kinase 2
CDK4	Cyclin Dependent Kinase 4
CDK6	Cyclin Dependent Kinase 6
CHK1	Checkpoint Kinase 1
CHK2	Checkpoint Kinase 2
cDNA	Complementary Deoxyribonucleic Acid
CK	Cytokeratin
CMA	Chaperone-Mediated Autophagy
CRDs	Cysteine Rich Domains
DCFDA	2,7-Dichlorofluorescein Diacetate
DD	Death Domain
DED	Death Effector Domain

DHEA	Dehydroepiandrostene
DIC	Differential Interference Contrast
DISC	Death Inducing Signalling Complex
DMEM	Dulbecco's Minimum Essential Medium Eagle
DMSO	Dimethyl Sulfoxide
DNA	Deoxyribonucleic Acid
DRAM	Damage-Regulated Autophagy Modulator
DR4	Death Receptor 4
DR5	Death Receptor 5
E2F	Elongation Factor 2
EGFR	Epidermal Growth Factor Receptor
EndoG	Endonuclease G
EOR	ER-Overload Response
ER	Estrogen Receptor
ER	Endoplasmic Reticulum
ERAD	ER-associated Degradation
ERK	Extracellular Signal-Regulated Kinase
FACS	Fluorescence Activated Cell Sorting
FADD	Fas Associated Death Domain
FITC	Fluorescein Isothiocyanate
FCS	Fetal Calf Serum
FFP	Front Focal Plane

FSC	Forward Scatter
GATA-6	GATA binding protein 6
GMNN	Geminin
h	Hours
HC	Immunohistochemical
HE	Hydroethidine
HER2	Human Epidermal Growth Factor Receptor 2
HIF	Hypoxia Inducible Factor
HIF-1	Hypoxia-Inducible factor 1
HIF-1α	Hypoxia-Inducible Factor 1α
HIFU	High Intensity Frequency Ultrasound
JNK	C-Jun N-Terminal Kinase
LAMPA-2A	Lysosomal-Associated Membrane Protein-2A
LDH	Lactate Dehydrogenase
MAD1	Mitotic Arrest-Deficient 1
MAD2	Mitotic Arrest-Deficient 2
MAD3	Mitotic Arrest-Deficient 3
MAPK	The P38 Mitogen Activated Protein Kinase
Mdm2	Murine Double Minute 2
MMP	Mitochondrial Membrane Potential
MMP-2	Matrix Metaloproteinases 2
MMP-9	Matrix Metaloproteinases 9

MOMP	Mitochondrial Outer Membrane Permeabilization
MPS1	Meiotic Recombination 11 Homolog
mRNA	Messenger RNA
mTOR	Mammalian Target Of Rapamycin
mTORC1	mTOR Complex 1
mTORC2	mTOR Complex 2
MTT	3-(4,5-Dimethylthiazol-2-Yl)-2,5-Diphenyltetrazolium Bromide
NADH	Reduced Nicotinamide Adenine Dinucleotide
NOS	Nitric Oxide Synthase
ORC	Origin Recognition Complex
PAI-1	Plasminogen Activator Inhibitor-1
PDGF-B	Platelet-Derived Growth Factor B
PBS	Phosphate Buffer Solution
PCD	Programmed Cell Death
PCNA	Proliferating Cell Nuclear Antigen
PCR	Polymerase Chain Reaction
PE	Phosphatidylethanolamine
PLASDIC	Polarization-Optical Transmitted Light Differential Interference Contrast
PgR	Progesterone Receptor Gene
PI3K	Phosphatidyllinositol 3-OH Kinase
PI3K/AKT	Phosphatidyl-3-Kinase
PPAR	Peroxisome Proliferators-Activator Receptors

PR	Progesterone Receptor
pRB	Retinoblastoma Protein
PS	Phospholipid Phosphatidylserine
RAPTOR	Regulatory-Associated Protein mTOR Complex 1
RICTOR	Rapamycin-Insensitive Companion Of mTOR Complex 2
ROS	Reactive Oxygen Species
SCF	Skp1/CUL1/F Box Protein
SSC	Side Scatter
STS	Steroid Sulfatase
TEM	Transmission Electron Microscopy
TIGAR	TP53-Induced Glycolysis And Apoptosis Regulator
TNF	Tumor Necrosis Factor
TNFR	Tumor Necrosis Factor Receptor
TNFR1	Tumor Necrosis Factor Receptor 1
Tao kinases	Thousand And One Kinases
TRAIL	Tumor Necrosis Factor Related Apoptosis-Inducing Ligand
TRADD	Receptor Associated Death Domain
TUNEL	Terminal Deoxynucleotidyl Transferase Nick End Labelling
Ubl	Ubiquitin-Like Protein
UCP-1	Uncoupling Protein 1
UCP-2	Uncoupling Protein 2
UPR	Unfolded Protein Response

VEGF	Vascular Endothelial Growth Factor
Vps	Vacuolar Protein Sorting
WAF-1	Wild-Type P53-Activated Fragment 1
WEE-1	Wee1-Like Protein Kinase

Graphical representation of signaling pathways

All graphical diagrams of signaling- and transduction pathways were demonstrated using Microsoft® Office Publisher (Microsoft office enterprise 2007, 2006 Microsoft Corporation, United States of America). Microsoft® Office Publisher provides flexible and precise design options for several purposes including posters. All figures were then saved as JPEG images.

Chapter 1

Literature review

1.1 Cancer

1.1.1 Overview of cancer incidence, risk factors and treatment

Breast cancer is the most common cancer diagnosed among women in South Africa (1). Studies have indicated that the probability of a woman developing breast cancer is one in eight (12%). Furthermore, 15% of female cancer deaths are due to breast cancer. The latter is also the leading cause of death of women between the ages of 44 to 50 years of age. Breast cancer survival rate varies between 98% for stage 1 to 16% for stage IV breast cancer (2). However, 40% of all patients with breast cancer suffer a recurrence and 60-70% suffer distal metastases that results in death (3). Studies conducted by means of complementary deoxyribonucleic acid (cDNA) microarrays and immunohistochemical (HC) markers have characterised different categories into which breast cancer can be classified including luminal A (estrogen receptor (ER) positive), progesterone receptor (PR) positive, human epidermal growth factor receptor 2 (HER2) negative, luminal B (ER positive and/or PR negative), HER2 overexpression (ER negative, PR positive, HER2 positive), basal-like (ER negative, PR negative, HER2 negative, cytokeratin (CK) 5/6 positive and/or epidermal growth factor receptor (EGFR) positive) and normal breast-like tumours (4).

Risk factors for breast cancer includes increasing age, high socioeconomic status, obesity, late onset of menopause, advanced age of first pregnancy carried to term, being Caucasian and having a first relative (especially mother or sister) diagnosed with breast cancer (5). The latter is suggested due to a mutation in breast cancer gene 1 (BRCA 1) or breast cancer gene 2 (BRCA 2) that increases the inherited susceptibility to breast cancer (6). Furthermore, mutations in p53 also increase the risk for breast cancer (7). Higher breast cancer incidence is found in Northern America and Northern Europe, as well in high socioeconomic status as women delaying childbearing, following a lifestyle with a western diet and lack exercise (8). Supplementing hormones in the form of oral contraceptives, estrogen replacement therapy and endogenous hormones also increase the risk to breast cancer. If breast cancer is diagnosed after the age of 45 years the prognosis worsens considerably. Environmental risk factors include cigarette smoke, caffeine consumption, exposure to diethylstilbestrol and radiation (9).

1.1.2 Current available breast cancer treatments

Primary breast cancer is localized; however, subclinical metastasis may occur. Secondary breast cancer is formed when cancer cells separate from primary breast cancer after treatment and metastasise to different parts of the body for example in the brain, lungs and liver.

Local treatment focuses on the area of the tumour and usually includes lumpectomy, mastectomy and radiotherapy; however metastasis may still take place. Disadvantages of these treatments include the psychological effects (although reconstructive surgery is also an option which has its own disadvantages) and the normal risks of surgery (10). Surgery risks include infection, pulmonary complications, cardiac arrhythmias, heart attack and stroke. Radiotherapy is an important part of preserving breast tissue in local therapy. Short-term side effects of radiotherapy are hyperpigmentation, dry or moist desquamation, fatigue and meylosuppression (7). Long-term side effects of radiotherapy are secondary cancer (contralateral breast cancer), myocardial infarction, pneumonitis, lymph oedema, brachial plexopathy and skin shrinkage. Radiotherapy is often combined with lumpectomy (7). High intensity frequency ultrasound (HIFU) uses high intensity beams that are focused on the tumour and surrounding tissues and damages target tissue. Since tissues are largely composed of fluids, HIFU can induce cavitation and significant cellular thermal damage (11).

Systemic treatment involves infusion of hormones and chemicals that affect the cell cycle and interrupt cell division. The specific course of treatment followed depends on several factors including the characteristics of the tumour, at which stage it is diagnosed, age, weight and the physical condition of the individual (12). Hormonal-dependent breast cancer treatment has typically been dependent on estrogen deprivation by means of ovarian ablation or estrogen receptor targeting action. Another frequently used treatment in estrogen-dependent breast cancer is aromatase inhibition which includes aminoglutethimide, formesatane, rogletimide, fadrozole, anastrozole, letrozole and exemestane. These compounds suppress the tumour by means of inhibiting estrogen production via blocking the conversion of androstenedione to oestrone (13, 14). The aromatse inhibition takes place by means of competing with the substrate of androgens. An example of the latter is anastrozole and letrozole where triazole groups are present and interacts with the heme group of aromatase (13). Aminoglutethimide, a non-selective aromatase inhibitor, is associated with lethargy and rashes while anastrozole is associated with headaches, hot flushes, gastrointestinal disturbances, weight gain, oedema, thrombo-embolic disturbances (15).

Research involving the prediction of responses to breast cancer treatment is currently being conducted. Several ER-positive tumours were analysed for differentially expressed genes between responders and non-responders to tamoxifen after primary surgery. Qualitative polymerase chain reaction (PCR) results revealed that HOXB14 and IL17BR mRNA levels are sufficiently able to predict the outcome of the therapy. *In vitro* research has shown that this gene confers motile and invasive properties of the MCF-10A mammary cell line (16, 17). The progesterone receptor (PgR) (estrogen-responsive) expression has been linked to benefits of tamoxifen treatment. It has been suggested that PgR transcription is regulated by means of Phosphatidyl-3-Kinase (PI3K/AKT) activation (13). Disadvantages of tamoxifen use include increased risk of deep vein thrombosis, pulmonary embolus, hot flashes, vaginal discharge, irregular menstruation, weight gain, depression, cataracts and an increased possible risk of stroke in postmenopausal women (10, 17). However, tamoxifen in combination with lapatinib results in rapid and profound antipropliferative effects than the drugs on its own. Lapatinib is also able to restore cells sensitivity to tamoxifen. Similar results were obtained from studies involving lapatinib and trastuzumab in various different ErbB-2-overexpressing cell lines. Side effects of lapatinib include diarrhoea, rash, nausea, vomiting, headache and anorexia (17, 18).

1.1.3 Involvement of the sulfatase pathway in breast cancer

Estrone sulphate is present in the blood in high concentrations (14.25nM +/- 2.94) (19). It has been reported that estrone sulphate is necessary for various physiological and pathological processes, including supplying estrone to breast target tissues. Estrone is weaker than estrogen, however, estrone exerts the same function as estrogen including playing an essential role in the oestrus cycle and promoting secondary female characteristics. In addition, several studies have reported that breast tissue contains estrone sulfate and aromatase (20).

Estrogen synthesis requires various enzymes including aromatase, hydrogenase and sulfatase. These enzymes are present in non-tumorigenic and tumorigenic breast tissues. Steroid sulfatase (STS) (also known as aryl-sulfatase C) is responsible for the conversion of estrogen sulphate to estrone. STS activity is a thousand times higher in the breast tissues than aromatase activity (21). Furthermore, estrone synthesis in breast tumour tissue is ten times higher by means of the sulfatase pathway (89%) when compared to the aromatase pathway (89%) (22, 23). The latter suggests that steroid sulfatase may have a central role in the regulation of estrogen synthesis in breast tissues (21).

STS is one of twelve sulfatases that have been characterized in human cells. In addition, seven of these twelve STS's are found in lysosomes and play a vital role in the lysosome function in an acidic environment. These seven lysosomes play a critical role in the glycoaminoglycan-and sulpholipid degradation. The remaining five

STS's are involved with the intracellular membranes and abide by a neutral pH. STS can cleave all steroid sulphates, contradicting to earlier views. (24). STS takes part in hydrolysis of oestrone sulphate to oestrone (25). This is believed to contribute to oestradiol production in breast tumour tissues. STS also partakes in the conversion of dehydroepiandrostene (DHEA) from DHEA-sulphate (26). DHEA is found significantly increased in tumorigenic breast tissue (23). Androstenediol (Adiol) is produced by the reduction of DHEA. Adiol can bind to the estrogen receptors and stimulate breast cancer cell growth. Adiol production is thus dependent on the sulfatase pathway. Studies have shown that STS mRNA expression is higher in malignant than in normal breast tissue and also suggested that high levels of STS mRNA expression in breast tumours are associated with poor prognosis (27). Inhibition of STS can thus be considered for cancer treatment.

1.2 Overview of the cell cycle

The cell cycle is a complicated series of orchestrated steps leading to cellular proliferation, senescence and cell death. The cell cycle in a eukaryotic cell consists of five stages: quiescent phase (G_0), the synthesis (S) phase, the mitotic phase (M) and two gap phases (G_1 and G_2). The S phase involves deoxyribonucleic acid (DNA) replication, the M phase consist of the segregation of two complete sets of chromosomes to two resulting daughter cells. The G_1 separates the M phase and the S phase, G_2 separates the S phase and M phase (28).

The cell cycle is regulated by protein heterodimer complexes that comprises of a cyclin and an associated kinase moiety. The latter is referred to as cyclin-dependent kinases (CDKs). Kinase activity requires the presence of cyclins (28). There are 11 CDK family members recognised presently. CDK1, 2, 3, 4 and 6 play essential roles in the cell cycle and CDK7 activates the CDKs involved in the cell cycle (29, 28). A cyclins are of importance in the control of cells moving from the S phase to the M phase. B cyclins are essential in G_2M transition and the regulation of cells in the M phase. H cyclins are plays a role in CDK-activating kinase process (30).

Phosphorylation and dephosphorylation of CDK and cyclins also plays an important role in the cell cycle since it regulates kinase activity (31). Phosphorylation is performed by means of cyclin-activating kinase and dephosphorylation is mediated by members of the CDC25 family of dual-specificity protein phosphatases (32). For example in, $p34^{cdc2}$, the phosphorylation of threonine 14 and tyrosine 15 results in inactivation of CDC2/cyclin B complexes for the regulation of cells entering the M phase. When the cells are ready for the G_2M transition, CDC25 removes the phosphates from the kinase (31). CDK-activating kinase (CAK) is an enzyme responsible for the activation by means of phosphorylation of CDK1, CDK2, CDK4 and CDK6 and is composed of 3 subunits: CDK7, cyclin H and MAT1 (33). The subunit of CAK is CDK7. Active human CAK

contains additional polypeptides of approximately 36 and 32-kDa. The 32kDa polypeptide is also known as cyclin H (31).

1.2.1 Cell cycle phases

1.2.1.1 The G_1 phase

The G_1 phase assesses whether a cell is prepared to enter the S phase based on nutrients and growth factor availability (28). The latter is achieved by means of the Retinoblastoma (RB)/E2F/DP pathway (30). In the G_1 phase, D cyclins are synthesized and bind to CDK4 and CDK6. The RB gene is phosphorylated by CDK4-cyclin D and CDK6-cyclin D resulting in transcription factor E2F release. This leads to transcription of genes necessary for the G_1/S transition and S phase. CDK2-Cyclin E also phosphorylates Rb and E2F ensures its own transcription; these two actions create a positive feedback loop promoting the S phase (28). The E2F family can be divided into 2 categories based on the function namely, activating E2F (E2F1, E2F2 and E2F3) and repressing E2F's (E2F4 and E2F5). Activated E2Fs upregulates target gene transcription during the G_1/S transition. Repressed E2F's mediates gene silencing during G_0/G_1. pRB, p107 and p130/Rbl2 confer cell cycle dependent regulation to the E2F activities by means of phosphorylation and dephosphorylation. During the G_1/S transition, the above-mentioned genes are hyperphosphorylated by CDK-complexes liberating E2F1, E2F2 and E2F3 that will activate gene transcription necessary for DNA synthesis and cell cycle progression (34).

1.2.1.2 The S phase

The genome is duplicated by DNA replication where each identical copy segregates into two daughter cells. Furthermore, in eukaryotes this process is complicated by the genome fragmentation into various chromosomes (35). Initiation of DNA replication during the S-phase involves six-subunit complexes called origin recognition complex (ORC) binding to chromosomal regions called origins of replication (36). There are 6 ORCS currently known, ORC1 to ORC6, named in descending molecular mass; which is located among six chromosomes (37). Cdt1 and Cdc6 bind and recruit the MCM2-7 complex to the origin. The MCM2-7 is the putatative replication origin that winds down the DNA and permits downstream factors to access DNA and to initiate replication. The ORC, Cdt1, cell division cycle (CDC) 6, MCM2-7 complex is known as the pre-replicative complex (pre-RC). The latter acts in the M and G_1 phases (38). Geminin (DNA replication inhibitor also known as GMNN which prevents chromosomal polyploidy while also contributing to progression of the cell cycle and cell proliferation) binds to Cdt1 and prevents MCM loading. CDC6 is phosphorylated and removed from the nucleus (38).

1.2.1.3 G_2M phase

The remainder of the cell cycle namely the G_2 phase and the S phase is driven by activated CDK1-cyclin A and CDK1-cyclin B complexes. Cyclin B production is steadily upregulated in the G_2 phase. When cyclin B reaches the threshold, depending on this kinase the cell will enter mitosis. Mitosis consists of several phases including prophase, metaphase, telophase and anaphase. Cyclin B activity continuous till late mitosis and is degraded in anaphase. The loss of CDK1 activity results in the activation of the mitotic exit and completion of the cell cycle (39). Mitotic exit comprises of an organised series of events leading to the segregation of sister chromatids to completion of mitosis by means of cytokinesis. Anaphase initiation is caused by the anaphase promoting complex (APC) ubiquitination and its activator CDC20 (APC^{CDC20}). The latter results in the degradation of securin leading to the release of separase which cleaves cohesions and initiates chromatid separation (40). Furthermore, APC^{CDC20} targets mitotic cyclins for degradation and CDK downregulation (41). The APC is a unit consisting of multi-subunit E3 ubiquination ligase responsible for the control of transitions in the cell cycle. A subunit *emb-30* is required for the metaphase-anaphase transition and encodes APC4 (41).

1.2.2 Protein degradation in the cell cycle

Protein degradation is vital to various cellular processes. The degradation of various proteins regulates the cell cycle transitions and degradation of cell cycle regulators by means of two ubiquitin E3-ligase complexes namely, Skp1/CUL1/F box protein (SCF) and anaphase promoting complex/cyclosome (APC/C) (42). Ubiquitin-protein ligase is responsible for the addition of small ubiquitin molecules to other proteins (43). Proteins carry domains and sequence motifs that function as degradation signals for proteolysis by proteases. These regions are proline-, glutamic acid-, serine- and threonine-rich and indicate that the protein has a short lifetime (44). In eukaryotic cells the majority of proteins are degraded by the 26S proteases that consist of 20S core and 19S regulatory complexes. The 20S core unit contains two chymotrypsin-like sites that cleaves peptide bonds, two trypsin-like sites that cleaves basic residues and two caspase-like proteolytic sites that cleaves acidotic residues (44, 45).

The ubiquitin/proteasome-dependent proteolysis of cyclin A and cyclin B requires a short sequence near their N terminus called the destruction box (D-box). The ubiquitin ligase E3 for cyclin B1 in mitosis is the anaphase-promoting complex/cyclosome complexed with CDC20. Cyclin A is probably also degraded by anaphase-promoting complex/cyclosome-CDC20, although the difference in the timing of degradation between cyclin A and cyclin B1 argues for the involvement of distinct mechanisms (45).

As previously mentioned, eukaryotic cells respond to cellular stress by means of various checkpoints in the cell cycle that is responsible for the delay of the cell cycle. Two major cell cycle checkpoints have been classified namely, G_1/S and the G_2M checkpoint. The p38 mitogen activated protein kinase (MAPK) pathway is involved in both of these checkpoints (46).

1.2.3 Cell cycle checkpoints

1.2.3.1 G_1/S checkpoint

The G_1/S checkpoint is involved before and after DNA replication (46). It has been reported that cellular damage results in slower DNA replication leading to the discovery of Ataxia Telangiectasia Mutated (ATM which phosphorylates various proteins involved in checkpoint signaling). The mechanism used by the cell to slow DNA replication down remains elusive; however, two mechanisms have been suggested. The checkpoint possibly slows down DNA replication. The second mechanism involves the inhibition of the origin of replication or replication fork progression is slowed down (47). Cellular stress activates ATM or ATM and Rad3-related kinase (ATR) in the cell. ATM activates Chk2. Chk2 phosphorylates CDC25A leading to its degradation. ATR activates chk1 resulting in the degradation of CDC25A in response to UV radiation. CDC25A phosphatase degradation prevents dephosphorylation and activation of CDK2-cyclin E that results in inhibition of the origin of fire (47). Double strand breaks of the DNA results in activation of p38 MAPK that is dependent in the activation of Ser/Thr protein kinases. The latter serves as DNA damage sensors and includes ATM and ATR. Furthermore, ATM may be necessary for p38 MAPK activation. Nonetheless, it appears that ATM is unable to phosphorylate p38 MAPK activation as the consensus motif recognised by ATM is not present in the p38 MAPK family members. p38 MAPK activation is induced by Thousand and one (TAO) kinases which are activated by ATM. However, p38 MAPK activation occurs in the presence of caffeine which is an ATM inhibitor and thus p38 MAPK activation can occur by alternative signaling pathways other than the ATM/ATR pathway. Furthermore, signaling pathways which results in the activation of p38 MAPK alternative to ATM/ATR pathway still remains elusive and requires more research (46).

1.2.3.2 Restriction point

Retinoblastoma protein (pRB) is the product of retinoblastoma tumour suppressor gene. pRB exerts its effects in the G_1 phase (48). The transition from the serum-dependent (cells entering G_1 from mitosis requires serum mitogens) to the serum-independent state is known as the Restriction (R) point (49). Cyclins of the D class (D1, D2 and D3) and their partners CDK4/CDK6 are involved in the initial pRB phosphorylation (49, 50). Furthermore, pRB phosphorylation in the entry and exit of the S phase are mediated by CyclinE/CDK2. If

pRB is hypophosphorylated the cell cannot enter S phase due to pRB physically associating with a group of E2F transcription factor members (E2F1-5). E2F1-3 binds to pRB, E2F4 and 5 binds to pRB-related proteins p107 and p130 (50). Thus, the E2F transcription factors act as effectors in the cell cycle dependent switch. After the cell passes the restriction point, the cell is committed to DNA replication even when proliferative signals are no longer present (33).

1.2.3.3 G_2M checkpoint

In response to double strand breakage of DNA, p38 MAPK is activated and results in the activation of the G_2M checkpoint (46). The pathway by which p38 MAPK induces G_2M arrest remains elusive, however, two pathways have been suggested. One pathway involves the phosphorylation and activation of p53 resulting in the G_2M checkpoint. The above-mentioned action leads to the dissociation of p53 and Murine double minute 2 (Mdm2) resulting in p53 accumulation. Mdm2 is a protein that activates p53 and promotes degradation of p53 by means of ubiquitination. p53 activation leads to the activation of several genes (DNA damage inducible factor α, p21 and 14-3-3) involved in the G_2M checkpoint (46). Furthermore, p38 MAPK induces the G_2M checkpoint by inhibition and phosphorylation of CDC25B. CDC25B dephosphorylates CDC2, activating cyclin B/CDC2 that is responsible for cell cycle progression. CDC25B phosphorylation inhibits its own activity by promoting association with 14-3-3 proteins that are sequestered in the cytoplasm. MAPK promotes CDC25B phosphorylation by means of activating MK2, a substrate of p38 MAPK. MK2 activation has been indicated as a required component for G_2M checkpoint induction (46).

CDK1/cyclin B1 complex controls mitosis entry, cyclin B degradation exit allows for the cell to enter mitosis (51). Inappropriate CDK1/cyclin B1 complex activation results in a cell cycle progression, while bypassing G_2M checkpoint resulting in improper mitosis entry and formation of tetraploidy cells with damaged DNA (52). Tyner (2009) reports that p21 is responsible for degradation of cyclin B; however, the mechanism remains elusive. Research has indicated that cyclin B associates with p21 after the occurrence of DNA damage. Furthermore, Cyclin B1 then is directed to the APC/C. APC/C then targets cyclin B1 for destruction. This would also result in additional safeguards to prevent replication of compromised DNA (51).

1.2.3.4 Mitotic checkpoint

In mitosis replicated chromosomes segregate to each of the daughter cells. The sister chromatids attach to the bipolar mitotic spindle during prometaphase and then progresses through the rest of mitosis. Incorrect attachment of the chromatids to mitotic spindle results in unequal separation of chromosomes. The spindle checkpoint is responsible for delaying the transition of metaphase to anaphase until the chromosomes are

attached in the correct bipolar way to the mitotic spindle (53). The mitotic checkpoint delays anaphase by means of inhibitory signals to avert APC/C activation. This leads to high levels of cyclin B and securin that avoid anaphase onset. The inhibitory signals are produced by the kinetochore. The kinetochore is a protein responsible for the assembly of centromeres. However, unattached kinetochore catalyses inhibitory signal production. When the chromosomes attach at the sister kinetochores, the inhibitory signals stops being generated, resulting in the transition of the cell into anaphase (54).

The APC is inactive in cells arrested by the mitotic checkpoint. The APC is thus believed to be the target of the mitotic checkpoint. It has been reported that several genes, including MAD1, MAD2, MAD3, BUB1, BUB2, BUB3 and MPS1 are involved in the mitotic checkpoint machinery (55). Bub1 and Mad1 function as scaffolds for recruitment of Mad2 and BubR1/Mad3 that are capable of generating inhibitory signals. Mad2 interacts with Cdc20; this is necessary for inhibition of APC by the mitotic checkpoint (53).

1.3 Mechanisms of cell death

Various modes of cell death including: apoptosis, oncosis, autophagy, mitotic catastrophe, metabolic catastrophe and necrosis are recognised and will be discussed below. Cell death can be classified according to its morphological appearance (which may be apoptotic, necrotic, autophagic or associated with mitosis), enzymological criteria (the possible involvement of nucleases of proteases, such as caspases, cathepsins and transglutaminases), functional aspects (programmed or accidental) or immunological characteristics (immunogenic or non-immunogenic) (56, 57, 58). Programmed cell death (PCD) is crucial for the development, regulation and maintenance of multicellular organisms. Although PCD is used several times as a synonym for apoptosis, other forms of PCD also exist including autophagy. However, necrosis and metabolic catastrophe are types of uncontrolled cell death (56, 57).

1.3.1 Apoptosis

The expression ‘apoptosis’ was initially coined to describe structural alterations in cells observable by transmitted light and electron microscopy during cell death (58, 59). Apoptosis is defined as an energy-dependent irreversible systematic elimination of unneeded or abnormal cells by a series of controlled molecular steps mediated by an intracellular program (60). Apoptosis is considered a vital component of various processes including normal cell turnover, proper development and functioning of the immune system, hormone-dependent atrophy, embryonic development and chemical-induced cell death. Dysregulation of apoptosis has serious consequences including neurodegenerative diseases, ischemic damage, autoimmune

disorders and several types of cancer (60). In mammalian cells, apoptosis is classified as one of two modes namely, intrinsic and extrinsic. The extrinsic pathway involves death receptors and the intrinsic pathway entails the mitochondria and the BCL-2 family (58). Intrinsic and extrinsic apoptosis are triggered by cell death stimuli from intra- and extracellular environments, respectively. The latter results in the activation of caspases which are the core components of the apoptotic machinery (60). Furthermore, the two pathways are linked and that molecules in one pathway can influence the other (61). Apoptosis is characterised by rounding of the cell, retraction of pseudopodes, cytoplasmic and nuclear condensation (pyknosis), chromatin condensation, nuclear fragmentation (karyorrhexis), classically little or no ultrastructural modifications of cytoplasmic organelles, plasma membrane blebbing (but membrane integrity is maintained until the final stages of the process) and engulfment by resident phagocytes (58, 59). Another important feature of apoptosis is the externalization of the cell's lipid phosphatidylserine bilayer governed by activation of a calcium-dependent phospholipid scramblase activity in combination with the aminophospholipid translocase inactivation at the cell surface (56, 59, 61, 62). This leads to the expression of cell surface markers that produces early phagocytic recognition by adjacent cells of apoptotic cells, allowing for phagocytosis with minimal damage to the neighbouring tissue (56).

1.3.1.1 Caspase-dependent apoptosis

Caspases is a family of cysteinyl aspartate proteinases (cysteine proteases that cleave their substrates at specific aspartyl residues) and are instrumental to the execution of apoptosis (63, 64). Apoptotic caspases belongs to one of two categories; initiator (upstream) caspases or effector/executioner (downstream) caspase (65). Initiator caspases that trigger apoptosis include caspases 2, 4, 8, 9, and 10 (66). Effector caspases includes caspases 3, 6, and 7 (65). There are increasing amounts of data supporting nonapoptotic roles for caspases in cells. For example it has been reported that caspase 9 plays a role in muscle differentiation (67). There are three caspase-dependent cell death pathways including the mitochondrial pathway (intrinsic), death receptor pathway (extrinsic) and the endoplasmic-specific pathway (56). Although the intrinsic and extrinsic cell death pathways act independently to initiate the cell death in some cellular networks, in most tumorigenic cells there is a delicate crosstalk between these two pathways which results in the activation of executioner caspases (68).

1.3.1.2.1 Death receptor pathway (extrinsic)

The extrinsic pathway eradicates abnormal or unnecessary cells during development and is initiated by the ligand-bound death receptors at the plasma membrane, including tumor necrosis factor/tumor necrosis factor

receptor 1 (TNF-TNFR1), FasL-Fas and TRAIL-DR4 or -DR5 (Figure 1.1) (69, 70). Death receptors belong to the tumour necrosis factor receptor (TNFR) gene superfamily and have several functions including initiating apoptosis. The TNF receptor (TNFR) superfamily is characterised by the occurrence of cysteine rich domains (CRDs) that mediate binding between ligands and type I transmembrane domain receptors including TNFR1 (TNF receptor-1), CD95 (also known as Apo-1 or Fas) and the TRAIL receptors DR4 and DR5. Furthermore, TRAIL receptors DR4 and DR5 are best characterized for initiation of apoptosis. A soluble Fas decoy receptor, DcR3, and three decoys for TRAIL, DcR1, DcR2 and OPG were also identified (68, 70). After the extrinsic pathway is initiated, death receptors accumulate at the cell surface following ligand binding to their extracellular domains. This results in recruitment of adaptor molecules to the aggregated intracellular domains of the receptors (70). One of the adaptor molecules Fas associated death domain (FADD) consists of two domains. The death domain (DD) either interacts with DD directly or through another adaptor molecule namely, TNF receptor associated death domain (TRADD) (56, 68). The second FADD protein interaction domain, death effector domain (DED) that interacts with the DED of the zymogen, pro-caspase 8 forms an intracellular multiprotein complex namely, death inducing signalling complex (DISC) (68). DISC facilitates the cleavage of caspase 8 leading to the activation of effector caspases 3- and 7 (Figure 1.1) (8, 71). These effector caspases are responsible for degradation of more than 280 cellular proteins identified so far. These proteins are involved in scaffolding of the cytoplasm and nucleus, signaling transduction, regulation of cell cycle progression and DNA replication and repair (72, 73).

.

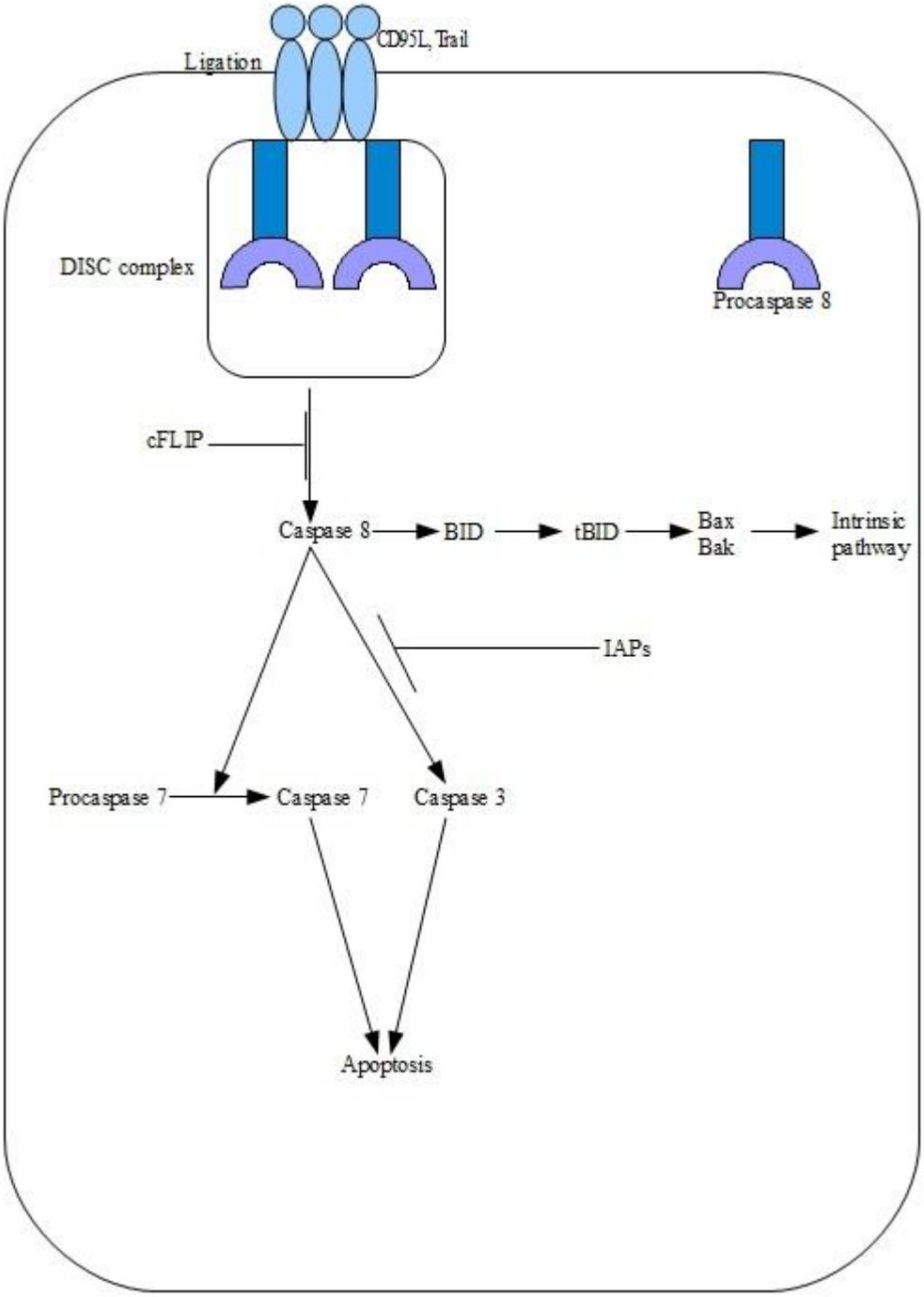

Figure 1.1: The death receptor (extrinsic) pathway is initiated when the ligand binds to the receptor namely CD95 and TRAIL receptors resulting in DISC formation. DISC formation is regulated by several inhibitory mechanisms including c-FLICE inhibitory proteins (c-FLIP) that acts by interacting with FADD to block initiator caspase activation. DISC facilitates cleavage of caspase 8. Caspase 8 can act via BID, a pro-apoptotic protein that interacts with BAX resulting in the activation of the mitochondrial (intrinsic) pathway and cytochrome *c* release. On the other hand after caspase 8 activation the cell can continue following the death receptor pathway by means of activation of caspase 7 or caspase 3 resulting in apoptosis.

1.3.1.2.2 Death receptor pathway its involvement in cancer treatment

Some chemotherapeutic agents initiate apoptosis by altering death receptors on the surface. For example, doxorubin increases the FAS expression on tumour cell surfaces (74). In addition, Apo-2 ligand (Apo-2L) is a member of the TNF-superfamily with structural and functional similarities to Fas/Apo-1L (75). Apo-2L induces apoptosis in tumours; furthermore, Apo-2L in combination with 5-fluorouracil (CPT-11) results in significant tumour regression or complete tumour ablation (74). In addition, data suggest that TRAIL alone is not sufficient in treating cancer as resistance often occurs. The receptor regulation and cytosolic factors that modulate apoptosis and is induced by TRAIL often results in the resistance to TRAIL. For example, cell lines that possess FADD mutations are resistant apoptosis induced by TRAIL. Furthermore, infant neuroblastoma cells possessing a silent caspase 8 gene are resistant to TRAIL (76). However, chemotherapy agents including subtoxic concentrations of doxorubicin, epirubicin and cisplatin associated with TRAIL is successful in treating TRAIL-resistant renal, prostate and bladder carcinomas as the chemotherapeutic agents sensitize the tumorigenic cells to TRAIL (77, 78).

1.3.1.3.1 Mitochondrial (intrinsic) pathway

The intrinsic pathway instigates apoptosis via the involvement of the mitochondria and is initiated by DNA damage as a result of irradiation, chemicals, lack of growth factors or oxidative stress (Figure 1.2) (70). The fundamental occurrence in the mitochondrial pathway is the mitochondrial outer membrane permeabilization (MOMP). During this process, the electrochemical gradient across the mitochondrial membrane collapses through the formation of pores in the mitochondria by B-cell lymphoma-2 (BCL-2) proapoptotic family members proteins (Figure 1.2) (79, 80, 81, 82, 83). The BCL-2 family consists of anti-apoptotic and pro-apoptotic proteins, these proteins share regions of sequence homology within conserved regions known as BCL-2 (BH) domains. Proapoptotic protein members (BCL-2 and BCL-X_L) and the proapoptotic protein subset (BAX and BAK) are multidomain proteins sharing sequence homology within three or four BH domains (84). The BCL-2 Homology Region 3-subset (BH3) of proapoptotic molecules, including BAD, BID, BIM, NOXA, BIK, HRK, and PUMA. The latter shows sequence homology only within single a helical segment, the BH3 domain, which is also known as the minimal death domain required for binding to multidomain BCL-2 family members (84, 85). Once MOMP occurs, it precipitates cell death through either the release of molecules involved in apoptosis, or the loss of mitochondrial functions essential for cell survival. Permeabilization of the outer membrane results in release of cell death activating factors into the cytosol, including cytochrome *c*, second mitochondria-derived activator caspase/direct IAP protein with low PI (Smac/DIABLO), apoptosis-inducing factor (AIF) and endonuclease G (Figure 1.2). These cell death

activating factors activates caspases that cleave cellular substrates resulting in destruction of the cell (86). Once cytochrome *c* is in the cytosol, the apoptosome forms and acts as a molecular platform for caspase 9 activation (87). The apoptosome consists out of three constituents namely, cytochrome *c*, apoptosis activating factor 1 (APAF-1) and ATP/dATP. APAF-1 comprises of three domains including an N-terminal caspase-recruiting domain (CARD), an expanded nucleotide domain and a 12-13 WD40 repeats domain (negative regulatory element which binds to CARD) at the carboxy terminal (88, 89). CARD interacts with the prodomain of caspase-9 and in combination with the nucleotide binding domains are responsible for oligomerization of APAF-1 in the presence of cytochrome *c*. The WD repeats interact with cytochrome *c* for the removal of this domain. The above-mentioned activities results in caspase 9 activation. Furthermore, the binding of cytochrome *c* and APAF-1 result in hydrolysis of ATP to dATP and exogenous heat (90). Active caspase 9 cleaves executioner caspases to induce apoptosis mainly through the activation of caspase 3 (91, 92).

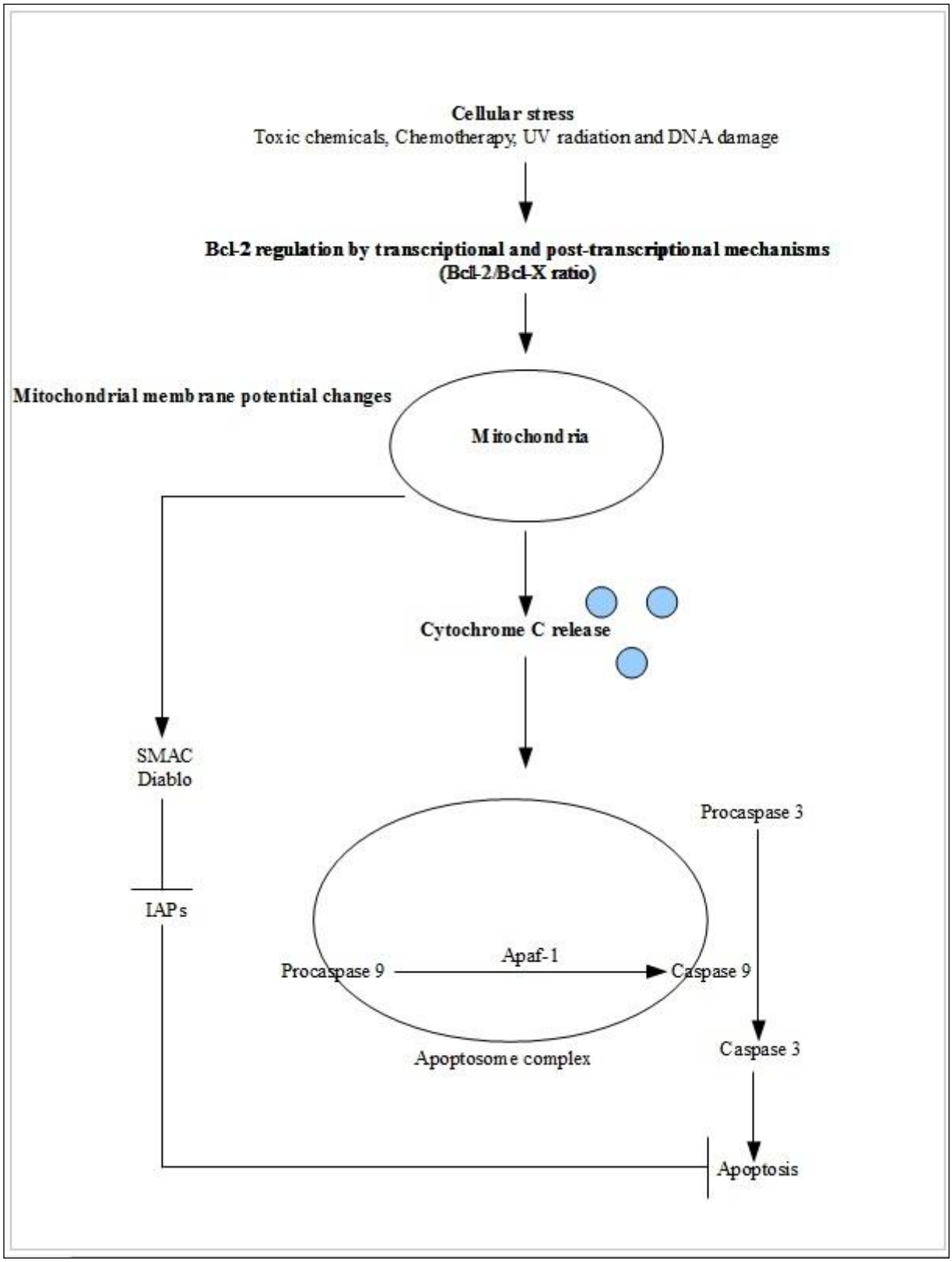

Figure 1.2: The mitochondrial (intrinsic) pathway is activated by cellular stress (toxins and DNA damage) that alters the Bcl-2/Bcl-X ratio. The latter results in cytochrome *c* release from the mitochondria. Caspase 9 is

activated by means of Apaf-1. Caspase 9 is required for caspase 3 activation. Furthermore, IAPs that inhibits apoptosis is also inhibited by SMAC/Diablo.

1.3.1.3.2 Mitochondrial pathway and its involvement in cancer treatment

The apoptosome is a target in several cancer types. One approach currently under study is cytochrome *c* mimetics which results in the APAF-1 conformational change necessary for apoptotome assembly and caspase 9 activation (93, 94). Another approach under investigation is the use of agents including Triacsin c, to facilitate the release cytochrome *c*. The latter results in the induction of apoptosis (95). Furthermore, a number of cytotoxic agents such as 2-chloro-s'-deoxyadenosine, etoposide and paxitaxel induces apoptosis in a cell-free system by altering the MMP (96).

1.3.1.4 Endoplasmic reticulum pathway

The endoplasmic reticulum (ER) is a cellular organ that is highly sensitive to changes in the surrounding area including calcium (Ca^{2+}) homeostasis (97). The ER also has a vital role as being the major physiological source of Ca^{2+} within the cell. This Ca^{2+} resource is vital for numerous signaling pathways including fertilization, differentiation, proliferation and transcription factor activation thereby influencing gene transcription and expression, protein and steroid synthesis and apoptosis (98). Furthermore, chemical agents, inhibitors of glycosylation, oxidative stress and accumulation of misfolded proteins may disrupt ER function, this is known as ER stress. The latter results in unfolded protein response (UPR), ER-overload response (EOR) and ER-associated degradation (ERAD) (97). Prolonged ER stress may be result in the activation of apoptosis through both a mitochondrial dependent and independent pathway. The mitochondrial independent pathway is alleged to occur through initiator caspase 12. Activation of caspase 12 appears to be triggered only by various stimuli that activate ER stress. Caspase 12, localised in the ER membrane and expressed ubiquitously and is synthesized as an inactive proenzyme consisting of a regulatory prodomain and two catalytic subunits and is cleaved and activated by the Ca^{2+}-dependent protease m-calpain. Caspase 12, once activated, directly activates caspase 9; caspase 9 activates effector caspase 3 (97, 98). Caspase 12 is involved in the ER-mediated apoptotic pathway in murine cells (99). Caspase 4 is the human homolog of murine caspase 12 and is localized to the ER membrane and is specifically activated by and required for ER stress-induced apoptosis (100). Overexpression of the transmembrane portion of Bap31 results in the early release of Ca^{2+} into the mitochondria, resulting in the mitochondria being very sensitized to caspase 8 and cytochrome *c* (101). Recent findings demonstrated that Bcl-2 is involved in the ER pathway as well. Release of Ca^{2+} from the ER is taken up into the mitochondria resulting in reduced apoptosis in Bax and Bak knockout mice (102).

ER stress induces oligomerization of bax and bak to their active states and induces ER Ca^{2+} leak that results in apoptosis (99).

1.3.2 Caspase-independent apoptosis

Non-caspase proteases have been implicated as effectors of apoptosis. These include the cathepsins, calpains (cytosolic calcium activated cysteine proteases), granzymes, endonuclease G (endoG) and AIF (58,103). EndoG and AIF are released during the permeabilization of the outer mitochondrial membrane resulting in the destruction of the cell (86). EndoG and AIF translocate to the nucleus, where AIF induces DNA fragmentation and peripheral nuclear condensation. Furthermore, mitochondrial EndoG is a mitochondrial nuclease that assists with the maintenance of the mitochondrial genome by participating in mitochondrial DNA duplication and repair (104, 105). Following EndoG entrance into the nucleus, endoG cleaves the nuclear chromatin (56, 86). Calpain and cathepsin activated by the Ca^{2+} influx degrade cytoplasmic proteins resulting in the ultimate demise of the cell (70). Granzyme B is a serine protease family member exclusively expressed by cytotoxic T-lymphocytes. Granzyme subfamilies are first expressed as zymogens containing cytolytic granules. Following receptor-mediated fusion cytotoxic lymphocyte with an infected target cell, granzyme enters the cell and induces apoptosis. Granzyme B contains active sites similar to cysteine proteases of the caspase family. The latter allows for the cleavage of aspartate residues and activates the caspase cascade by activating several procaspases (106). Furthermore, granzymes are also able to cleave the proapoptotic Bcl-2 family members Bid and Bax, thereby inducing mitochondrial membrane permeabilization (107).

1.3.3 Autophagy

Autophagy literally means ‘self-eating when translated from the original Greek word (108). Autophagy refers to an evolutionary conserved multistep lysosomal pathway involved in long-lived proteins and organelles. The functions of autophagy include remodelling during development, production of amino acids, energy production and the elimination of unwanted or damaged organelles. Autophagy stimuli include stress, starvation, changes in cell volume, oxidative stress, accumulation of misfolded proteins, irradiation, TRIAL treatment and hormonal signalling (Figure 1.3). Two major systems involved in protein degradation include the ubiquintin-proteosome pathway and autophagic system (102). Autophagy consists of several steps including nucleation, expansion, maturation and docking and fusion. In nucleation an unidentified membrane source transports lipid bilayers for phogophore formation (preautophagosomal structure in yeast). The expansion step (also known as isolation membrane stage) refers to the formation of double-membrane vesicles by means of invagination from the preautophagosomal structure (Figure 1.3). During maturation the

autophagsosome undergoes numerous maturation steps including fusion events with multi-vesicular and endosomes. Docking and fusion refers to the fusion of the inner membrane compartment and its contents with the lysosome/autolysosome. The latter is then degraded by lysosomal hydrolases (108, 109). Various forms of autophagy have been described including chaperone-mediated autophagy (CMA), piecemeal microautophagy, macroautophagy and microautophagy. CMA refers to the translocation of unfolded proteins across the membrane at the lysosomal membrane. Piecemeal microautophagy occurs in yeast and degrades nucleus portions by transporting them to the vacuole yeast; this however only takes place in yeast. Macroautophagy makes use of specialised cytosolic vesicles that eventually fuses with the lysosome in order to sequester and degrade the cytoplasm. Microautophagy involves the direct uptake of cytoplasm at the lysosomal surface by invagination of the limiting membrane of the lysosome (110).

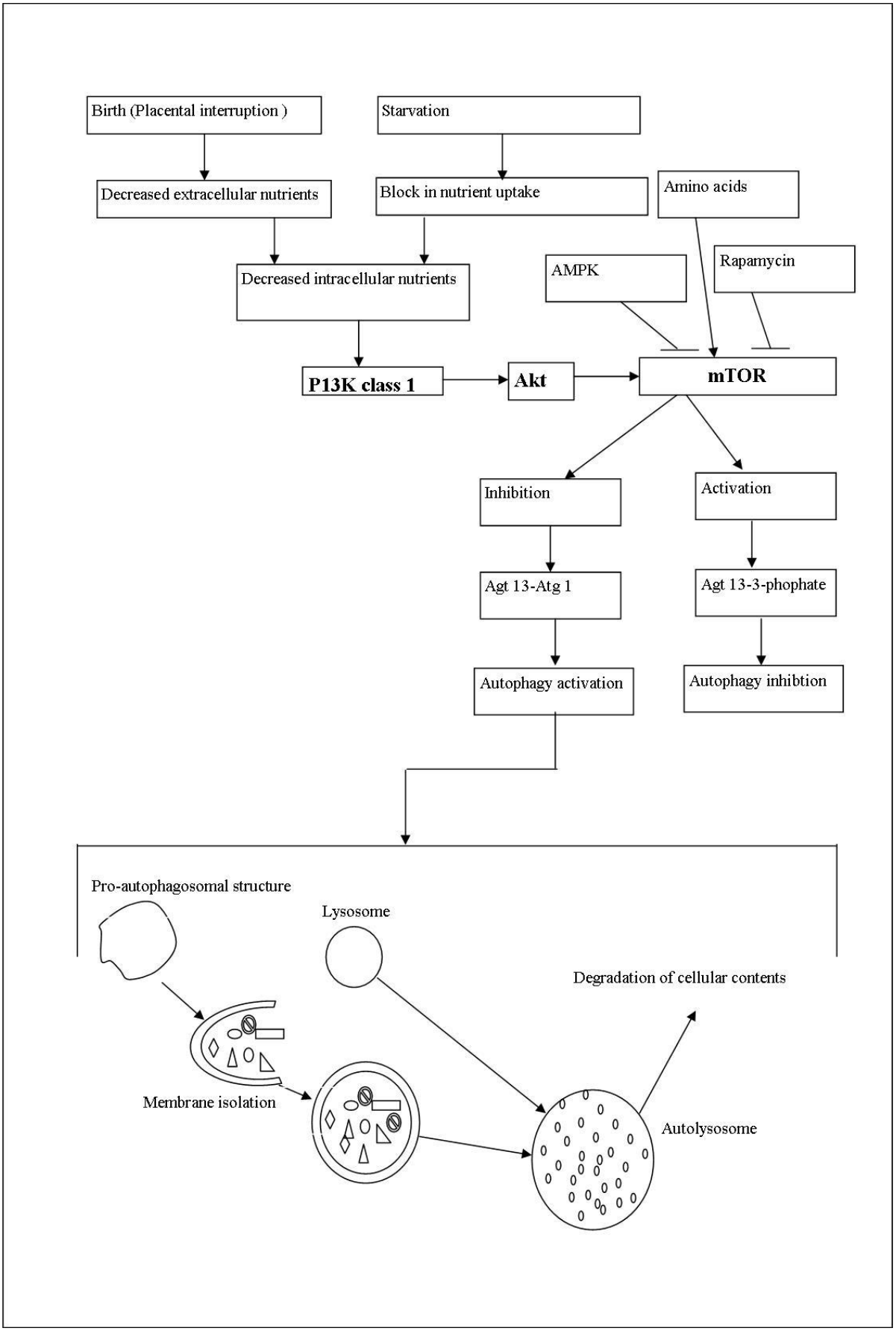
Birth (Placental interruption)
Starvation
Decreased extracellular nutrients
Block in nutrient uptake
Amino acids
Decreased intracellular nutrients
AMPK
Raparnycin
P13K class 1
Akt
mTOR
Inhibition
Activation
Agt 13-Atg 1
Agt 13-3-phophate
Autophagy activation
Autophagy inhibtion
Pro-autophagosomal structure
Lysosome
Degradation of cellular contents
Membrane isolation
Autolysosome

Figure 1.3: Autophagy is initiated by decreased cellular uptake or the blockage of nutrient uptake (starvation). This results in decreased nutrients within the cell, resulting in PI3K class 1 activation. In the case that mTOR is activated, autophagy does not take place. However, if mTOR is successfully inhibited by rapamycin, autophagy will take place where the cellular nutrients are sequestered and degraded.

1.3.3.1 Chaperone-mediated autophagy

CMA activated by long-term starvation results in protein degradation in a molecule-to-molecule fashion (111). CMA involvement has been found in autophagy induced by nutrient deprivation, oxidative stress and Parkinson's disease (wild-type α-synuclein degradation) (111, 112, 113). The substrate of CMA consists of cytosolic proteins recognised by the heat shock protein (hsp) 70 chaperones. The chaperone-substrate complex attaches to the CMA receptor, lysosomal-associated membrane protein-2A (LAMP-2A) (112). Three different isoforms of LAMP-2 exists by alternative splicing namely, LAMP-2A, LAMP-2B and LAMP-2C, however, only LAMP-2A acts as a receptor in autophagy. The role of LAMP-2B and LAMP-2C are uncertain (111, 112). Removal of all LAMP-2A isoforms results in accumulation of autophagic vacuoles in cytoplasm (114). A pool of LAMPA-2A residues in the lysosomal lumen is capable of reinserting themselves for CMA activation. In old liver cells this process is defective indicating that LAMP-2A levels in older cells are declining, suppressed or inactive. Nevertheless, the degradation rate of LAMP-2A is accelerated in senescent fibroblasts. This accelerated process is due to different proteases than proteases used in younger cells for LAMP-2A degradation. An increase in LAMP-2A transcription rate may restore CMA rates (111).

1.3.3.2 Macroautophagy

Macroautophagy involves the sequestration of internal cellular components and organelles into a double membrane arrangement recognized as autophagic vesicles followed by degradation by the lysosomes and endosomes (115). After the initiation event, autophagy-related (ATGs) genes arrange the configuration of autophagic vesicles from the phogophore or the segregation of the membrane to the phagosome and ultimately the autolysosome. The ULK-ATG13-FIP200 and the Beclin-1-hVps34-p150 complexes mediate nucleation events, whereas the ubiquitin-like conjugation systems (ATG5–ATG12 and LC3-II) direct vesicle elongation and autophagosome formation. Cellular contents are ultimately sequestered within the autophagosome and thereby removed from the cytoplasm. Intracellular material is degraded into autolysosomes, which is the product of lysosomes and autophagosomes fusion (108). The autolysosome is an acidic vesicle in which the intracellular material is degraded by lysosomal hydrolases, for example cathepsins. Amino acids and other end products generated in this catabolic process are then released from the autolysosome to fuel cellular processes

and maintenance of the cell (108, 115). Macroautophagy is activated by starvation, hypoxic conditions and high temperatures (116).

Research has identified 30 ATG genes in yeast including ATG genes involved in starvation-induced autophagy and cytoplasm-to-vacuole targeting pathway. The core machinery consists of Atg9 and the recycling system (ATG9 and the ATG1 kinase complex, ATG2 and ATG18), phosphatidyllinositol 3-OH kinase (PI3K) complex (vacuolar protein sorting (Vps) 34, Vsp15, ATG6, ATG14) and the ubiquitin-like protein (Ubl) system which consists of two Ubl proteins (ATG8 AND AGT12), an activating enzyme namely AGT7, two analogues of ubiquintin-conjugating enzyme (AGT10 and AGT3), Agt8 modifying protease (Agt4) and the protein target of Atg12 attachment (ATG5) and ATG 16 (Figure 1.4) (110). Vesicle nucleation development is dependent on PI3K activity, hVsp34 and the formation of the complex with Beclin 1 (Agt6) and hVps35. Vesicle elongation and completion is dependent on two Ubl systems which is activated by ATG7 and subsequently binds to AGT10 which is transferred to ATG5. ATG5 then forms a multimeric complex (ATG12-ATG5-ATG16) with ATG16. Several ortholoques has been identified in mammalian cells namely MAP1LC3 (LC3), GABARAPL2 (GATE16), GABARAP and GABARAPL1 (ATG8L) (52). LC3 is targeted by post-translational modifications. LC3-I (distributed in the cytoplasm) is converted to LC3-II by a series of reactions catalyzed by Apg7 and Apg3 (117). Furthermore, LC3 competes with LC3-I to bind to phosphatidylethanolamine (PE) to form LC3II on the autophagosome surface (Figure 1.4) (108, 117). Enhancement of LC3-I conversion to LC3-II results in the upregulation of autophagy. Thus, detection of LC3-II is a useful indication for the presence of autophagy (118).

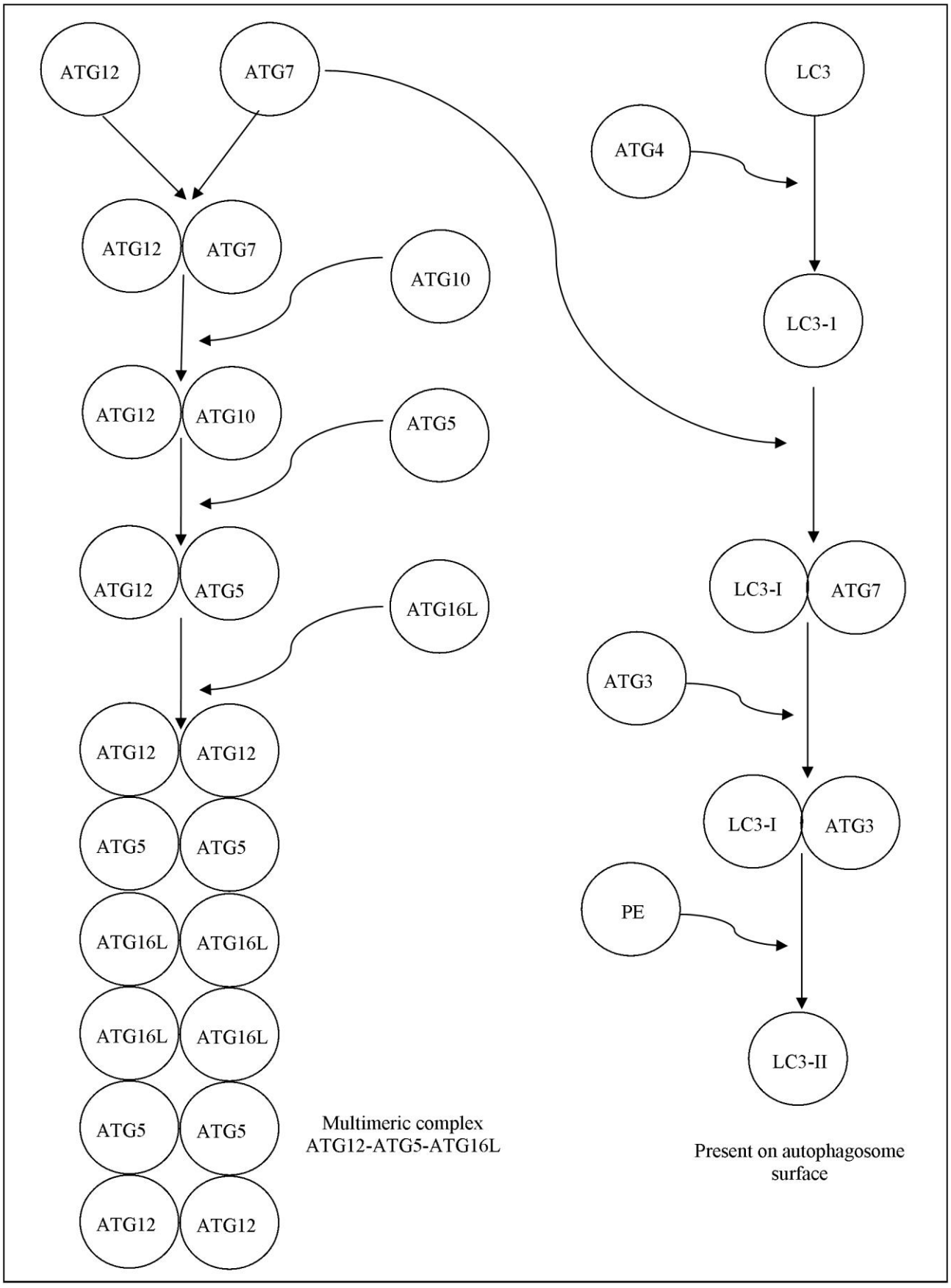
ATG12
ATG7
ATG12
ATG7
ATG10
ATG12
ATG10
ATG5
ATG12
ATG5
ATG16L
ATG12
ATG12
ATG5
ATG5
ATG16L
ATG16L
ATG16L
ATG16L
ATG5
ATG5
ATG12
ATG12
Multimeric complex
ATG12-ATG5-ATG16L
LC3
ATG4
LC3-1
LC3-I
ATG7
ATG3
LC3-I
ATG3
PE
LC3-II
Present on autophagosome
surface

Figure 1.4: Elongation and completion of macroautophagy is dependent on the interaction between several components and genes. ATG12 interacts with ATG7, ATG5 and ATG16L to form a multimeric complex consisting of ATG12-ATG5-ATG16L. LC3-II is formed by several steps including LC3 interacting with ATG4, LC3-1 binds to ATG7 and ATG3 and lastly with PE to form LC3-II on the autophagosome surface.

Autophagy is regulated by negative feedback as the final product namely, amino acids, acts as a negative feedback regulator (119). Furthermore, inhibition of serine/threonine kinase mTOR (mammalian target of rapamycin) that contains ULK1/2 induces autophagy, even in the presence of amino acids. mTOR is an upstream mediator of amino acid-dependent suppression of autophagy (119). Inhibition of mTOR-induced phosphorylation of ULK and ATG13 liberates the kinase activity of ULK (120, 121). Furthermore, mTOR acts as the main kinase for two multiprotein complexes including mTOR complex 1 and mTOR complex 2 (mTORC1/2). Regulatory-associated protein mTOR complex 1 (RAPTOR) is part of TORC1 and mTORC1 and rapamycin-insensitive companion of mTOR complex 2 (RICTOR) is part of mTORC2. mTORC1 activation results in protein synthesis via RPS6KBI, ribosomal protein S6 kinase polypeptide (SKK1) and EIF4EBP1, eukaryotic translational initiation factor 4E binding protein 1 (4EBP1). It has been reported that mTORC2 activates AKT by phosphorylation and enhances hypoxia-inducible factor 1α (HIF-1α) (108). TORC1 activity regulated by TSC1, TSC2 and LKB1 which blocks mTOR activation by inhibiting small GTPase. AKT regulates mTOR function by phosphorylating and downregulation of TSC2, which in turn inhibits the function of the TSC1–TSC2 complex, enhancing mTOR activation (115).

Beclin 1 is the mammalian homologue of the yeast protein AGT14 (53). Beclin 1 forms a complex with PI3K. Beclin 1 is a haploinsufficient tumour suppressor and inhibited by anti-apoptotic proteins such as the BCL-2 family members (120). Beclin 1 forms a heterodimer that is stabilised by BCL-2 anti-apoptotic members through the BCL-2-homology domain 3 domain (108).This complex is found in the Golgi complex suggesting that it controls autophagy by providing phosphatidyllinositol 3-phosphate to the isolation membranes (119). Another function of Beclin 1 includes the proteolytic processing of procathepsin D from the Golgi apparatus to the lysosomes (120). In addition, MCF7 breast epithelial adenocarcinoma cells that express low levels of Beclin 1 do not demonstrate starvation-induced upregulation of autophagy. Beclin 1-mediated rescue of starvation-induced autophagy in MCF-7 cells is subdued by Bcl-2 and Bcl-X_L expression (120).

1.3.3.3 Microautophagy

Microautophagy refers to the degradation route in which portions of the cytoplasm and certain organelles including peroxisomes and intracellular components including the macromolecules are directly taken up and

internalised into the lysosomal matrix by the invagination of the limiting lysosomal membrane that produces intralysosomal vesicles (121). The lysosomal membrane invaginations is then believed to be pinched off and degraded along with the sequestered cytoplasm and cellular components. Microautophagy degradation contributes to the cytoplasmic degradation in intact cells. Microautophagy does not seem to directly have a necessity for autophagy-related proteins (Atg), although its exact physiological role is not known (122). Dubouloz *et al.* (2005) reported that rapamycin-sensitive mTOR signalling pathways positively regulates cell growth in response to availability of nutrients. mTOR depletion or treatment with rapamycin resulted in cells present in quiescent phase (123). Microautophagy in fungi is used for selective organelle degradation. However, the function of microautophagy in higher eukaryotes remains unknown (113, 124).

1.3.4 Mitotic catastrophe

'Mitotic catastrophe' was originally used to describe the lethal fate of cells forced to go into mitosis prematurely due to upregulation of CDC2 (125). Mitotic catastrophe is defined more broadly as the result of deficient mitotic checkpoints, anti-tubulin drugs or failure of cell arrest before mitosis followed by DNA damage, resulting in severe chromosomal structural abnormalities, segregation and finally cell death (125, 126, 127). In addition, mitotic catastrophe is just another entry point for apoptosis and necrosis (58, 126). Distinct morphological characteristics of mitotic catastrophe include fragmented nucleus, the formation of multinucleated, giant cells containing uncondensed chromosomes and micronucleation (58, 125). Multinucleated cells are the product of two or more nuclei with heterogeneous sizes that is derived from an incomplete separation during cytokinesis. Micronucleation results from evenly distributed chromosomes the daughter nuclei (58).

As previously mentioned the cell cycle consists of different phases including the M phase which consists out of mitosis (prophase, metaphase, anaphase and telophase) and cytokinesis (cytoplasm and cellular contents are divided into the cells) (125). It is the responsibility of the G_2 checkpoint (CDC2 not activated) to arrest the abnormal cell before it enters mitosis as DNA damage results in the release of various agents leading to cell arrest, apoptosis or DNA repair. Nonetheless, if the G_2 checkpoint is defective the damaged cell enters mitosis before the DNA damage can be repaired (70). Damaged mitotic checkpoints and anti-tubulin drugs may result in the unscheduled activation of CDC2 forcing the cell into mitosis (127). Also, mitotic cell fusion with interphase cells results in mitotic catastrophe due to the premature entry in mitosis and incomplete S and G_2. Furthermore, the G_2 checkpoint also involves ATR, CHK1 and WAF1 that leads DNA damaged cells to mitotic catastrophe (95). Cells that have damaged spindle checkpoints result in a 'wait anaphase' message being forwarded to the anaphase promoting complex (128).

Mitotic catastrophe is a highly conserved stress response that the cell experiences when damaging agents disrupt the mitotic spindle. For example, paclixatel exposure results in abnormal metaphase where the sister chromatids do not segregate properly. CDC2 activation is prolonged and mitotic catastrophe is induced (102).

1.3.5 Metabolic catastrophe

Tumorigenic cells have altered metabolic systems characterised by the increased glycolysis and glucose uptake. Several tumour cells *in vivo* and *in vitro* displayed an unusual high rate of glucose consumption accompanied by lactate secretion; known as the Warburg effect (129). Glycolysis is an essential cellular process where glucose is catalyzed to form pyruvate and 2 ATP molecules. In non-tumorigenic cells pyruvate is converted to acetyl coenzyme A that enters the citric acid cycle and the product undergoes oxidative phosphorylation. However, in cancer cells pyruvate is converted to lactate. Tumour hypoxia and hypoxia-inducible factor (HIF) activation also undoubtedly plays a role in tumorigenesis, angiogenesis and higher glycolysis levels (130). HIFs play a dual role in tumor growth by enabling both cell survival and angiogenesis. Hypoxia-inducible factor 1 (HIF-1) has been implicated in angiogenesis-independent tumor growth in part via effects on glucose metabolism and biosynthetic pathways (131). According to Rankin *et al.* (2008) hypoxia is the best-characterised mechanism of HIF activation in tumours since 50-60% of solid tumours contain hypoxic/anoxic tissues that develop as a result of an imbalance between oxygen availability and oxygen consumption. HIF can activate the expression of several pro-angiogenic genes including vascular endothelial growth factor (VEGF), plasminogen activator inhibitor-1 (PAI-1), angiopoietins (ANG-1 and -2), Platelet-derived growth factor B (PDGF-B) and matrix Metaloproteinases (MMP-2 and -9) (132). Various genes that play a role in glucose uptake and glycolysis are HIF-1 target genes. This results in increased lactate production and an increase in the acidotic environment from the enhanced anaerobic glycolysis (133). The genes controlling glucose metabolism is modulated by peroxisome proliferators-activator receptors (PPAR). During starvation conditions PPAR and AMP-dependent protein kinase cooperates to induce metabolic catastrophe (134). Increased glycolysis may result in mutations contributing to enhanced cellular proliferation and a hypoxic tumour environment. In addition, signalling pathways enabling uncontrolled cellular proliferation also inhibit autophagy that may lead to genomic instability and enhanced tumour growth (135). Furthermore, constant PI3 kinase pathway activation and induced oxidative metabolism in tumorigenic cells may also lead to metabolic catastrophe (134, 135).

1.3.6 Oncosis

Oncosis is derived from the greek word ‘onco’ which means swelling and was first coined by von Recklinghausen in 1910 (136). The morphological hallmarks of oncosis include cellular swelling, membrane blebbing, vacuolization, protein denaturing and increased membrane permeability with a non-specific DNA fragmentation pattern (136, 137). Oncosis is a passive cell death process induced by severe tissue damage as a result of ischemia, heat or toxic agents with the expression of UCP-2 (136, 138). The molecular signaling pathway of oncosis remains a mystery, although autophagy, apoptosis and oncosis possibly share common signaling pathways in the early cell death pathway. A common stimuli triggers cell death and may follow apoptosis, autophagy or oncosis pathways depending on the energy and magnitude of the cell (139). Furthermore, oncosis evolves to necrosis within 24h (136). The most popular proposed mechanism responsible for oncosis refers to failure of ion pumps of the plasma membrane and decreased ATP levels (136, 140).

1.3.7 Necrosis

Necrosis refers to the energy-independent passive degradation process accompanied with cellular changes the cell undergoes after the cell death (141, 142). The morphological characteristics of necrosis includes cellular swelling, karyolysis, pyknosis, karyorrhexis, disruption of the cell membrane, minor cytoplasmic vacuoles, formation of cytoplasmic blebs, swollen or disrupted mitochondria, ribosome detachment, disrupted organelle membranes and swollen or disrupted lysosomes. Disruption of the cell membrane results in release of cellular constituents into the surrounding environment (56, 74). The latter sends chemotatic signals resulting in inflammation and cytokine release (70, 143). It has been reported that necrosis involves death domain receptors, Toll-like receptors, CA^{2+}, ceramide and the C-Jun N-terminal kinase (JNK)/p38 pathway and TNF-R1 via the RIP-dependent pathway (70, 144). Furthermore, disturbances of pH balance, ion transport and energy production can also result necrosis (70).

1.3.8 Reactive oxygen species and cell death

Reactive oxygen species (ROS) are ions or molecules generated from incomplete one-electron reduction of oxygen (145). ROS are produced by the mitochondrial electron transport chain, arachidonic acid metabolizing enzymes, lipoxygenase and cyclooxygenase, cytochrome P450, xanthine oxidase, NAD(P)H oxidases, uncoupled nitiric oxide synthase (NOS), peroxidase and hemoproteins. Reactive oxygen species include hydrogen peroxide, superoxide, singlet oxygen, hydroxyl radicals, hypocholorous acid and nitric oxide (146).

Furthermore, ROS are produced as a normal by-product of cellular metabolism and function including signaling transduction involved in proliferation, senescence, apoptosis, necrosis and autophagy (147, 148). Under standard physiological conditions, the production and elimination of ROS is maintained. As ROS is dangerous and potentially extremely dangerous it must be eliminated by superoxide dismutase, peroxidases and redox molecules (149). Superoxide is derived from the reduction of oxygen. The latter can be converted to various other ROS (148). Superoxide is constantly being produced by the mitochondria by means of cellular metabolism (149). Superoxide can be catalyzed by superoxide dismutase to produce hydrogen peroxide. Hydrogen peroxide can generate hydroxyl radicals in the presence of transitional metals (148). As superoxide is produced by the mitochondria and various ROS can be produced from the superoxide, the mitochondria are considered the major source of ROS production (149). In addition, ROS is involved in various pathological conditions as increased ROS results in oxidative stress that leads to damage of nucleic acid, proteins and lipids. The latter results in chromosomal instability, mutations and membrane damage leading to cancer. ROS produces in the redox cycle also has been reported to contribute to p53 mutations (G-toT transversions) (148).

ROS production is regulated by Ras on the transcriptional level. When GATA binding protein 6 (GATA-6) is phosphorylated at the serine residue by MEK-activated extracellular signal-regulated kinase (ERK), GATA-6 DNA binding is facilitated. An site-directed mutation (PYA (120) P to PYA (120)P) of GATA-6 eliminates the trans-activation activity which inhibits epithelial colorectal adenocarcinoma cells (CaCo-2). In addition, NOX1 (homolog of the catalytic subunit of the superoxide-generating NADPH oxidase of phagocytes, gp91phox) is required for tumorigenic angiogenesis and transcription is enhanced by means of Ras signaling (148).

Increased ROS production results in the release of cytochrome *c*. Cytochrome *c* binds to apaf-1 in the presence of dATP and ATP. The latter results in the activation of caspase 9 that triggers apoptosis (149). Furthermore, Myc is a transcription factor that regulates the expression of genes that plays a role in cellular proliferation, metabolism and apoptosis. Studies indicated that ROS production resulted in c-Myc activation. However, c-Myc treatment results in decreased ROS production (147).

A low ROS level contributes to the regulation of autophagic cell death (150). Caspase inhibition resulting in autophagic cell death requires ROS accumulation, membrane lipid oxidation and compromised cell membrane integrity (57). ROS plays a central role in starvation-induced autophagy that regulate Agt4 activity. Starvation induces the formation of hydrogen peroxide that directly targets cysteine protease Agt4. The latter contributes to the lipidation of Atg8 that promotes autophagosome formation. In another study, nerve growth factor deprived neurons resulted in ROS accumulation in the mitochondria. This resulted in lipid peroxidation and

loss of mitochondrial lipid cardiolipin leading to autophagy (151). Furthermore TP53-induced glycolysis and apoptosis regulator (TIGAR) inhibits glycolysis and decreases ROS. TIGAR modulates ROS in response to nutrient deprivation and can thus inhibit autophagy induction (146). Induction of ROS production can thus be considered as a potential anticancer therapy.

1.4 Overview of 2-methoxyestradiol-bis-sulphamate

It has been reported that the natural metabolite of estradiol, namely 2-methoxyestradiol (2ME2) exerts antiproliferative, antiangiogenic and antitumor *in vitro* and *in vivo* activity (152). The angiogenic activity is decreased by 2ME2 by affecting invasion through a collagen matrix and decreased tubule formation. 2ME2 has shown potential as an anticancer agent, in particular breast cancer. Inhibition of proliferation results mainly from the induction of apoptosis as it appears that 2ME2 targets active proliferating cells and thus quiescent cells are not affected. 2ME2 has a low affinity for estrogen receptors and the antiproliferating effect is independent of the presence of estrogen receptors (152, 153).

2ME2 exposure resulted in the induction of apoptosis in various cell lines including MDA-MB-435s, Ewing's sarcoma cells, MCF-7, osteolytic breast cancer tumour cells, leukaemia cells, non-small cell carcinoma (154, 155, 156). 2ME2 induces apoptosis in cultured arterial endothelial cells in a time- and concentration-dependent manner, and the migration of these vascular endothelial cells is also inhibited *in vitro*. Administration of this estradiol metabolite to animals strongly inhibits angiogenesis *in vivo.* The strong antiangiogenic effect of 2ME2 and its potent cytostatic effect on the growth of cultured tumour cells may both contribute to the inhibitory effect of 2ME2 on tumour growth in animal models (157).

2ME2 induces change in various proteins that play a role in cell cycle progression and these changes usually culminate in apoptosis (152, 158). Target proteins include co-factors of DNA replication and repair, proliferating cell nuclear antigen (PCNA), cell division cycle kinases and regulators (p34 and cyclin B), transcription factor modulators and upregulation of death receptor 5 (DR5). Increased expression of wild type p53 and inhibiting tubulin polymerization result in apoptosis (152, 158). 2ME2 activates both the intrinsic and extrinsic apoptotic pathways. Increased reactive oxygen species generation and caspase-dependent and caspase-independent mechanisms are involved in 2ME2-mediated apoptosis (159).

Although, 2ME2 has been reported to exert antitumor activities; literature from previous studies implies that effects of 2ME2 are biphasic and dose-and cell line-dependent (160, 161, 162). Phase II clinical trials for 2ME2 (Panzem^{TM}) have been conducted for multiple myeloma (163), ovarian cancer (164) and glioblastoma multiforme (165), breast cancer and prostate cancer (166).

However, due to low oral bioavailability and fast metabolic degradation several promising analogues of 2ME2 have been developed in recent years. 2-MeOE2bisMATE is a bis-sulphamoylated derivative of 2ME2 with antiproliferative activity and inhibits steroid sulphatase (STS) activity (167, 168). Other promising analogues include methylcoumarin-sulphamate (667 Coumate), 2-methoxyestradiol-sulphamate (2-MeOE2MATE) and STX213 (a second-generation steroid sulfatase inhibitor). All these compounds are potent STS inhibitors (169, 170). In addition 667 Coumate has weak aromatase abilities and is in Phase I clinical trials for postmenopausal women with advanced or metastatic breast cancer (166). 2-MeOE2MATE exerts antiproliferative-and antiangiogenic activity and induces a G_2M block (170). In addition, STX213 inhibit the proliferation of ER positive/ER negative breast cancer cells *in vitro* and to cause regression of nitrosomethylurea (NMU)-induced mammary tumours in rodents (169).

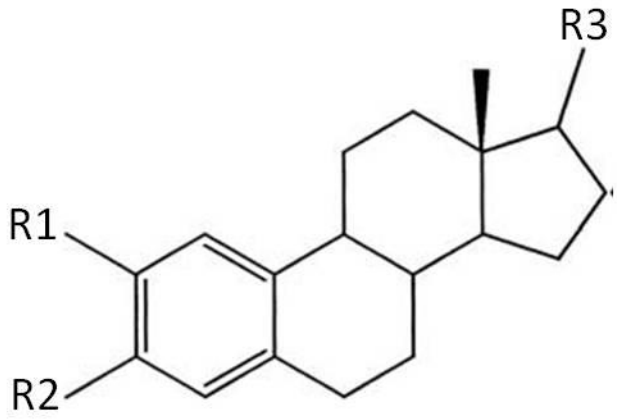

Compound	R1	R2	R3
2-Methoxyestradiol	-OCH3	-OH	-OH
Compound 14	-CH4	-OSO2NH2	-OSO2NH2
Compound 16	-CH4	-OSO2NH2	-OH

Figure 1.5: Structural differences between 2ME2 and 2-MeOE2bisMATE are illustrated.

Previous reports indicate that the novel 2-MeOE2bisMATE is tenfold more potent than 2ME2 with increased bioavailability and a superior pharmacokinetic profile due to its ability to bind to carbonic anhydrase II in red blood cells (167,171). Leese *et al*. cocrystalized 2-MeOE2bisMATE with carbonic anhydrase II (CA II) and determined that the 17-*O*-sulphamate moiety is needed to bind to the catalytic zinc ion of CA II. Carbonic anhydrases (CAs) are ubiquitous zinc metalloenzymes present in vertebrates regulating the acid/base homeostasis by controlling the CO_2/bicarbonate ratio. Various cancer cells are known to have a high rate of aerobic glycolysis and this in turn contributes to the upregulation of lactic acid coinciding with a drop in pH in

the immediate environment of the hyper proliferative neoplastic cells (171). The acidotic environment contributes to metastatic processes associated with malignant cancers. Two membrane bound CA isozymes (IX and XII) are overexpressed in many tumors and contribute to the adaptation of tumorigenic cells in an acidotic environment. Both these isoenzymes are thus targets for drug design that could be specifically targeted towards malignant cancer phenotypes with an abrogated acid/base homeostasis. The binding affinity of towards these tumor-associated CAs is unknown at present, however for CA-binding drugs to be effective, they need to have a higher binding-affinity towards tumor-associated CAs (171). Other reports indicate that the increased potency of 2-MeOE2bisMATE is due to the sulphamate group that is added to the original 2ME2 molecule (23). 2-MeOE2bisMATE is a potent inhibitor of STS activity (172). It has been reported that 2-MeOE2bisMATE inhibits proliferation of estrogen receptor positive- and negative breast cancer cell lines. This indicates a STS independent action mechanism.

In silico modeling suggests that 2ME2 and 2-MeOE2bisMATE share a common tubulin binding mode and the principle mechanism of action of 2-MeOE2bisMATE is believed to be derived from its ability to disrupt microtubule dynamics. Disruption of microtubule dynamics results in a G_2M block in MCF-7 cells (estrogen receptor positive human breast adenocarcinoma cell line), the MCF-7 $_{DOX}$40 cells (drug resistant human adenocarcinoma cell line), fibroblasts and the MDA-MB-231 cells (highly tumorigenic breast carcinoma cell line) (176, 177, 178, 179, 180, 181, 182, 183). Furthermore, apoptosis induction in the CAL51 breast adenocarcinoma cells by 2-MeOE2bisMATE is dependent on caspase activaton (178). The induction of apoptosis is supported in previous data and literature studies where 2-MeOE2bisMATE induced apoptosis in MCF-7, MDA-MB, PC-3 (prostate cancer cells), HUVEC (human umbilical vein endothelial cell), MCF-7_{DOX}, MCF-7_{WT} and the CAL51 cell line (178, 179, 180, 181).

Due to its antiproliferative activity, STS inhibiting activity, 2-MeOE2bisMATE holds therapeutic promise anticancer agent (179). The effects of 2-MeOE2bisMATE on tumorigenic and non-tumorigenic cell lines remain unclear and warrant further investigation. This project investigated the *in vitro* effects on an adenocarcinoma cell line and a non-tumorigenic epithelial breast cell line. This project contributed to the embedded scientific knowledge regarding the unravelling of the signal transduction of 2-MeOE2bisMATE in tumorigenic and non-tumorigenic cell lines.

1.5 Relevance and aim of study

This research project is regarded as a preclinical *in vitro* study and data cannot directly be extrapolated to an *in vivo* environment. Scientific information gained from this study contributed to the knowledge of the differential influences of 2-MeOE2bisMATE on tumorigenic and non-tumorigenic cell lines.

The aim of this study was to investigate and compare the signaling transduction mechanism of 2-MeOE2bisMATE in tumorigenic MCF-7 and non-tumorigenic MCF-12A cell lines by:

a) performing time- and dose dependent growth studies in order to determine the effect of 2-MeOE2bisMATE on cell numbers.
b) determining the effects of 2-MeOE2bisMATE on lactate dehydrogenase production as an indicator of cell membrane integrity.
c) studying morphological changes induced by 2-MeOE2bisMATE in MCF-12A and MCF-7 cell lines with haematoxylin and eosin staining, Hoechst 33342, acridine orange and propidium iodide triple fluorescent staining and transmission electron microscopy techniques.
d) determining the influence of 2-MeOE2bisMATE on reactive oxygen species production.
e) investigating the effects that 2-MeOE2bisMATE exerts on cell cycle progression, apoptosis and autophagy.

Chapter 2

Materials and methods

2.1 Cell lines

The MCF-12A cell line is a non-tumorigenic spontaneously immortalized adherent human breast epithelial cell line and forms domes in confluent cultures. The MCF-12A cells were a gift from Professor Parker (Department of Medical Biochemistry, University of Cape Town, South Africa).

MCF-7 is a tumorigenic adherent breast epithelial cell line and was derived from metastatic sites in adenocarcinoma. MCF-7 cells were supplied by Highveld Biological (Pty) Ltd. (Sandringham, South Africa).

2.2 General cell culture maintenance procedure

2.2.1 Materials

Dulbecco's minimum essential medium eagle (DMEM), Trypsin-EDTA and crystal violet were supplied by Sigma Chemical Co. (St. Louis, MO, USA). Heat-inactivated fetal calf serum (FCS), sterile cell culture flasks and plates were acquired through Sterilab Services (Kempton Park, Johannesburg, South Africa). Penicillin, streptomycin and fungizone were obtained from Highveld Biological Pty (Ltd) (Sandringham, SA). All other chemicals of analytical grade were purchased from Sigma Chemical Co. (St. Louis, MO, USA), Southern Cross Biotechnology Pty (Ltd) (Cape Town, SA), Amersham Biosciences Pty (Ltd) (Pittsburgh, PA, USA) and Agilent Technologies Pty (Ltd) (Palo Alto, CA, USA). 2-MeOE2bisMATE was synthesized by Professor Vleggaar from the Department of Chemistry (University of Pretoria, Pretoria, South Africa), since the compound is not commercially available.

2.2.2 General cell culture procedures

Cell were grown and maintained in 25cm^2 sterile tissue culture flasks in a humidified atmosphere at 37°C, 5% CO_2 in a Forma Scientific water-jacketed incubator (Ohio, United States of America). MCF-7 cells were cultured in DMEM and supplemented with 10% heat-inactivated FCS (56°C, 30min), 100U/ml penicillin G, 100µg/ml streptomycin and fungizone (250µg/l). MCF-12A maintenance medium consisted of a 1:1 mixture of DMEM and Ham's-F12 medium, 20ng/ml epidermal growth factor, 100ng/ml cholera toxin, 10µg/ml

insulin and 500ng/ml hydrocortisone, supplemented with 10% heat-inactivated FCS (56°C, 30min), 100U/ml penicillin G, 100µg/ml streptomycin and fungizone (250µg/l).

Phosphate buffered saline (PBS) was prepared by diluting a ten times concentrated solution consisting of 80g/l NaCl, 2g/l KCl, 2g/l KH_2PO_4 and 11.5g/l Na_2HPO_4 (purchased from Merck (Munich, Germany)) to a 1 times concentrated solution. Diluted PBS solution was autoclaved (20min, 120°C, 15psi) before use (Sterilizer Technologies CC, South Africa).

Growth medium was replaced at one to three day intervals. When confluent, cells were trypsinized by removing growth medium, washing with sterile PBS and incubating in trypsin/versene for approximately 25min or when the cells appeared round and easily detached. The tissue culture flask was gently tapped against the hand in order to detach the cells. Fresh medium was added to the detached cells and was either divided into subcultures, used in experiments or frozen away in cryotubes at -70°C in a freezer. Freeze medium consists of 10% growth media, 10% dimethyl sulphoxide (DMSO) and 80% FCS.

Aseptic techniques were applied throughout, with all work being conducted in a laminar flow cabinet from Labotec (Midrand, South Africa). Solutions were filtered-sterilized (0.22µm pore size) and all glassware and non-sterile equipment were sterilized by autoclaving (20min, 120°C, 15psi).

2.2.3.2 General methods for experiments

For experiments, cells were seeded in a 96-well (5 000 cells per well) tissue culture plates, on heat-sterilized coverslips in 6-well culture plates (350 000 cells per well) or in 25cm^2 tissue culture flasks (500 000 cells per flask). Cells were incubated for 24h to allow for attachment after which medium was removed and cells were exposed to 2-MeOe2bisMATE at appropriate concentrations. A stock solution of $2x10^{-3}$M 2-MeOE2bisMATE dissolved in DMSO was prepared and diluted with medium to the desired concentrations prior to exposure of the cells. Media of all control experiments were supplemented with an equal volume of DMSO (vehicle). The DMSO content of the final dilutions never exceeded 0.05% (v/v). A 24h incubation period at 37^oC was allowed for cell adherence, medium was discarded and cells were exposed to 2-MeOE2bisMATE with concentrations ranging from 0.2-1µM including vehicle-treated controls and incubated for 48h at 37^oC. These conditions were selected since previous studies in our laboratory have demonstrated successful antiproliferative activity in tumorigenic cell lines within this [0.2-1µM] series. Sample controls for apoptosis- and autophagy were also included. Controls for apoptosis comprised of cells exposed to actinomycin D with a concentration of 0.1µg/ml in growth medium for 48h. Controls for autophagy consisted of cells that were starved (1:3 ratio relative to growth medium: phosphate buffered saline

(PBS)). Cells were harvested by tripsinization as described above and were counted by making use of a haemocytometer (184). 20µl of suspended cells where mixed with 80µl PBS, 20µl of that solution was then resuspended in 20µl Trypan blue to provide a concentration of cells with a dilution factor 10X. Dead cells take up the dye and are consequently stained blue, which is then left uncounted.
The number of viable cells per ml is determined by:

Cells/ml

= Average count of viable cells in corner squares in haemocytometer x dilution factor x 10^4

2.3 Analytical experimental protocols

2.3.1 Polarization-optical transmitted light differential interference contrast

Optical transmitted light differential interference contrast (PlasDIC) is a polarization-optical transmitted light differential interference contrast method. PlasDIC is an improved method for polarization-optical transmitted light differential interference contrast, where, unlike conventional Smith-Nomarski's method, linearly polarized light is only generated after the objective. PlasDIC displays the required phase profile which is relative to the product of the section thickness and the refractive index difference between the environment and the average refractive index of quartz. PlasDIC provides high-quality imaging of individual cells, cell clusters and thick individual cells in plastic cell culture vessels (185).

A) Materials

No additional materials needed.

B) Methods

Exponentially growing MCF-7 and MCF-12A cells were seeded in 96 well tissue culture plates at a cell density of 5 000 cells per well. Cells were incubated at 37°C for 24h to allow for attachment. Images were captured, medium was discarded and cells were exposed to 0.4µM 2-MeOE2BisMATE. Images were also captured after 48h exposure period by the Zeiss Axiovert 2000 microscope (Zeiss, Oberkochen, Germany).

2.3.2 Cell growth

Crystal violet staining

Quantification of fixed monolayer cells were spectrophotometrically determined by employing crystal violet that stains DNA. Staining cell nuclei of fixed cells with crystal violet allows for rapid, accurate and reproducible quantification of cell numbers in cultures grown in 96-well plates (186, 187). Quantification is possible by solubilising the adsorbed dye into a solution of Triton X-100 and determining optical density using spectrophotometry. Absorbance of the dye measured spectrophotometrically at 570nm corresponds to cell numbers. According to Berry *et al.* (1996) crystal violet staining of samples containing an abnormally high proportion (>30%) of stationary binucleated cells will yield higher cell concentrations than trypan blue or Coulter counter methods (188). MCF-7 and MCF-12A cells contain less than 1% stationery binucleated cells and will therefore not lead to anomalous results (189, 190).

A) Materials

Glutaraldehyde, crystal violet and Triton X-100 were purchased from Merck (Munich, Germany).

B) Methods

Exponentially growing MCF-12A cells were seeded in 96 well tissue culture plates at a cell density of 5 000 cells per well. Cells were incubated at 37°C for 24h to allow for attachment. Medium was discarded and cells were exposed to a 0.2-1µM 2-MeOE2bisMATE concentration series for 24h, 48h and 72h respectively 37^{o}C. Appropriate vehicle-treated controls were also included. A baseline was also included, seeded in a separate 96 well plate and cells were stained before exposure to determine the starting number. Cells were fixed with 100µl of 1% gluteraldehyde (incubation for 15min at room temperature). Subsequently, glutaraldehyde was discarded and cells were stained using 100µl 0.1% crystal violet (incubated at room temperature for 30min). The crystal violet solution was discarded and the 96 well plate was submersed under running water. Crystal violet dye was solubilized using 200µl 0.2% Triton X-100 and incubated at room temperature for 30min. 100µl of the solution was transferred to a new microtitre plate. Afterwards, the absorbance was read at 570nm using an EL_x800 Universal Microplate Reader (Bio-Tek Instruments Inc., Vermont, United States of America). It was important to select a dose that would cause antiproliferative activity in tumorigenic cell lines with minimal antiproliferative effects on non-tumorigenic cell lines. Therefore, a concentration was selected with increased susceptibility in tumorigenic cell lines when compared to a non-tumorigenic cell line. The 50% growth inhibitory concentration (IC_{50}) was calculated in an adenocarcinoma cell line (MCF-7) as described by the National Cancer Institute in order to determine the growth inhibition induced by 2-MeOE2bisMATE (191). The IC_{50} that was found in the latter study was incorporated in subsequent studies as described below and differential effects of 2-MeOE2bisMATE on tumorigenic MCF-7 and non-tumorigenic MCF-12A cell lines were investigated.

2.3.3 Cell viability and metabolism

Lactate dehydrogenase assay

Lactate dehydrogenase (LDH) is a soluble cytosolic enzyme that catalyzes the interconversion of lactate and pyruvate. Cells release LDH during injury or cell damage, following the loss of membrane integrity consequential from either apoptosis or necrosis. LDH activity, therefore, can be used as an indicator of cell membrane integrity and serves as a means to assess cytotoxicity resulting from exposure to chemical compounds. Cytotoxicity was determined by measuring the amount of LDH found in the medium after exposure to 2-MeOE2bisMATE. This LDH colorimetric assay is based on the reduction of 3-(4,5-Dimethylthiazol-2-yl)-2,5-diphenyltetrazolium bromide (MTT) in a nicotinamide adenine dinucleotide (NADH)-coupled enzymatic reaction to a reduced form of MTT which exhibits an absorption maximum at 565 nm. The purple colour intensity is directly proportional to the enzyme activity.

A) Materials

Lactate dehydrogenase assay kit was acquired from BIOCOM biotech Pty (Ltd) (Clubview, South Africa).

B) Methods

Cells were seeded in 96 well plates at a cell density of 5 000 cells per well with an overnight attachment policy (incubated at 37°C at 5% CO_2). After 24h, cells were exposed to 2-MeOE2bisMATE and appropriate controls were included. Subsequently, 200µl medium was transferred and centrifuged at 5 000 rpm for 10min. Afterwards, 10µl was transferred to a clear 96 well plate. Subsequently, 100µl of the LDH reaction mix (mixed according to the kit pamphlet instructions) was added to the sample. After 90min incubation at room temperature, the absorbance was read at 460nm, with a reference wavelength of 630nm by means of EL_x800 Universal Microplate Reader (Bio-Tek Instruments Inc., Vermont, United States of America). Various controls were included in the experiment namely background control, low control and high control. The background control consists of growth medium only. The low control refers to cells resuspended in growth medium and the high control to cells resuspended in growth medium with cell lysis solution added to the cells shortly before the experiment was terminated (according to the manufacturer's instructions).

2.3.2 Morphology studies

2.3.2.1 Light microscopy

Haematoxylin and eosin staining

The influence of 2-MeOE2bisMATE on cell morphology was conducted by staining the nucleus and cytoplasm of MCF-7 and MCF-12A with haematoxylin and eosin (H & E) respectively (192).

A) Materials

Bouin's fixative was purchased from Sigma-Aldrich ((St. Louis, United States of America). Haematoxylin, eosin, ethanol, xylol and Entellam® fixative were purchased from Merck (Munich, Germany).

B) Methods

Cells (500 000 per well) were seeded on sterile coverslips in 6 well plates and incubated overnight. Cells were exposed to 0.4µM 2-MeOE2bisMATE for 48h and the appropriate controls were included. Coverslips were transferred to staining dishes and cells were fixed with Bouin's fixative for 30min. Subsequently Bouin's fixative was discarded and 70% ethanol was added for 20min to the coverslips at room temperature before they were rinsed with tap water. Mayer's haematoxylin was added to the coverslips for 20min. Coverslips were rinsed with tap water for 2min. Afterwards 70% ethanol was added to the coverslip followed by 1% eosin for 5min. Eosin was discarded and coverslips were consecutively rinsed twice for 5min with 70%, 96%, 100% and xylol. Coverslips were mounted on microscope slides with resin and left to dry. Photos were taken with a Zeiss Axiovert MRc microscope (Zeiss, Oberkochen, Germany). Mitotic indices were also determined from the haematoxylin and eosin-stained cells. Quantitative data for mitotic indices were obtained by counting 1000 cells on each slide of the biological replicates and expressing data as a percentage of cells in each phase of mitosis, interphase and abnormal cells were also counted. Distinction was made between mitotic cells (prophase, metaphase, anaphase and telophase), cells in interphase and cells that displayed hypercondensed chromatin, membrane blebbing, apoptotic bodies; as well as abnormal chromosome segregation. This H & E staining provided both qualitative and quantitative information.

2.3.2.2 Transmission electron microscopy

Transmission electron microscopy (TEM) was used to determine the ultra structure of intracellular components of exposed and control cells. TEM is an imaging technique whereby a beam of electrons is

focused onto a specimen. The electron beam is partially transmitted through the very thin specimen and carries information about the inner structure of the specimen (193).

A) Materials

Aqueous osmium tetroxide, glutaraldehyde, phosphate buffer quetol, Reynolds' lead citrate, aqueous uranyl acetate were purchased by the Electron Microscopy Unit of the University of Pretoria from Merck Co. (Munich, Germany). The Multi-purpose Philips 301 transmission electron microscope (TEM) (Apollo Scientific SA, Midrand, South Africa) of the Electron Microscopy Unit (University of Pretoria, Pretoria, South Africa) was used for viewing the prepared samples.

B) Methods

Cells were seeded in a 25cm^2 flask at a density of 500 000 cells per flask with an overnight attachment policy. Subsequently, medium was discarded and cells were exposed to 0.4µM 2-MeOE2bisMATE for 48h and appropriate controls were included. After 48h, cells were trypsinized and resuspended in 1ml medium. Cells were fixed with 2.5% glutaraldehyde in 0.075M phosphate buffer for 1h, rinsed thrice with 0.075M phosphate buffer, fixed with osmium tetroxide for 30min, rinsed thrice with distilled water and dehydrated with increasing ethanol concentrations (30%, 50%, 70%, 90%, and 100%). Cells were infiltrated with 50% quetol in ethanol for 1h and then with 100% quetol for 4 to 6h. Ultra-thin sections were prepared using a microtome and contrasted by means of 4% uranyl acetate-staining for 10min and rinsed with water. Images were taken using TEM (Electron Microscopy Unit, University of Pretoria, Pretoria, South Africa).

2.3.2.3 Fluorescent microscopy

Apoptosis, autophagy and necrosis detection

Fluorescent microscopy was employed to differentiate between viable, apoptotic, autophagic and oncotic cells. A triple fluorescent dye staining method was developed utilizing acridine orange (green), Hoechst 33342 (blue) and propidium iodide (red) fluorescent dyes. Acridine orange is a lysosomotropic fluorescent compound that serves as a tracer for acidic vesicular organelles including autophagic vacuoles and lysosomes (194). Cells undergoing autophagy will have an increased tendency for acridine orange staining when compared to viable cells, however acridine orange is not a specific marker for autophagy and therefore other techniques are needed to verify the appearance of increased autophagic activity. Hoechst 33342 is a fluorescent dye that can penetrate intact cell membranes of viable cells and cells undergoing apoptosis and stain the nucleus. Propidium iodide is a fluorescent dye that is unable to penetrate an intact membrane and therefore stains the nucleus of cells that have lost their membrane's integrity due to necrotic processes.

A) Materials

Acridine orange, bisbenzimide (Hoechst 33342) and propidium iodide were purchased from Sigma-Aldrich (St. Louis, United States of America).

B) Methods

Cells (500 000) per well were seeded in 6 well plates and incubated overnight. Afterwards, cells were exposed to 0.4µM 2-MeOE2bisMATE and appropriate controls were included. 0.5ml of Hoechst 33342 solution (3.5µg/ml in phosphate buffered saline (PBS)) was added to the medium to provide a final concentration of 0.9µM and was incubated for 25min at 37°C. Subsequently, 0.5ml of acridine orange solution **(**4µg/ml in PBS) was added to the medium to give a final concentration of 1µg/ml and incubated for 5min at 37°C and 0.5ml of propidium iodide solution (40µg/ml in PBS) was added to the medium to provide a final concentration of 12µM. Cells were washed three times with PBS. Photos were taken with the appropriate filters in a dark room to prevent quenching. Zeiss Axiovert CFL40 microscope and Zeiss Axiovert MRm monochrome camera (Zeiss, Oberkochen, Germany) were used employing a Zeiss filter 2 for Hoechst 33342 stained blue-cells and a Zeiss filter 9 for acridine orange-stained (green) cells and a Zeiss filter 15 for propidium iodide-stained (red) cells.

2.3.3 Flow cytometry

2.3.3.1 Cell cycle progression

Flow cytometry was employed to analyze the influence of 0.4µM 2-MeOE2bisMATE on cell cycle progression of MCF-7 and MCF-12A cells. Analysis was conducted by ethanol fixation and propidium iodide staining of cells. Propidium iodide was used to stain the nucleus in order to determine the amount of DNA present. The latter present correlates with stages of the cell cycle during cell division. In flow cytometry a laser beam of a single frequency is directed onto a hydrodynamically focused stream of fluid. A number of detectors are aimed at the point where the stream passes through the light beam; one in line with the light beam (Forward Scatter (FSC)) and several perpendicular to it Side Scatter (SSC) and one or more fluorescent detectors. Each suspended particle passing through the beam scatters the light. Fluorescent chemicals in the particle may be excited into emitting light at a lower frequency than the light source. This combination of scattered and fluorescent light is detected by the detectors. By analyzing fluctuations in brightness at each detector (one for each fluorescent emission peak) it is possible to deduce the size, quantity and fluorescent intensity (DNA content when stained with propidium iodide) of cells. FSC correlates with cell volume and SSC depends on inner complexity of the particle *e.g.* amount of DNA, shape of nucleus, etc.

A) Materials

99.9% ethanol was from Merck Co. (Munich, Germany). Propidium iodide was purchased from Sigma-Aldrich (St. Louis, United States of America).

B) Methods

Exponentially growing MCF-7 and MCF-12A cells were seeded at 500 000 cells per 25cm^2 flask. After 24h attachment medium was discarded and cells were exposed to 0.4µM 2-MeOE2bisMATE and incubated for 48h. Cells were trypsinized and resuspended in 1ml growth medium. 1x10^6 cells were centrifuged for 5min at 300 x g. The supernatant was discarded and cells were resuspended in 200µl of ice-cold PBS containing 0.1% FCS. 4ml of ice-cold 70% ethanol was added in a drop wise manner and cells were stored at 4ºC for 24h. After 24h, the cells were pelleted by centrifuging them at 300 x g for 5min. The supernatant was removed and cells were resuspended in 1ml of PBS containing propidium iodide (40µg/ml) and incubated at 37ºC, 5% CO_2, for 45min.

Propidium iodide fluorescence (relative DNA content per cell) was measured with a fluorescence activated cell sorting (FACS) FC500 System flow cytometer (Beckman Coulter South Africa (Pty) Ltd) equipped with an air-cooled argon laser excited at 488nm. Data from at least 10 000 cells were analyzed with CXP software (Beckman Coulter South Africa (Pty) Ltd). Data from cell debris (particles smaller than apoptotic bodies) and clumps of 2 or more cells were removed from further analysis. Cell cycle distributions were calculated with Cyflogic 1.2.1 released 2008/11/19 (Perttu Terho & Cyflo Ltd) by assigning relative DNA content per cell to sub-G_1, G_1, S and G_2M fractions. Propidium iodide molecules emit light at 617nm therefore, data obtained from the log forward scatter detector nr 3 (FL3 log, detects 600nm emissions) was represented as histograms on the *x*-axis.

2.3.3.2 Apoptosis detection analysis

Annexin V-FITC

Flow cytometry was employed to analyse apoptosis in MCF-7 and MCF-12A cells. Cells were stained with Annexin V and propidium iodide. One of the earliest indications of apoptosis is the externalization of the membrane phospholipid phosphatidylserine (PS) layer of the plasma membrane. Once exposed to the extracellular environment, binding sites on PS become available for Annexin V, a 35-36 kDa, Ca^{2+}-dependent, phospholipid binding protein with a high affinity for PS. Annexin V is conjugated to a fluorochrome, fluorescein isothiocyanate (FITC) and used for identification by flow cytometry for stages of apoptosis. Propidium iodide is used to distinguish between necrotic and apoptotic cells.

A) Materials

Annexin V-FITC Kit was purchased from BIOCOM biotech Pty (Ltd) (Clubview, South Africa).

B) Methods

Exponentially growing MCF-7 and MCF-12A cells were seeded at 500 000 cells per 25cm^2 flask. After 24h attachment the medium was discarded, cells were exposed to 0.4µM 2-MeOE2bisMATE and incubated for 48h. Cells were trypsinized, 10^6 cells were resuspended in 1ml of 1x Binding Buffer and centrifuged at 300 x g for 10min. The supernatant was removed and cells were resupended in 100µL of 1x Binding Buffer. 10µl of Annexin V-FITC was added and samples were incubated for 15min in the dark at room temperature. After 15min, cells were washed by adding 1ml of 1x Binding Buffer and centrifuged at 300 x g for 10min. The supernatant was carefully pipetted off and cells were resuspended in 500µl of 1x Binding Buffer solution. Immediately prior to analysis, 5µl of propidium iodide (100µg/ml) was added and gently mixed.

Propidium iodide fluorescence (oncotic cells) and annexin V fluorescence (apoptotic cells) were measured with a fluorescence activated cell sorting (FACS) FC500 System flow cytometer (Beckman Coulter South Africa (Pty) Ltd) equipped with an air-cooled argon laser excited at 488nm. Data from at least 30 000 cells were analyzed with CXP software (Beckman Coulter South Africa (Pty) Ltd). Data from cell debris (particles smaller than apoptotic bodies) and clumps of 2 or more cells were removed from further analysis. Propidium iodide molecules emit light at 617nm and FITC emit at 530nm therefore, data obtained from the log forward scatter detector nr 1 (Fl Lin, detects 515-545nm emissions) and the log forward scatter detector nr 3 (Fl3 Lin, detects 600nm emissions) were represented as a single dot-plot. FL3 log (propidium iodide) was represented on the *x*-axis and FL1 log (FITC) was represented on the *y*-axis. The FL3 log/FL1 log dot-plot was divided into for quadrants. The bottom-left quadrant was assigned to measure the viable cells with minimal propidium iodide and FITC staining. Medium only control MCF-7 cells were calibrated to include 98% of cells within the viable cell quadrant. MCF-12A cells have a higher rate of apoptosis than MCF-7 cells therefore, the medium only control MCF-12A cells were calibrated to include 96% of cells within the viable cell quadrant. The top left quadrant was assigned to cells in the early stages of apoptosis, the bottom-right quadrant was assigned to cells undergoing oncosis and the top-right quadrant was assigned to cells in the late stages of apoptosis which have become necrotic. Distributions of cells within the quadrants were calculated with Cyflogic 1.2.1 released 2008/11/19 (Perttu Terho & Cyflo Ltd).

2.3.3.3 Detection of changes in mitochondria membrane potential

Mitocapture mitochondrial kit

The mitocapture mitochondrial kit provided quantitive apoptosis information. The reduction of the mitochondrial membrane potential is an early feature during apoptosis due to loss of the electrochemical gradient across the mitochondrial membrane. A unique cationic dye, 5,5',6,6'-tetrachloro-1,1',3,3'-tetraethylbenzimidazolylcarbocyanine iodide was used to detect loss of the mitochondrial membrane potential. In healthy cells, the dye concentrates in the mitochondrial matrix to form red fluorescent aggregates. In any event that reduces the mitochondrial potential, such as apoptosis induced by 2-MeOE2bisMATE, the dye remains in the cytoplasm in a green fluorescent monomeric form. Intensity of fluorescence in cells was measured by flow cytometry analysis.

A) Materials

MitoCaptureTM Mitochondrial Apoptosis Detection Kit was purchased from BIOCOM biotech Pty (Ltd) (Clubview, South Africa).

B) Methods

Exponentially growing MCF-7 and MCF-12A cells were seeded at 500 000 cells per 25cm^2 flask. After 24h of attachment, medium was discarded, cells were exposed to 0.4µM 2-MeOE2bisMATE and incubated for 48h. Cells were trypsinized and centrifuged at 13 000 x g. 500 000 cells were resuspended in 1ml of diluted Mitocapture solution (1µl mitocapture: 1ml pre-warmed incubation buffer). Cells were incubated at 37°C, 5% CO_2 for 20min and centrifuged thereafter at 500 x g. After the supernatant was discarded, cells were resuspended in 1ml of prewarmed incubation buffer at 37°C. Cells were analyzed immediately after following the above-mentioned step using fluorescence activated cell sorting (FACS) FC500 System flow cytometer (Beckman Coulter South Africa (Pty) Ltd). Apoptotic cells were detected in the FITC channel (usually FL1) showing diffused green fluorescence. Healthy cells were detectable in the PI channel (usually FL2) showing punctuate red fluorescence.

2.3.3.4 Autophagy detection

Rabbit polyclonal anti-LC3B conjugated to DyLight 488

There are 16 proteins participating in the autophagy pathway in humans. The autophagy protein LC3, a mammalian homologue of Atg8, was initially identified as microtubule-associated protein 1 light chain 3. LC3 is the only recognized mammalian protein identified that stably associates with the autophagosome membranes. LC3-I is cytosolic; furthermore, the LC3-II is membrane bound and enriched in the autophagic vacuole fraction. The detection of the conversion of LC3-I to LC3-II is a useful and sensitive marker for identifying autophagy in mammalian cells. LC3B antibody allowed for autophagy detection and confirmation (results provided by light microscopy and Hoechst 33342, propidium iodide and acridine orange staining) in mammalian cells during fluorescence microscopy by binding to the autophagosome membrane.

A) Materials

Formaldehyde, methanol, Triton X-100, propidium iodide and bovine serum albumin (BSA) were purchased from Sigma-Aldrich (St. Louis, United States of America). Rabbit polyclonal anti-LC3B conjugated to DyLight 488 was supplied by BIOCOM biotech Pty (Ltd) (Clubview, South Africa).

B) Methods

Exponentially growing MCF-7 and MCF-12A cells were seeded at 500 000 cells per 25cm^2 flask. After 24h attachment the medium was discarded and cells were exposed to 0.4µM 2-MeOE2bisMATE and incubated for 48h. Cells were washed with cold PBS and pelleted. Cells were fixed with 3ml 0.01% formaldehyde in PBS for 10min at 4˚C. Cells were centrifuged and resuspended in 200µl PBS, followed by 1ml ice-cold methanol (-20˚C) for 15min at 4˚C. Afterwards cells were washed twice with cold PBS. Cells were stained with the 0.5ml antibody cocktail (0.05% Triton, 1% BSA, 40µg/ml propidium iodide and 0.5µg/ml conjugated rabbit polyclonal anti-LC3B antibody) prepared in PBS for 2h at 4˚C. Cells were washed trice with PBS/0.05% Triton x-100/1% BSA and analyzed with flow cytometry. Data from at least 10 000 cells were analyzed by means of Cyflogic version 1.2.1 software (Pertu Therho, Turko, Finland).

2.3.3.5 Reactive oxygen species (ROS) detection

Flow cytometry was employed to analyze the influence of 0.4µM 2-MeOE2bisMATE on ROS production in MCF-7 and MCF-12A cells. 2,7-dichlorofluorescein diacetate (DCFDA) is a non-fluorescent probe, which upon oxidation by ROS and peroxides, is converted to the highly fluorescent derivative DCF. The latter was used to detect hydrogen peroxide. Superoxide generation was evaluated using hydroethidine (HE). HE is oxidized by superoxide and not by hydroxyl radicals, superoxide, hydrogen peroxide or nitrogen radicals to a red fluorescing compound.

A) Materials

DCFDA, HE and PBS were acquired from BIOCOM biotech Pty (Ltd) (Clubview, South Africa).

B) Methods

Hydrogen peroxide detection

Exponentially growing MCF-7 and MCF-12A cells were seeded at 500 000 cells per 25cm^2 flask. After 24h of attachment, medium was discarded, cells were exposed to 0.4µM 2-MeOE2bisMATE and incubated for 48h. Cells were trypsined and washed with PBS. After centrifuging, 1000 000 cells were resuspended in 1ml PBS. 1µl DCFDA stock solution (10 mM) was added to the cells and samples were incubated for 25min at 37°C. Cells were analysed using a fluorescence activated cell sorting (FACS) FC500 System flow cytometer (Beckman Coulter South Africa (Pty) Ltd). Data from at least 10 000 cells were analyzed by means of Cyflogic version 1.2.1 software (Pertu Therho, Turko, Finland).

Superoxide detection

Exponentially growing MCF-7 and MCF-12A cells were seeded at 500 000 cells per 25cm^2 flask. After 24h of attachment, medium was discarded and cells were exposed to 0.4µM 2-MeOE2bisMATE and incubated for 48h. Cells were trypsined, thereafter cells were washed with PBS. After centrifuging, 1000 000 cells were resuspended in 1ml PBS. 1µl HE stock solution (10 mM) was added to the cells and samples were incubated for 15min at 37°C. Cells were analysed using a fluorescence activated cell sorting (FACS) FC500 System flow cytometer (Beckman Coulter South Africa (Pty) Ltd). Data from at least 10 000 cells were analyzed by means of Cyflogic version 1.2.1 software (Pertu Therho, Turko, Finland).

2.4 Statistical planning

Qualitative data was supplied by PlasDIC, light microscopy (haematoxylin and eosin staining), transmission electron microscopy and fluorescent microscopy (apoptosis, autophagy and necrosis detection). Quantitative information was gained by means of time- and dose dependent studies (crystal violet staining), cell viability and cytotoxicity assay (lactate dehydrogenase), mitotic indices, apoptosis detection (annexin V-FITC), detection of changes in mitochondrial membrane potential, autophagy detection (anti-LC3B conjugated to DyLight 488) and reactive oxygen species detection. Data obtained from three independent experiments (each conducted in six replicates) are shown as the mean ±SD and data for mitotic indices were obtained by

counting 1000 cells (repeated three times) on each slide of the biological replicates. Data were statistically analysed for significance using the analysis of variance (ANOVA)-single factor model followed by a two-tailed Student's *t*-test. Means are presented in bar charts, with T-bars referring to standard deviations. *P*-values < 0.05 were regarded as statistically significant and are indicated by a star (★). Flow cytometry analysis involved 10 000 events and was repeated thrice.

Chapter 3

Results

3.1 Polarization-optical transmitted light differential interference contrast

The Plasdic system that was developed by Zeiss is a particular design of Köhler-DIC configuration in which a slit in the course of shear is placed symmetrically with respect to the optical axis in the front focal plane (FFP) of the condenser. Therefore, partially coherent transfer function is derived only for Köhler-DIC (195). PlasDIC displays the required phase profile which is relative to the product of the section thickness and the refractive index difference between the environment and the average refractive index of quartz. PlasDIC provides high-quality DIC imaging of individual cells, cell clusters and thick individual cells in plastic cell culture vessels possible for the first time (185). Cells were photographed before exposure, as well as after the 48h exposure period to determine the *in vitro* effects of 2-MeOE2bisMATE on morphology of MCF-7 and MCF-12A cells and to investigate if characteristics of apoptosis and autophagy were present in these cell lines.

PlasDIC photo's taken of MCF-7 cells before exposure revealed no signs of distress. Cells propagated in growth medium and vehicle-treated cells were confluent and displayed no features of distress with the nucleus membrane and nucleoli clearly visible (Figure 3.1 and Figure 3.2). However, 0.4µM 2-MeOE2bisMATE-treated cells revealed a decrease in cell density. Cells were shrunken and several apoptotic bodies were observed. Furthermore, 0.4µM 2-MeOE2bisMATE-treated cells appeared very similar to the apoptosis-induced cells (Figure 3.3).

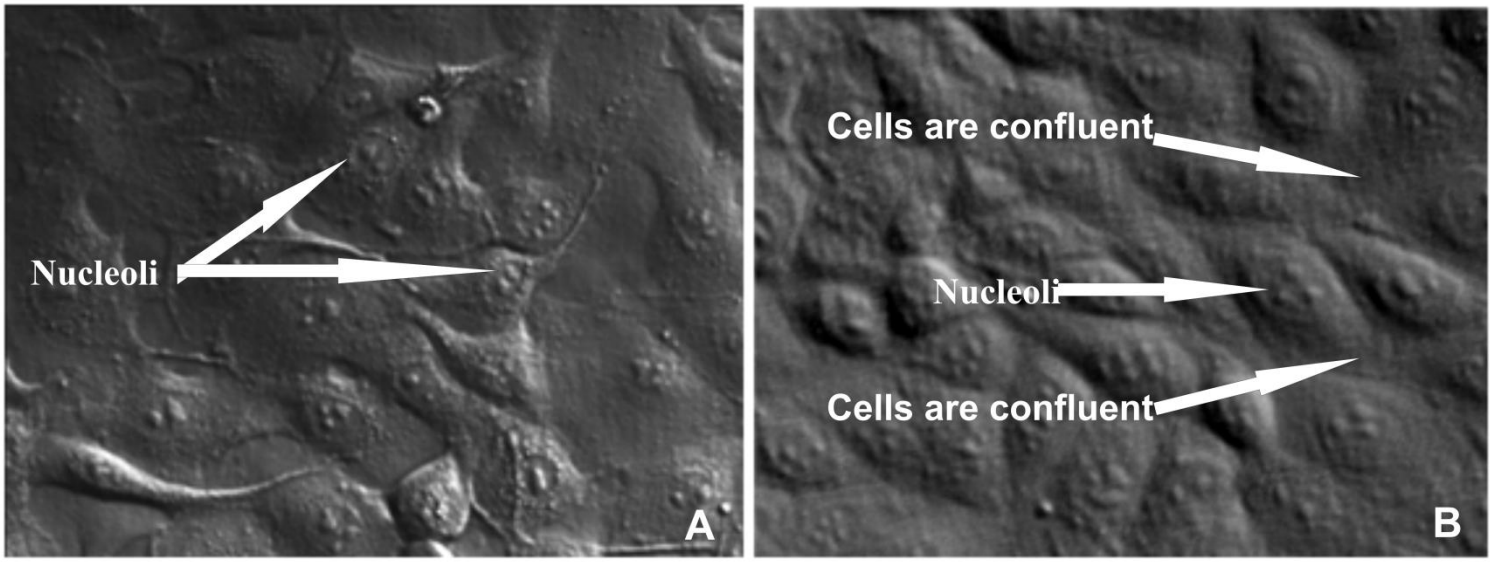

Figure 3.1: PlasDIC MCF-7 photo (A) taken before exposure revealed cells with no signs of distress (40X magnification). PlasDIC photo MCF-7 cells propagated in growth medium after 48h (B). Cells are confluent with nucleoli clearly visible (40X magnification).

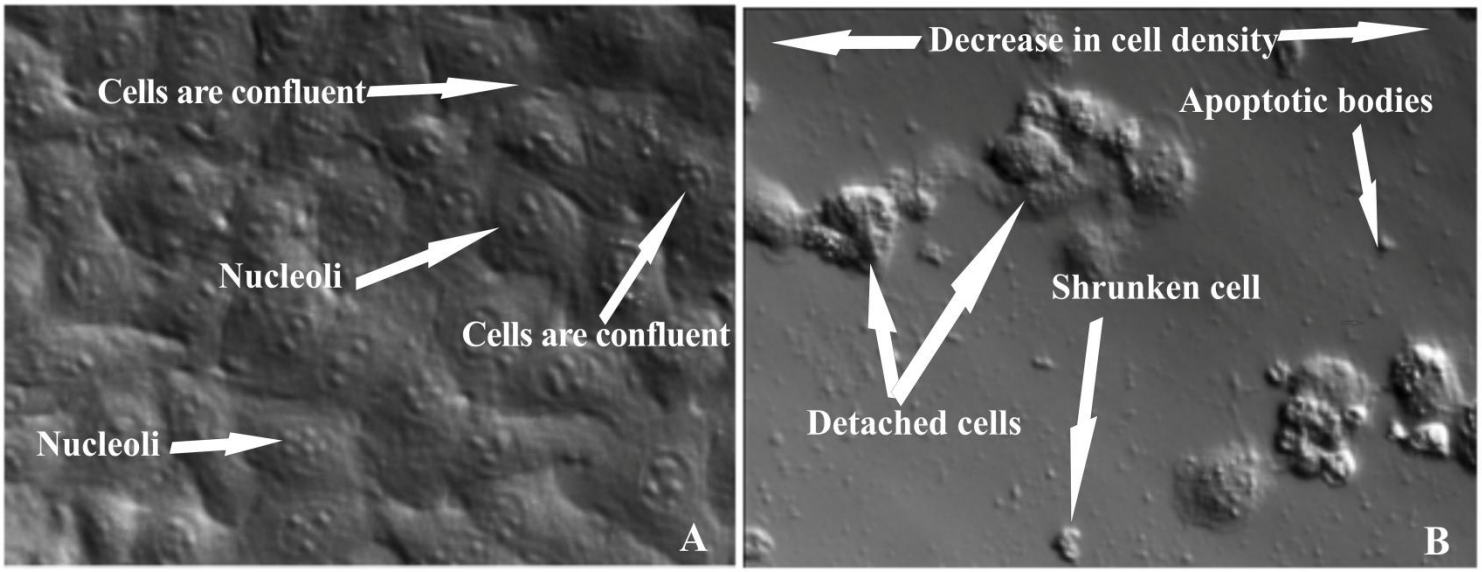

Figure 3.2: Morphology of MCF-7 vehicle-treated cells (A). No morphological effects were observed due to exposure of MCF-7 cells to DMSO. Furthermore, cell density was not affected (40X magnification). PlasDIC revealed a decrease in cell density in the MCF-7 cells treated with 2-MeOE2bisMATE (B) when compared to the vehicle-treated control and to cells propagated in growth medium. 2-MeOE2bisMATE-treated cells were shrunken and detached from the surface. Apoptotic bodies were also observed in the 2-MeOE2bisMATE-treated cells (40X magnification).

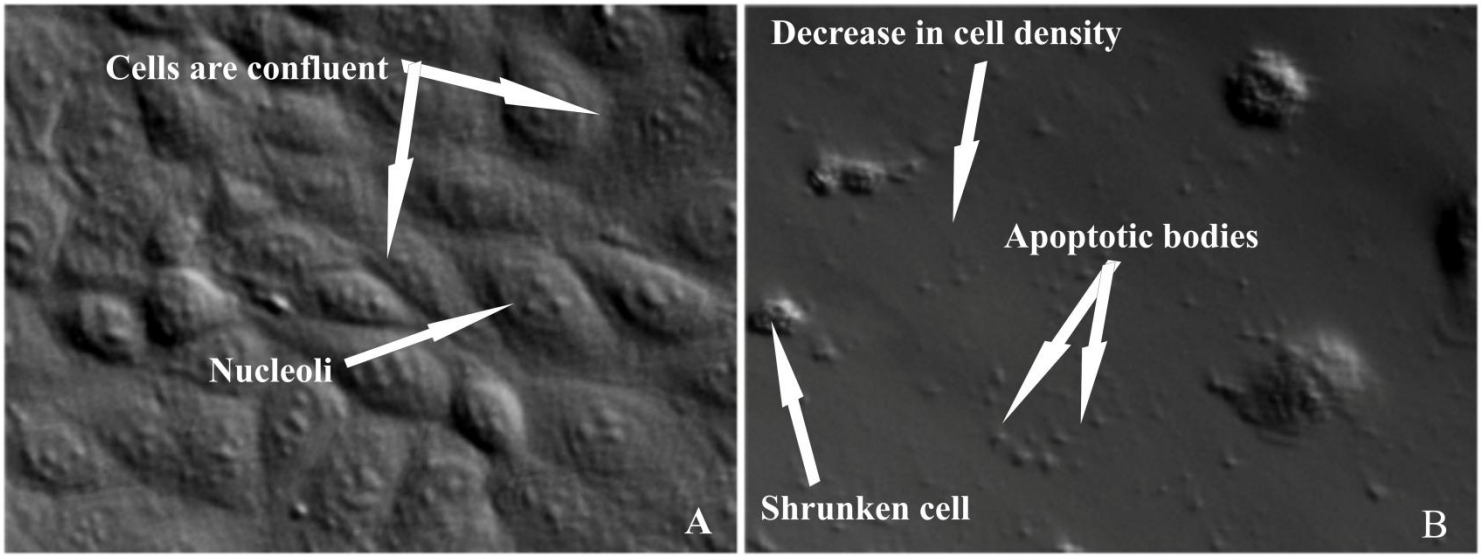

Figure 3.3: MCF-7 cells with induced starvation that as a positive control for induction of autophagy (A). Cells were not displaying any characteristics of distress. The cells depicted in this photo are confluent with the nucleoli clearly detectable (40X magnification). Cells exposed to actinomycin D (0.1µg/ml) as the positive control for inducing apoptosis are illustrated in B. A decrease in cell density was observed when compared to the cells propagated in growth medium and the vehicle-treated cells. Furthermore, cells were shrunken with several apoptotic bodies present (40X magnification).

PlasDIC micrographs taken of MCF-12A cells before exposure revealed healthy viable cells with enough space to proliferate for 48h without risk of contact inhibition (Figure 3.4). MCF-12A cells propagated in growth medium and vehicle-treated cells are confluent presenting with the nucleoli clearly (Figure 3.5). However, MCF-12A 2-MeOE2bisMATE–treated cells revealed the initial rounding of cells when compared to vehicle-treated control cells and cells propagated in growth medium. Cells were still confluent (Figure 3.6). All observed morphological effects were more prominent in the MCF-7 cells when compared to MCF-12A cells.

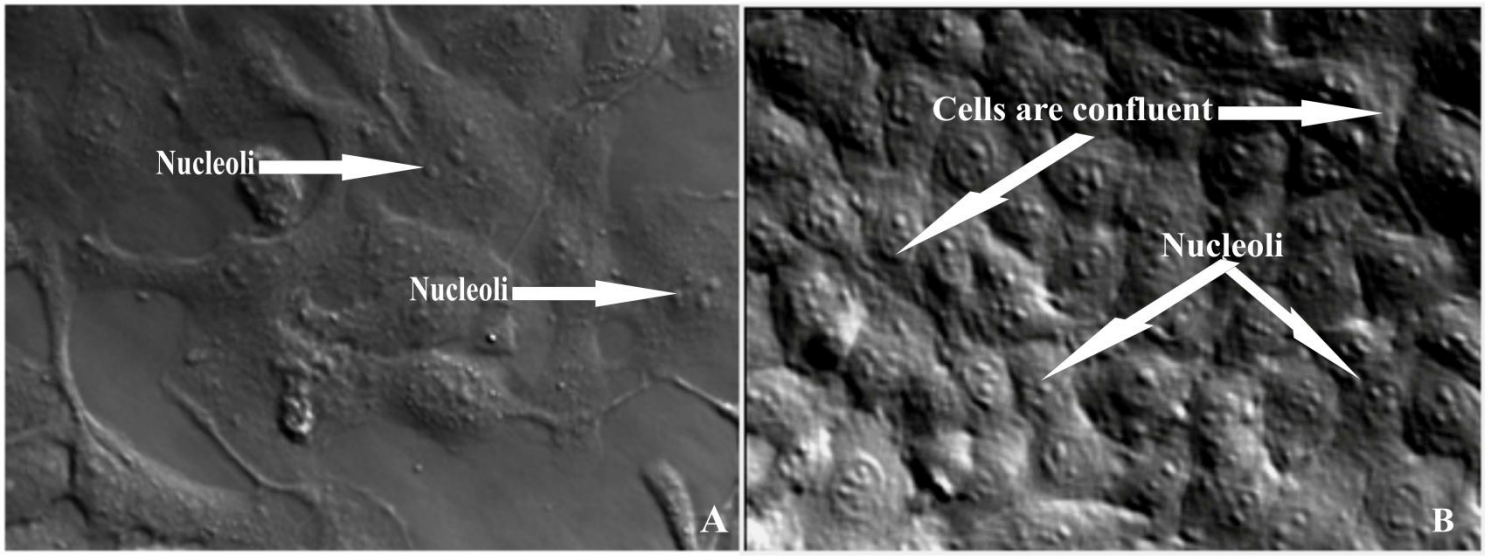

Figure 3.4: PlasDIC photo's of MCF-12A cells (A) taken before exposure and MCF-12A cells (B) propagated in growth medium after 48h of exposure revealed confluent cells with no signs of distress (40X magnification).

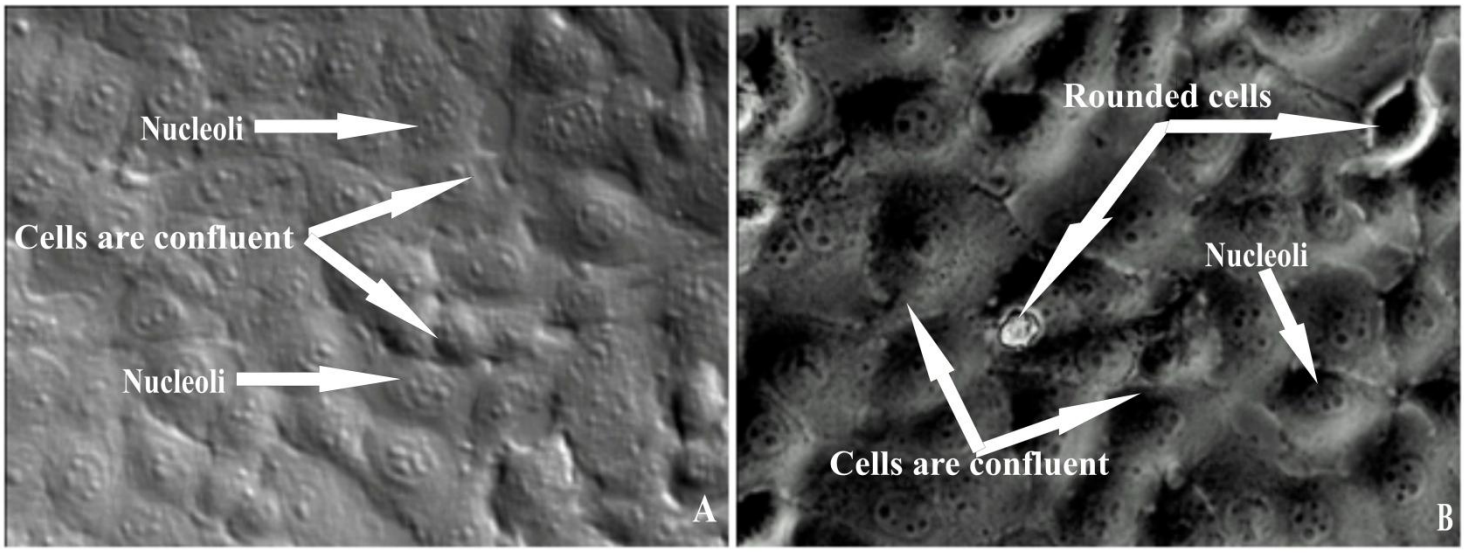

Figure 3.5: MCF-12A vehicle-treated control cells after 48h (A). No morphological effects were observed due to exposure of MCF-7 cells to DMSO with cell density unaffected (40X magnification). PlasDIC of MCF-12A 2-MeOE2bisMATE–treated cells revealed the rounding of cells when compared to vehicle-treated cells and cells propagated in growth medium (B). The cell density was not affected by 2-MeOE2bisMATE (40X magnification).

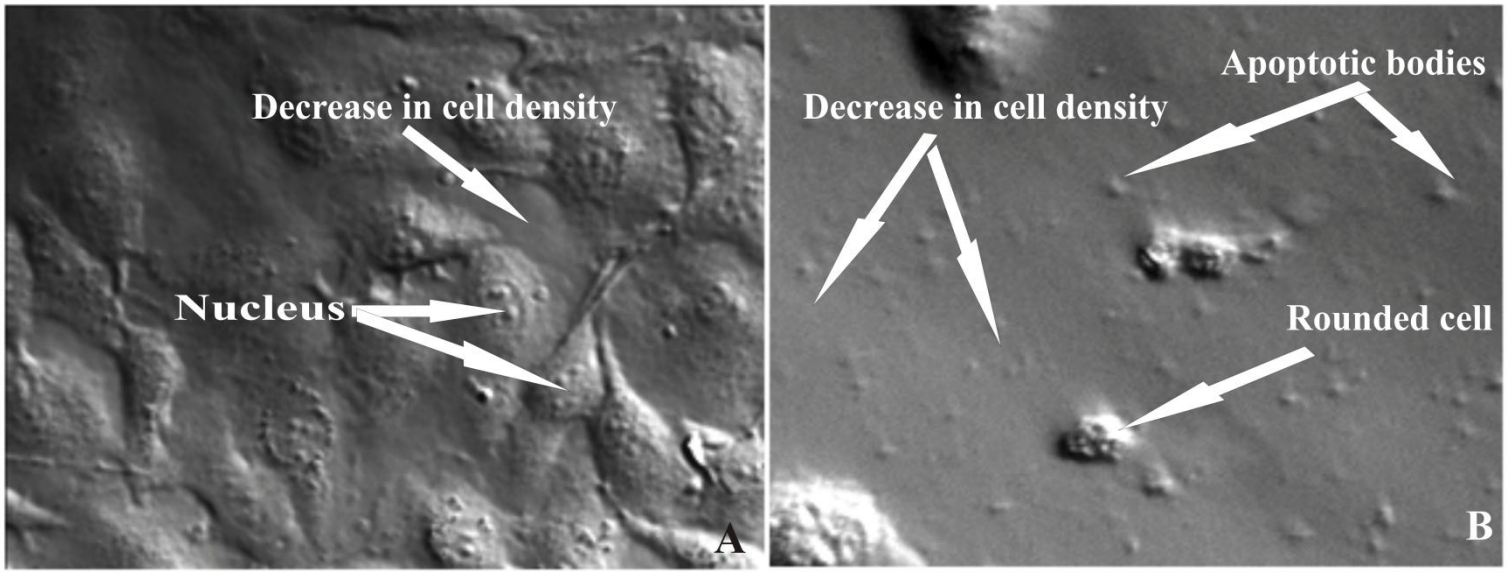

Figure 3.6: MCF-12A cells with induced starvation used as a positive control for autophagy (A). Cells were not displaying any characteristics of distress with the nucleoli clearly detectable. However, the cells were less confluent when compared to cells growing in growth medium and vehicle-treated cells (40X magnification). Cells exposed to actinomycin (1µg/1ml) as a positive control for inducing apoptosis is illustrated in B. A decrease in cell density was observed when compared to cells propagated in growth medium and vehicle-treated cells. Furthermore, cells appear rounded with numerous apoptotic bodies present (40X magnification).

3.2 Cell growth studies

Crystal violet staining

Crystal violet is a method used to determine cell number by staining the DNA. Gillies *et al.* (1986) used crystal violet to quantify cell number in monolayer cultures as a function of the absorbance of dye taken up by the cells (185). Cell numbers were expressed as a percentage of the cells propagated in growth medium in order to determine antiproliferative effects of 2-MeOE2bisMATE on tumorigenic MCF-7 and non-tumorigenic MCF-12A cells. 5 000 cells were seeded per well in sterile 96 well plates and exposed to different 2-MeOE2bisMATE concentrations, ranging from 0.2µM to 1µM with time intervals of 24h, 48h and 72h since previous studies conducted by Newman *et al.* (2004) demonstrated successful antiproliferative activity within this concentration range in the MCF-7 cell line (179).

The 50% growth inhibitory concentration was calculated as described by the National Cancer Institute in order to compare the growth inhibition induced by 2-MeOE2bisMATE between the two cell lines (195).

$100 \times (T - T_0)/(C - T_0) = 50$

Where:

T is the optical density of the test well after background subtraction after 48h exposure to test conditions.

T_0 is the optical density after background subtraction at time zero.

C is the control optical density after background subtraction of the vehicle treated-control.

Cell numbers were affected in by 2-MeOE2bisMATE in both cell lines in a time- and dose-dependent manner. Minor cell growth inhibition was noted after the 24h exposure in the MCF-12A cell line; however, 2-MeOE2bisMATE decreased cell growth to 84% at 0.2µM, 75% at 0.4µM and 0.6µM, 77% at 0.8µM and 78% at 1µM when compared to cells propagated in growth medium (Figure 3.7). During the 48h exposure 2-MeOE2bisMATE, reduced cellular proliferation in the MCF-12A cell line to 79% at 0.4µM, 68% at 0.6 µM, 62% at 0.8µM and 53% at 1µM when compared to the cells propagated in growth medium in the MCF-12A cell line. Contrasting to the MCF-12A cell line, 2-MeOE2bisMATE reduced cell proliferation in the tumorigenic MCF-7 cell line during the 48h exposure to 55% at 0.2µM, 47% at 0.4µM, 37% at 0.6 µM, 35% at 0.8µM and 1µM when compared to cells propagated in growth medium. The GI_{50} for the MCF-7 cell line was found at 0.4µM at 48h (Figure 3.8). All subsequent experiments for this project were conducted with a concentration of 0.4µM at an exposure period of 48h. 72h of 2-MeOE2bisMATE exposure resulted in extreme inhibitory effects in the MCF-7 tumorigenic cell line (Figure 3.9A). Less severe inhibitory effects were observed in the MCF-12A non-tumorigenic cell line (Figure 3.9B). MCF-7 cell growth was decreased to 41%; when compared to the 78% in the MCF-12A cell line. A significant statistically difference between the MCF-7 and MCF-12A cell line growth (P-value < 0.05) was observed when exposed to 0.4µM 2-MeOE2bisMATE for 48h and 72h. 2-MeOE2bisMATE concentrations of 0.8µM and 1µM resulted in an inhibition of 24% and 21% decrease in cell growth in the MCF-7 cell line; 57% and 49% in the MCF-12A respectively. 1µM vehicle-treated cells cell growth decreased to 94% in the MCF-7 cell line and 96% in the MCF-12A cell lines. However, the 0.4µM vehicle control resulted in 98% cell growth in the MCF-7 cell line and 93% in the MCF-12A cell lines.

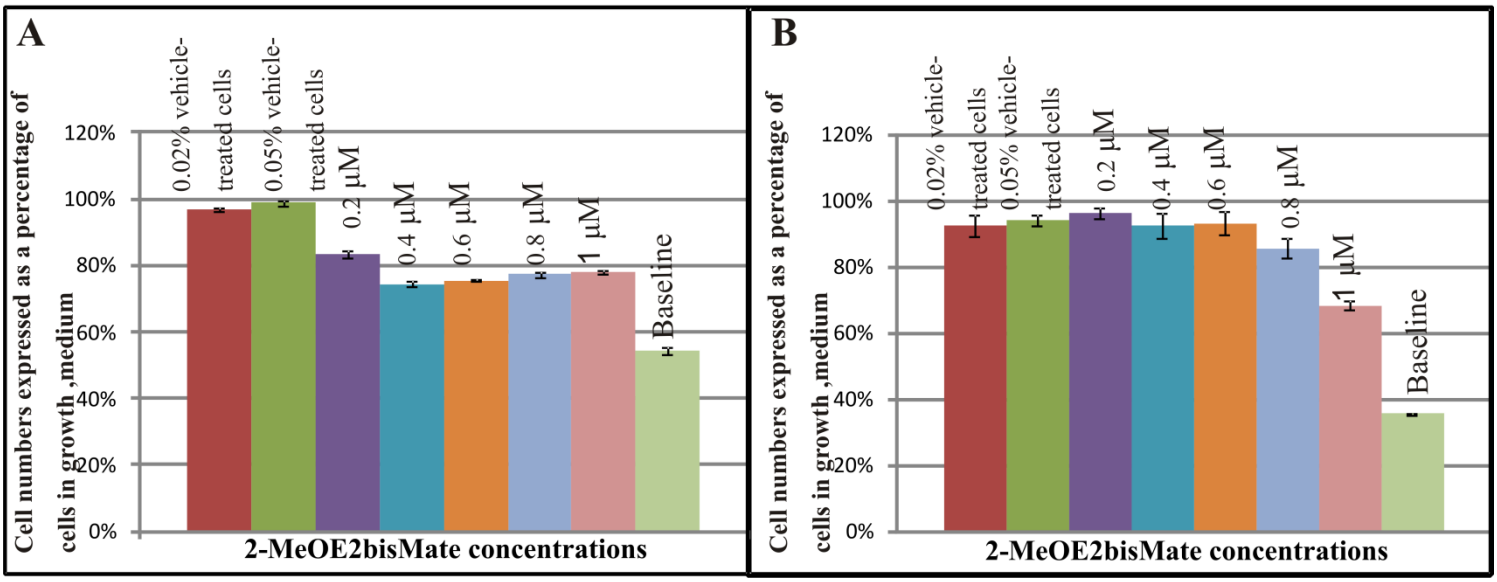

Figure 3.7: 24h of exposure of the MCF-7 cell line (A) and the MCF-12A cell line (B) to 2-MeOE2bisMATE resulted in significant growth inhibition in the MCF-7 cell line, however, growth inhibition in the MCF12A cell line was not as severe. 0.4µM 2-MeOE2bisMATE treatment decreased cell numbers to 75% in MCF-7 cells in contrast to 92% in MCF-12A cells.

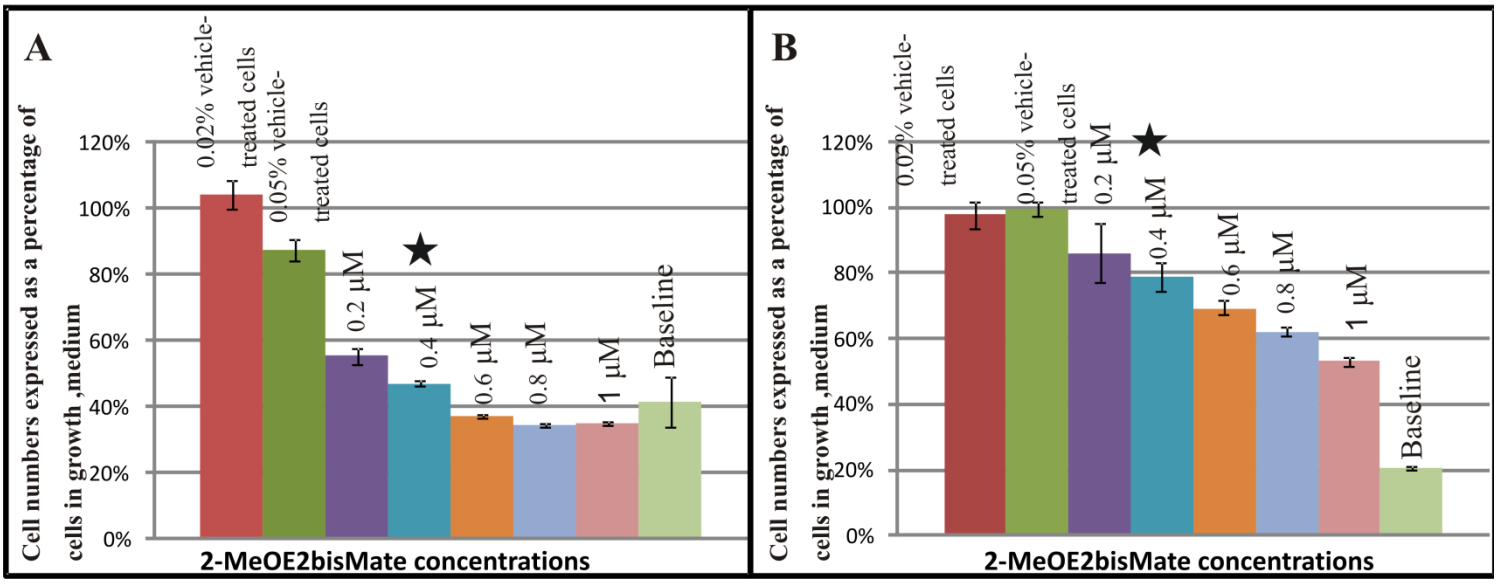

Figure 3.8: 48h of exposure of the MCF-7 cell line (A) and the MCF-12A cell line (B) to 2-MeOE2bisMATE resulted in 53% growth reduction in MCF-7 and 21% in MCF-12A cell number. A ★ indicates a statistical significant *P*-value < 0.05 difference for growth inhibition between the two cell lines.

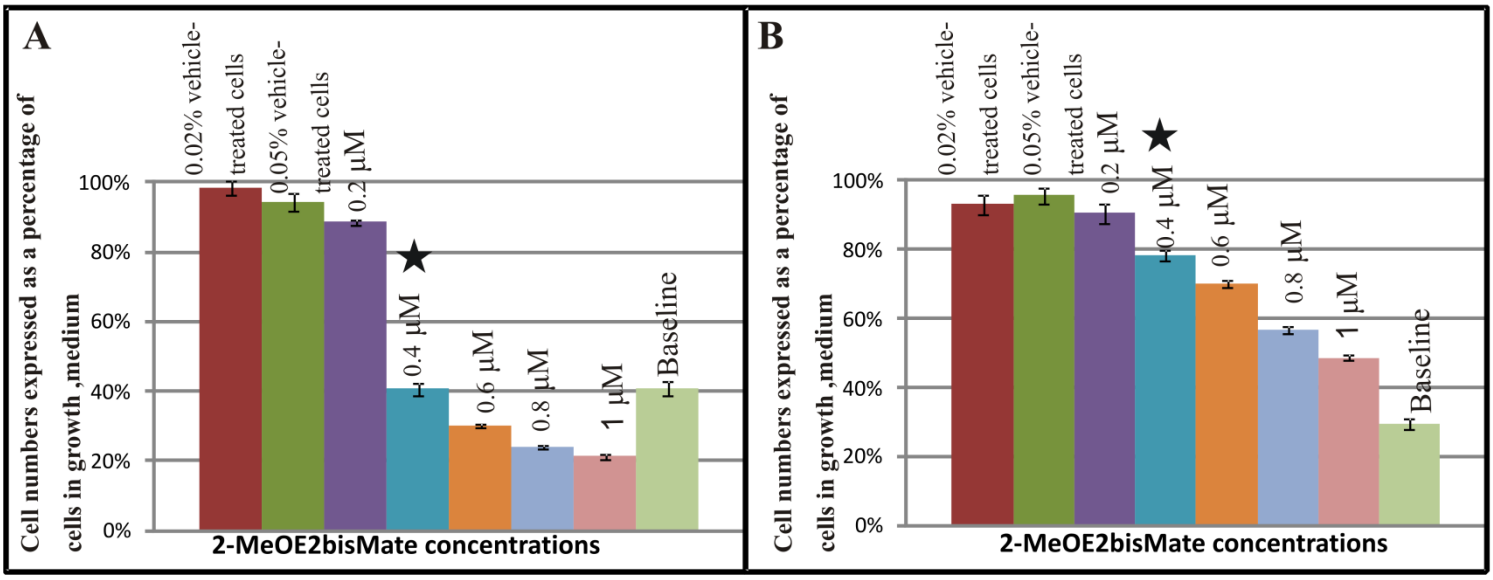

Figure 3.9: 72 H 2-MeOE2bisMATE exposures of MCF-7 (A) and MCF-12A (B) resulted in resulted in 41% cell growth when compared to control cells in growth medium. Cell growth at 0.4µM 2-MeOE2bisMATE in the MCF-12A cell line was 78%. A ★ indicates a statistical significant *P*-value < 0.05 difference for growth inhibition between the two cell lines.

3.3 Cell viability and metabolism

Lactate dehydrogenase detection

LDH production in the medium was measured after exposure of MCF-7 and MCF-12A cells to 2-MeOE2bisMATE by means of spectrophotometry. LDH is a soluble cytosolic enzyme that catalyzes the interconversion of lactate and pyruvate. Cells release LDH during injury or cell damage, following the loss of membrane integrity consequential from either apoptosis or necrosis. LDH activity, therefore, can be used as an indicator of cell membrane integrity and serves as a general means to assess cytotoxicity resulting from exposure to chemical compounds. Various controls were included in the experiment namely: background control, low control and high control. The background control consists of growth medium. The low control refers to cells propagated in growth medium, and the high control to cells propagated in growth medium with cell lysis solution added to the cells shortly before the experiment is terminated (according to manufacturer's instructions).

A statistically insignificant increase in LDH (Figure 3.10) production was found in the 2-MeOE2bisMATE-treated cells after exposure when compared to the vehicle-treated cells. However, these results were not statistically significant.

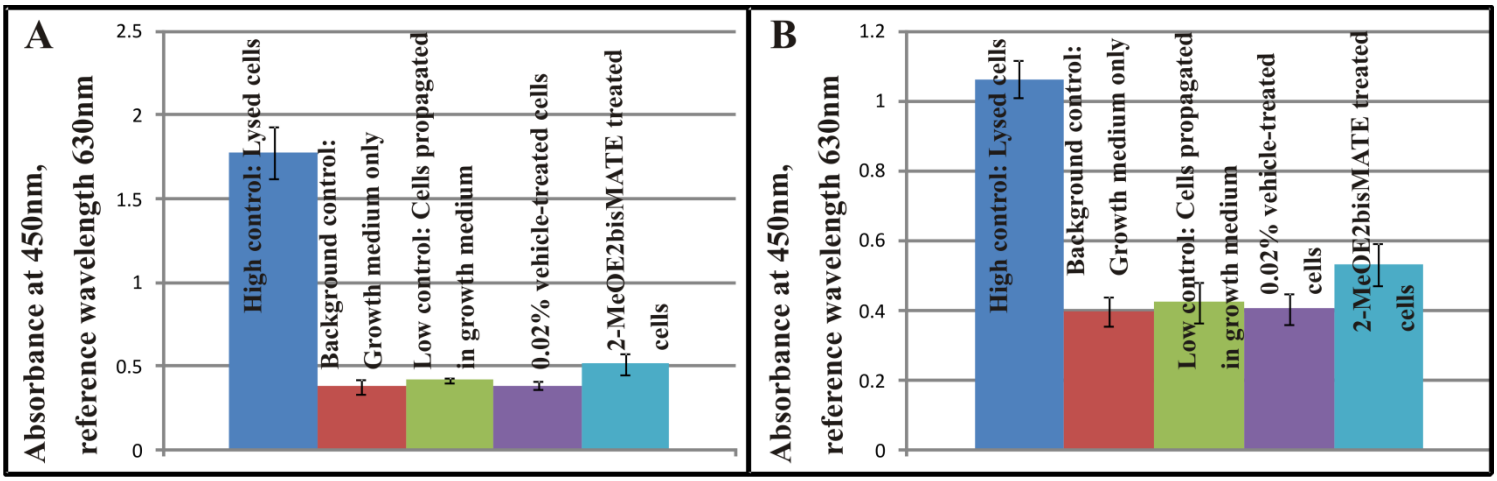

Figure 3.10: LDH production measured by means of spectrophotometry revealed a slight increase in 2-MeOE2bisMATE-treated cells after 48h of exposure when compared to the vehicle-treated control cells in the MCF-7 cell line (A) and MCF-12A cell line (B). The increase found in the exposed cells were however, not statistically significant.

3.4 Morphology

3.4.1 Light microscopy (haematoxylin and eosin staining)

Light microscopy was conducted to investigate the effects exerted by 0.4µM 2-MeOE2bisMATE after 48h of exposure on the morphology in the MCF-7 cell line and MCF-12A cell line. H & E staining was used to visualise the effects on the cytoplasm and nucleus since haematoxylin stains the cell nucleus blue and eosin stains the cytoplasm pink. H & E staining also allows for the identification of the different cell cycle phases, as well as apoptotic and abnormal cells. Quantitative data for mitotic indices were obtained by counting 1000 cells (repeated thrice) on each slide of the biological replicates and expressing data as a percentage of cells in each phase of mitosis, interphase and abnormal cells. Distinction was made between normal mitotic cells (included prophase, metaphase, anaphase and telophase), cells in interphase and abnormal cells which included cells displaying hypercondensed chromatin, membrane blebbing, apoptotic bodies and abnormal chromosome segregation. This technique provided qualitative and quantitative information.

H & E staining revealed hypercondensed chromatin, apoptotic bodies and compromised cell density in the 2-MeOE2bisMATE-treated MCF-7 cells when compared to cells propagated in growth medium and vehicle-treated cells (Figure 3.11 and Figure 3.12). Vehicle-treated cells displayed no signs of distress. Furthermore, cells with induced starvation used as positive control for autophagy showed decreased cell density (Figure 3.13). Cells exposed to 0.1µg/ml actinomycin for 48h were severely compromised accompanied with severe decreased cell density (Figure 3.13). Haematoxylin and eosin staining revealed no indications of apoptosis namely, hypercondensed chromatin or apoptotic bodies in the 2-MeOE2bisMATE-treated MCF-12A cells when compared to cells propagated in growth medium vehicle-treated cells (Figure 3.14 and Figure 3.15). In addition, there was no difference in cell density between the 2-MeOE2bisMATE-treated MCF-12A cells when compared to the vehicle-treated cells that displayed no cellular characteristics of distress. Mitotic indices were determined of the H & E-stained cells (Figure 3.17 and Figure 3.18). MCF-7 cells observed in metaphase experienced an 8% increase. MCF-12A cells observed in metaphase experienced a 5% increase when compared to the vehicle control cells.

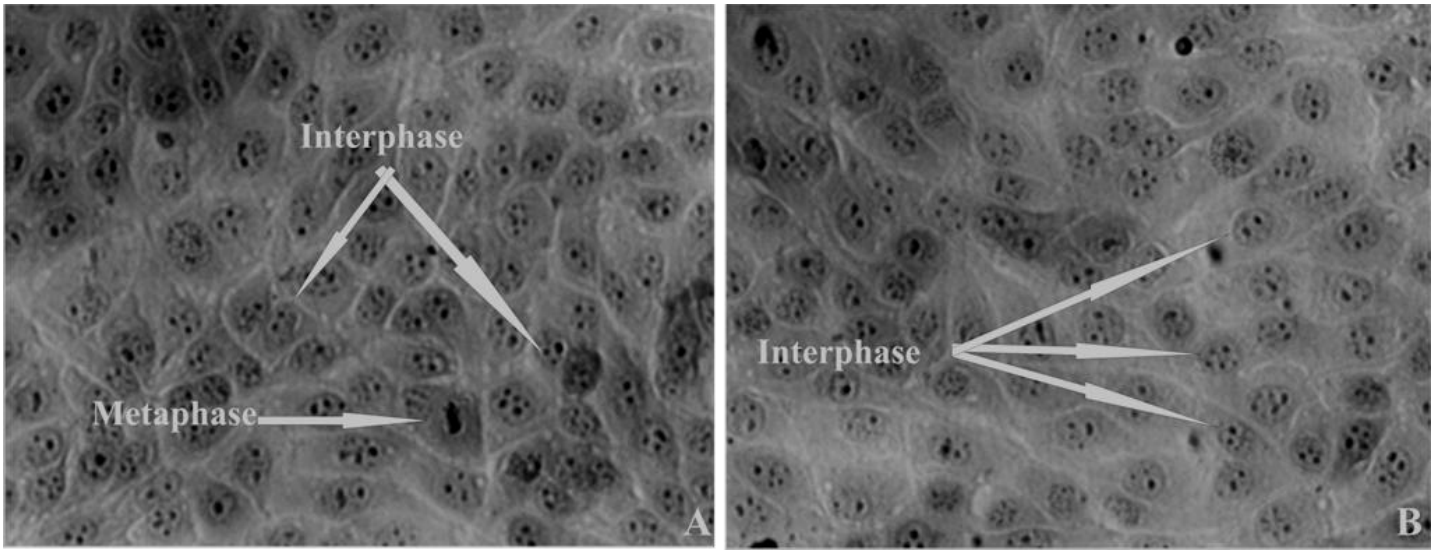

Figure 3.11: The MCF-7 cells in growth medium (A) and MCF-7 vehicle control cells (B) were mostly in found in interphase (40X magnification). Cells in both samples were confluent and displaying no characteristics of distress.

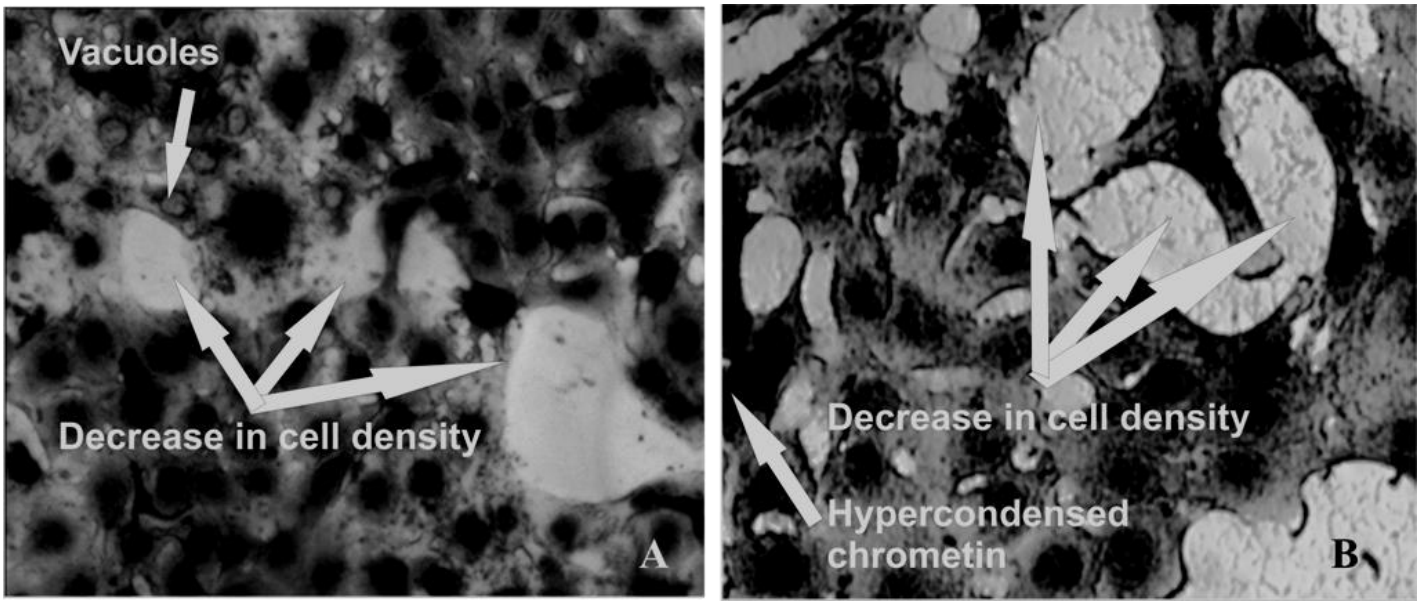

Figure 3.12: Both figures illustrate the effects of 0.4µM 2-MeOE2bisMATE after 48h in the MCF-7 cell line. 2-MeOE2bisMATE-treated cells after 48h of exposure revealed several apoptotic characteristics including hypercondensed chromatin and a decreased cell density (40X magnification in figure A and 100X magnification in B)

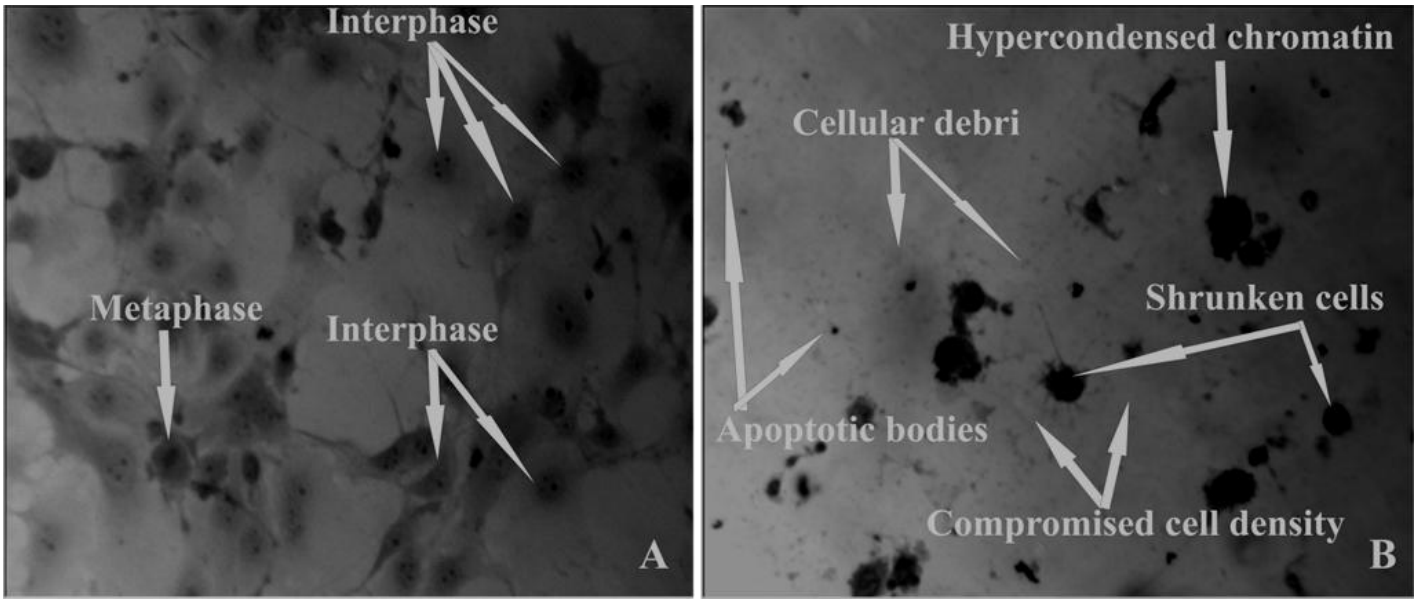

Figure 3.13: The MCF-7 cells with induced starvation as a positive control for autophagy (A) where growth medium was supplemented with PBS with a ratio of 1 growth medium: 3 PBS ($^{V}/_{V}$). The latter revealed cells mostly present in interphase (40 X magnifications). MCF-7 exposed to actinomycin as a positive control for apoptosis (B) resulted in severely compromised cells with decreased cell density (40X magnifications).

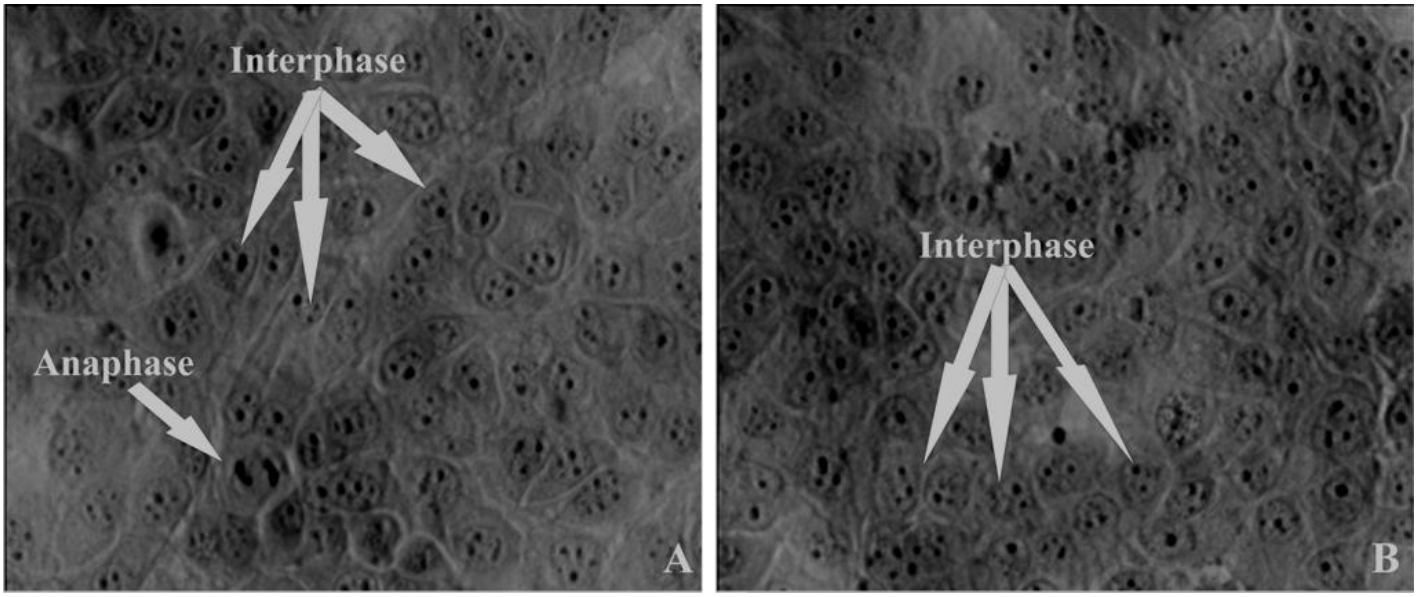

Figure 3.14: MCF-12A cells propagated in growth medium (A) and vehicle-treated MCF-12A cells (B) were confluent and found mostly in interphase (40X magnification).

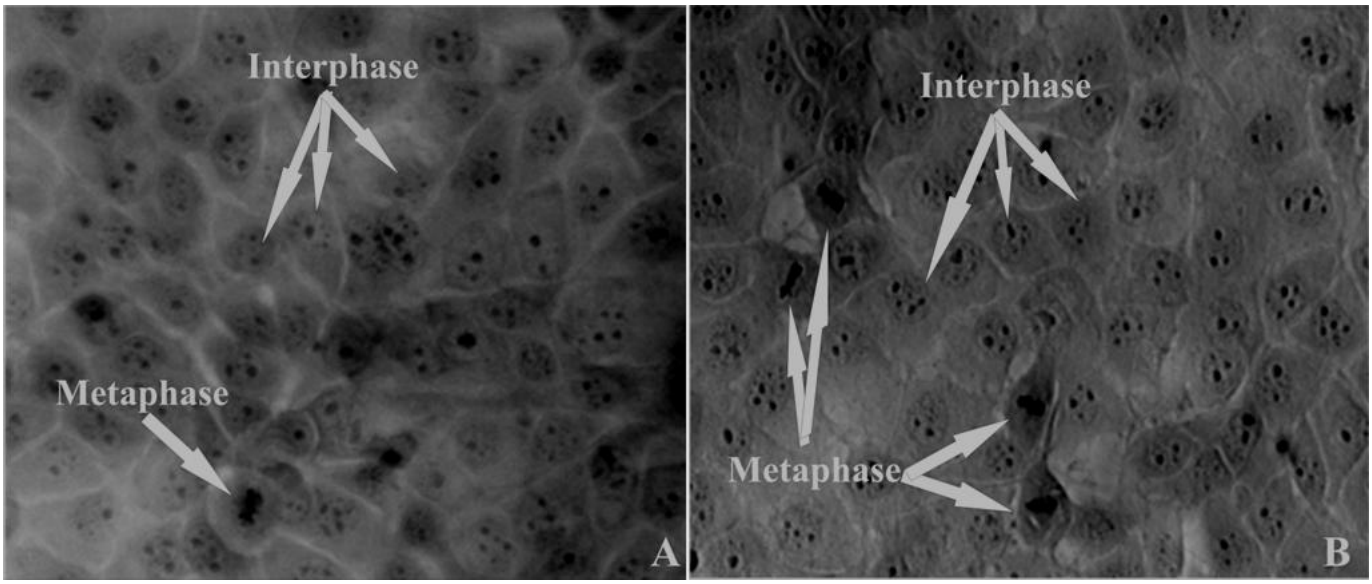

Figure 3.15: Images represents MCF-12A exposed to 2-MeOE2bisMATE after 48h where cells were found in interphase and metaphase (A and B). 48 h 0.4µM 2-MeOE2bisMATE MCF-12A-treated cells revealed no hypercondensed chromatin and cell density was unaffected (A and B) (40X magnification).

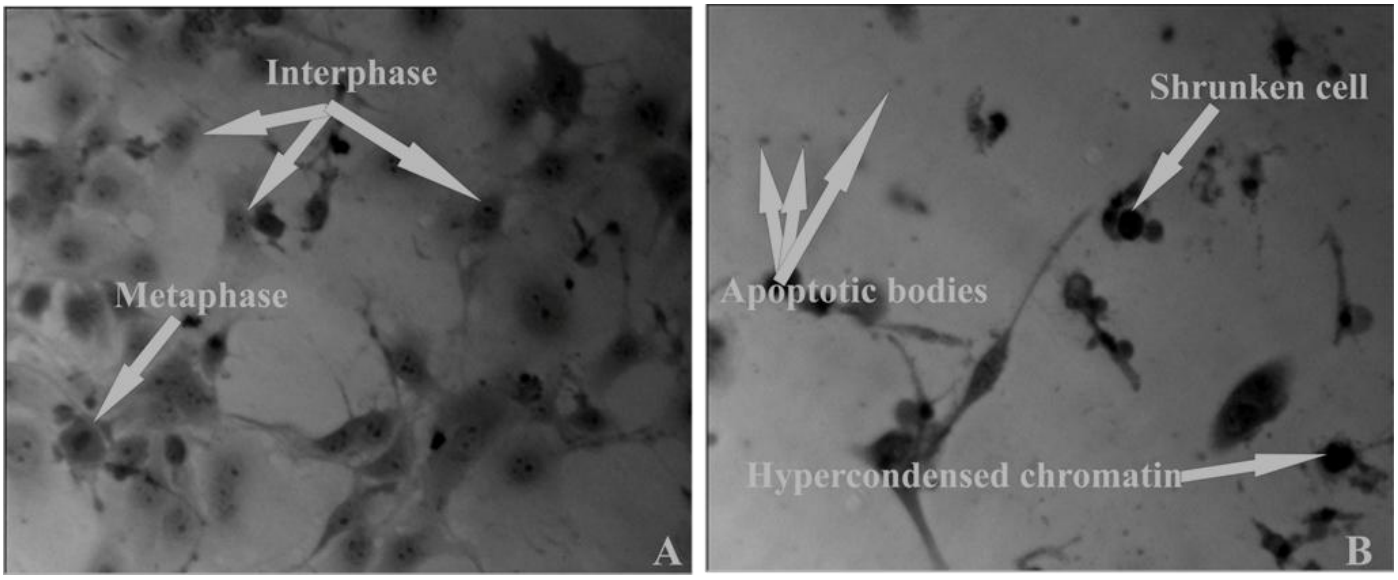

Figure 3.16: The positive control for autophagy where MCF-12A cells (A) were starved by supplementing growth medium with PBS with a ratio of 1 growth medium: 3 PBS ($^{V}/_{V}$). The latter illustrated where cells were observed mostly found in interphase accompanied with compromised cell density (40X magnifications). 48h MCF-12A exposure to 0.1µg/ml actinomycin as positive control for apoptosis (B) resulted in extensively compromised cells with severe decreased cell density (40X magnifications).

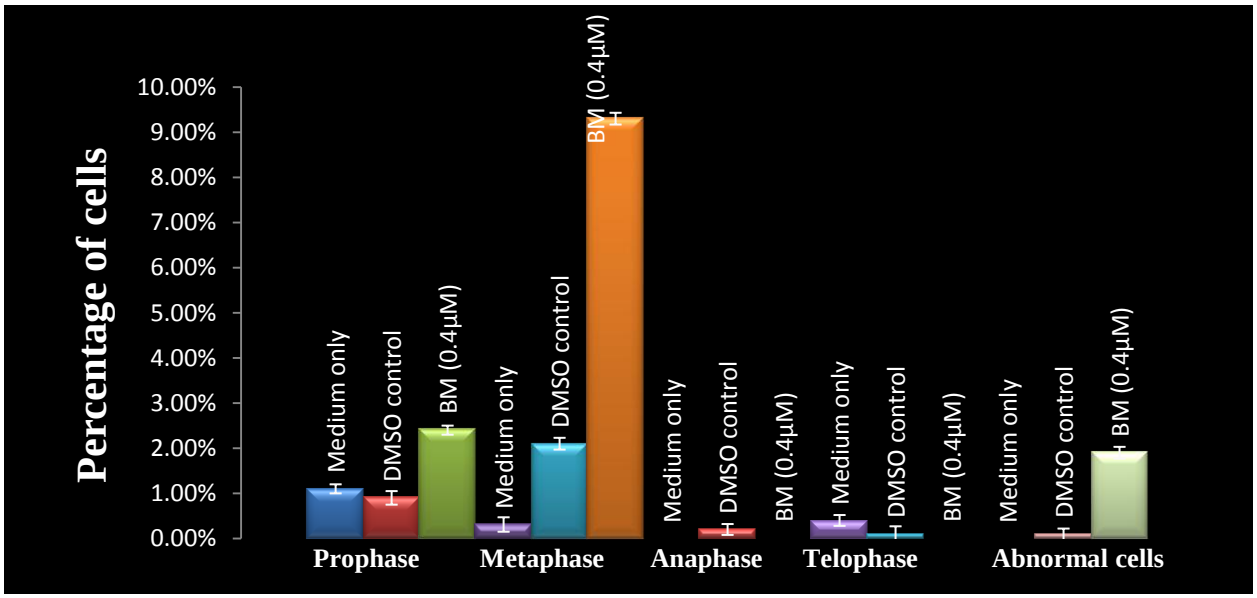

Figure 3.17: Mitotic indices of MCF-7 cells propagated in growth medium, vehicle-treated cells and 2-MeOE2bisMATE-treated cells. The 2-MeOE2bisMATE-treated cells revealed an increase in cells present in metaphase when compared to the cells propagated in growth medium and vehicle-treated cells.

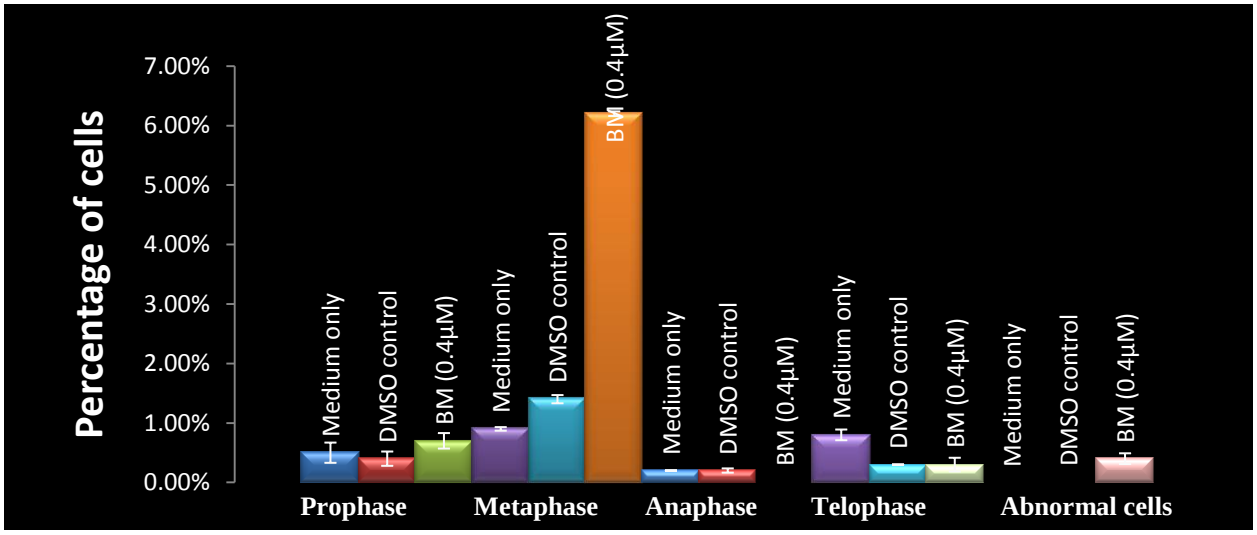

Figure 3.18: Mitotic indices of MCF-12A cells propagated in growth medium, vehicle-treated cells and 2-MeOE2bisMATE-treated cells. 2-MeOE2bisMATE-treated cells demonstrated an increase in cells present in metaphase when compared to cells propagated in growth medium and vehicle-treated cells.

3.4.2 Transmission electron microscopy

TEM was used to determine the ultrastructure of intracellular components of exposed and control cells. TEM allowed for the identification of chromatin condensation, membrane blebbing and apoptotic bodies. Furthermore, TEM was conducted to identify characteristics of autophagy, namely the autophagic vacuolization of the cytoplasm. These vacuoles are large double-membrane vesicles containing degenerating sequestered cytoplasmic constituents (196, 197). TEM provides an illustration of the interior of the cell at a much larger magnification than light microscopy. Thus, effects on cell morphology not visible by means of light microscopy were revealed by TEM.

TEM demonstrated hypercondensed chromatin, membrane blebbing, budding and mitochondria migration towards the nucleus in the 2-MeOE2bisMATE-treated-MCF-7 cells when compared to the vehicle control cells indicating the presence of apoptosis (Figure 3.19, Figure 3.20 and Figure 3.21). In addition, several intracellular vacuoles were observed in the exposed cells which is a hallmark of autophagy. The presence of extended sections of the cell membrane, nuclear fragmentation and apoptotic bodies in the 2-MeOE2bisMATE-MCF-12A cells-treated was observed when compared to the vehicle-treated control (Figure 3.23 and Figure 3.24). However, these effects were not as prominent when compared to MCF-7-treated cells. Intracellular vacuoles were not present in the 2-MeOE2bisMATE-treated MCF-12A cells,

suggesting the absence of autophagy. MCF-7 and MCF-12A cells treated with 0.1µg/ml actinomycin D as a positive control for apoptosis and cells with induced starvation as a positive control for autophagy resulted in severely compromised cells (Figure 3.22 and Figure 3.25).

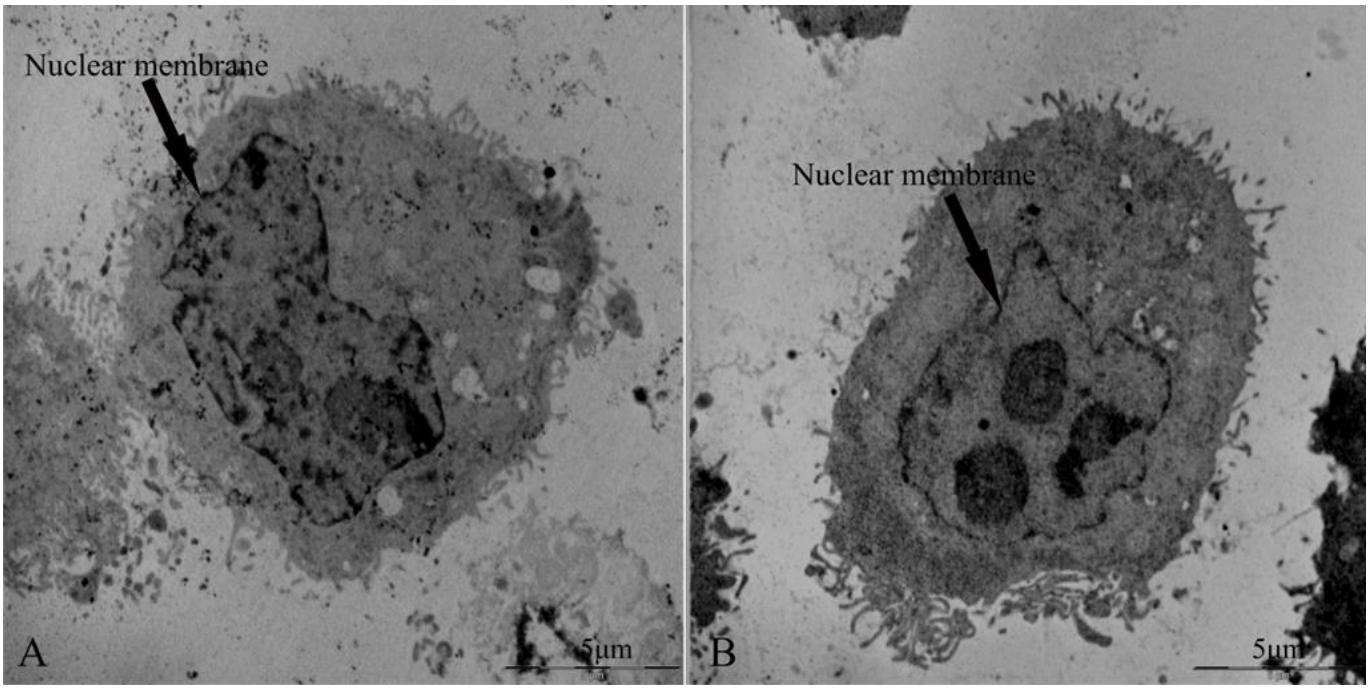

Figure 3.19: MCF-7 cells propagated in growth medium (A) and vehicle-treated cells (B) displayed minimum vacuoles with the nuclear membrane was visible (6000X magnification).

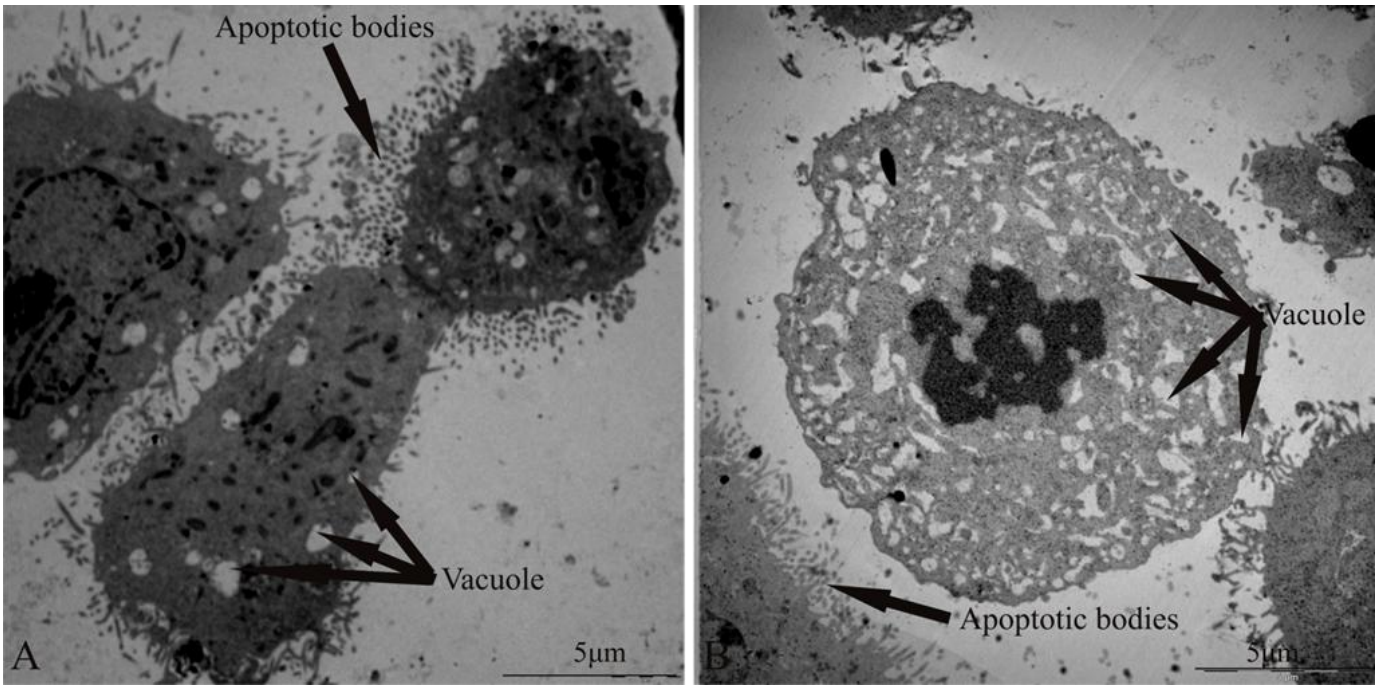

Figure 3.20: The MCF-7 2-MeOE2bisMATE-treated cells (A and B) were severely affected. The presence of several vacuoles and apoptotic bodies were observed (6000X magnification).

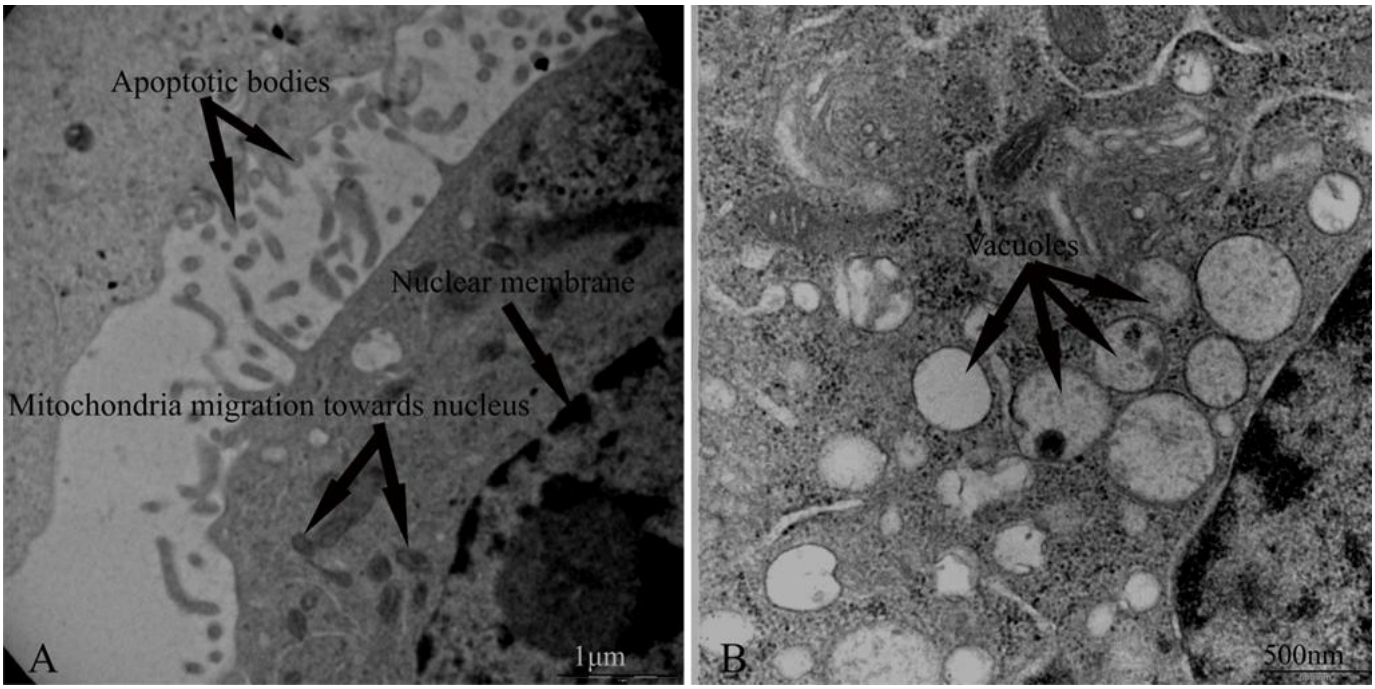

Figure 3.21: Micrographs of MCF-7 2-MeOE2bisMATE-treated cells revealed several apoptotic bodies (A) and vacuoles (B). Furthermore, the migration of mitochondria towards the nucleus was observed (A) (30 000X magnified in A and 40 000X magnification in B).

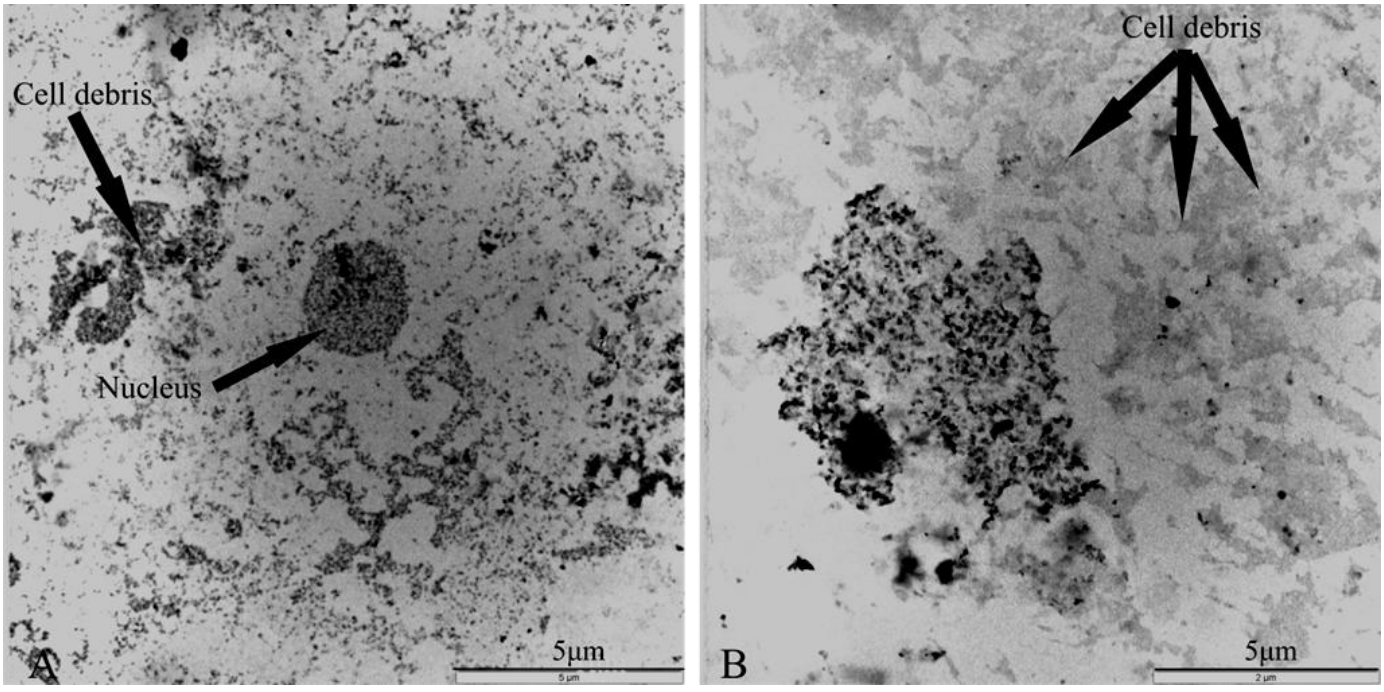

Figure 3.22: MCF-7 exposure to using 0.1µg/ml actinomycin D used as a positive control for apoptosis induction (A), and MCF-7 positive control cells for autophagy (starvation induction) (B) resulted in severely compromised cells.

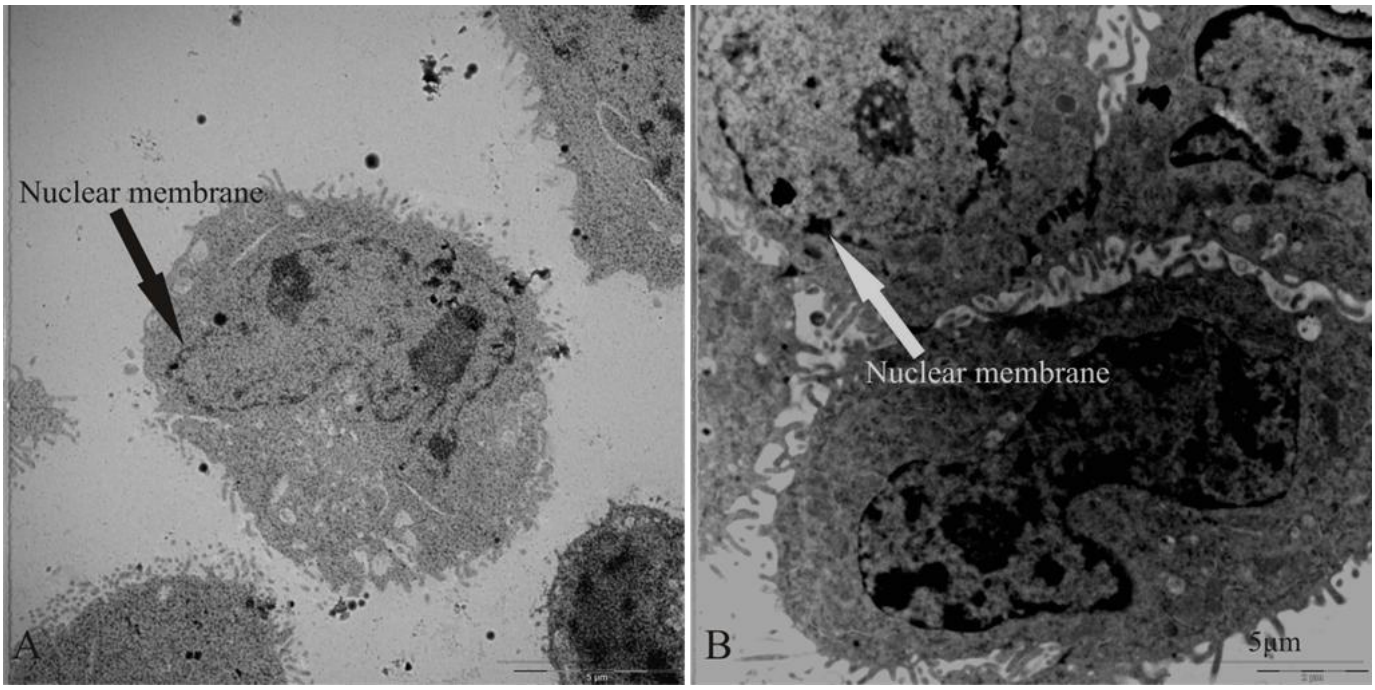

Figure 3.23: The MCF-12A cells propagated in growth medium and the vehicle-treated sample (A) revealed cells illustrating no signs of distress (B). The nucleus and nuclear membrane were both clearly visible (6000X magnification)

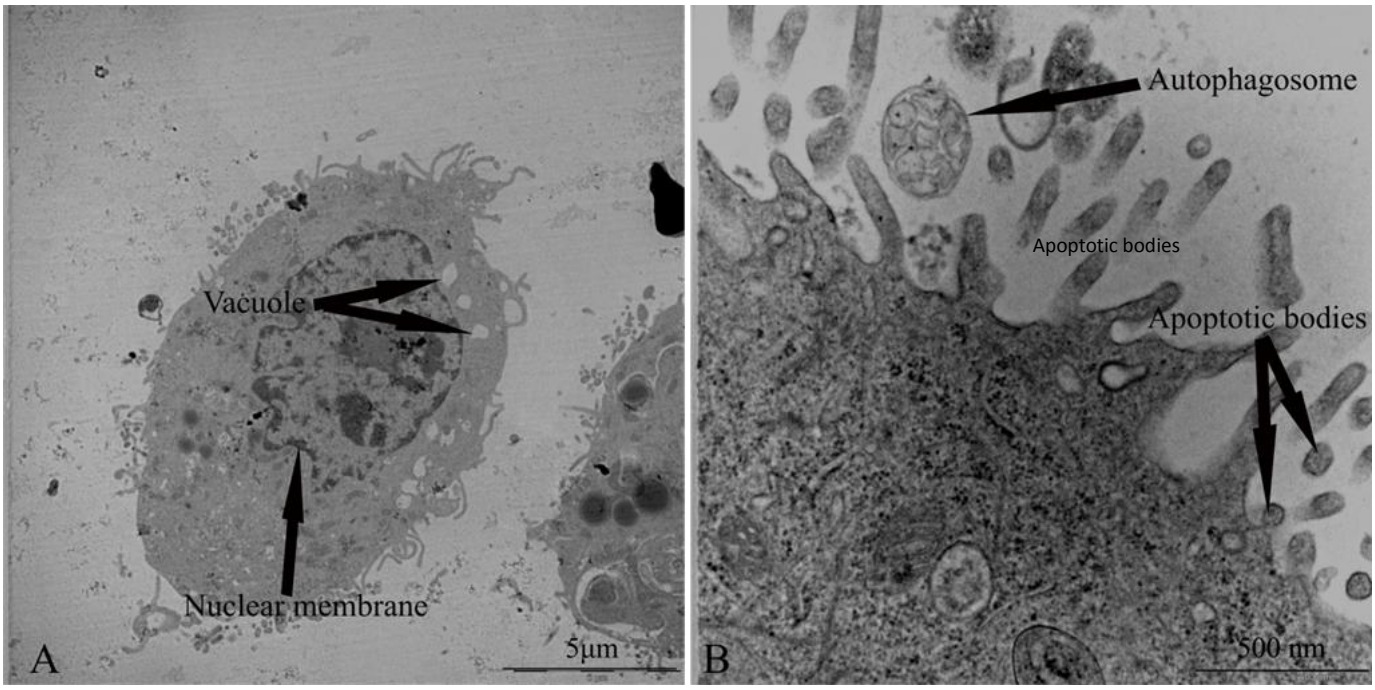

Figure 3.24: 0.4µM MCF-12A 2-MeOE2bisMATE-treated cells exposed for 48h revealed nuclear fragmentation, extensions of the cell membrane and apoptotic bodies (6000X magnification) (A). Figure B illustrated 0.4µM 2-MeOE2bisMATE-treated cells exposed for 48h revealed autophagosomes (40 000X magnification).

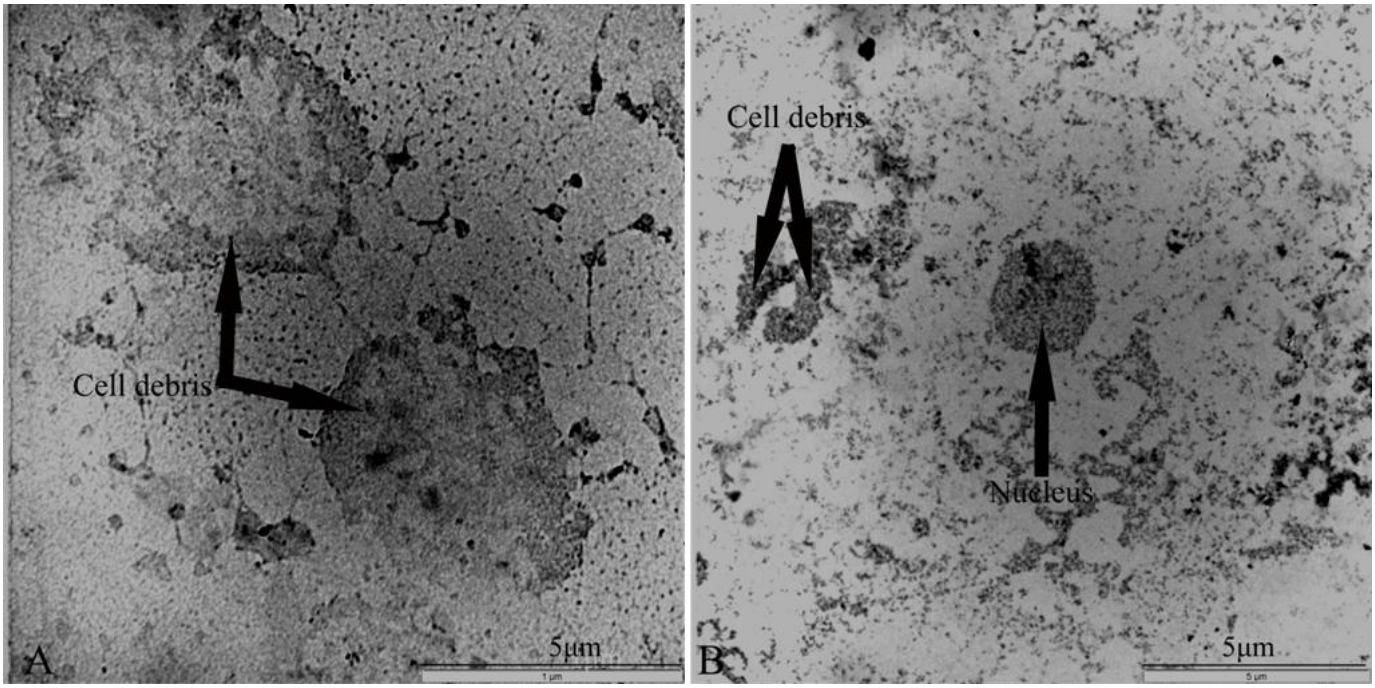

Figure 3.25: MCF-12A exposure to using 0.1µg/ml actinomycin D used as a positive control for apoptosis induction (A), and MCF-7 positive control cells for autophagy (starvation induction) (B) resulted in severely compromised cells.

3.4.3 Fluorescent microscopy

Apoptosis, autophagy and necrosis detection

A triple staining fluorescent microscopy method was employed to visualize autophagy and the influence of 2-MeOE2bisMATE on morphology and cell viability. A triple fluorescent dye staining method was developed utilizing acridine orange (green), Hoechst 33342 (blue) and propidium iodide (red) fluorescent dyes. Acridine orange is a lysosomotropic fluorescent compound that serves as a tracer for acidic vesicular organelles including autophagic vacuoles and lysosomes (198). Cells undergoing autophagy has an increased tendency for acridine orange staining when compared to viable cells, however acridine orange is not a specific marker for autophagy and therefore other techniques are needed to verify the appearance of increased autophagic activity. Hoechst 33342 is capable of penetrate intact cell membranes of viable cells and cells undergoing

apoptosis and stains the DNA. Propidium iodide is a fluorescent dye and unable to penetrate an intact membrane and therefore stains the nucleus of cells where the membrane is compromised due to oncotic or necrotic processes.

Increased lysosomal staining and a decrease in cell density were found in the 2-MeOE2bisMATE-exposed MCF-7 cells when compared to cells propagated in growth medium and vehicle-treated cells (Figure 3.26 and Figure 3.27). In addition, several 2-MeOE2bisMATE-exposed cells were found rounded. No propidium iodide staining was present in neither the treated cells, nor the vehicle control cells. Minor increased lysosomal staining was observed in the MCF-12A 2-MeOE2bisMATE-exposed cells when compared to cells propagated in growth medium and vehicle-treated cells (Figure 3.29 and Figure 3.30). No propidium iodide staining was found in neither the treated cells, nor the vehicle control cells, revealing the absence of necrosis. Cells exposed to 0.1µg/ml actinomycin D for 48h used in this project as a positive control for apoptosis induction revealed cells that were severely compromised accompanied with decreased cell density. Furthermore, cells with induced starvation used as a positive control for autophagy exhibited a dramatic increase in lysosomal staining (Figure 3.28 and Figure 3.31).

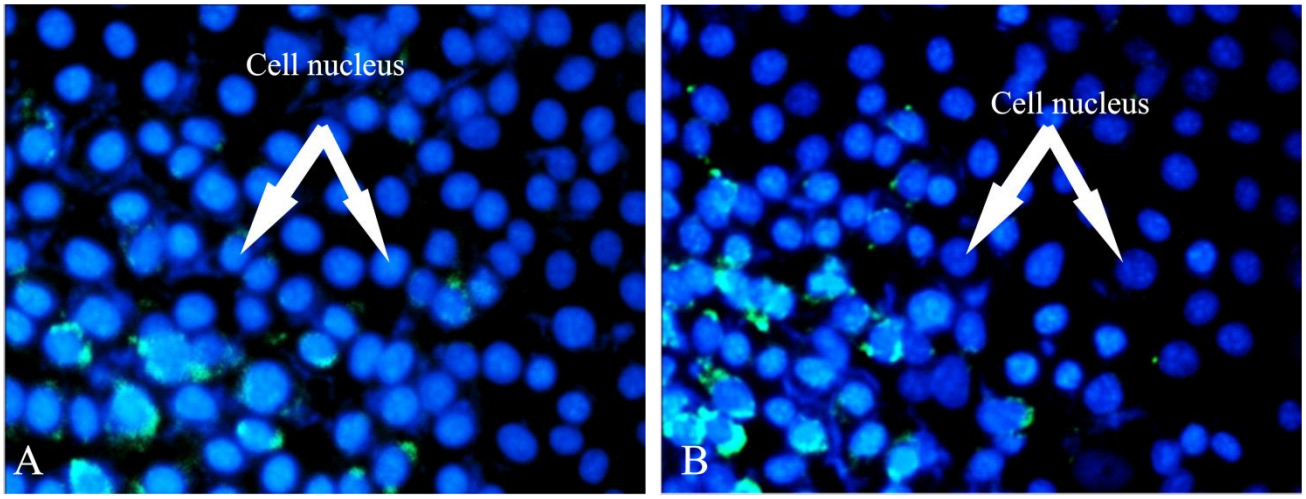

Figure 3.26: MCF-7 cells propagated in growth medium (A) and vehicle-treated control cells (B) were confluent. Since Hoechst 33342 stains the DNA, the nucleus can be identified. Background lysosomal staining (green) was observed (20X magnification).

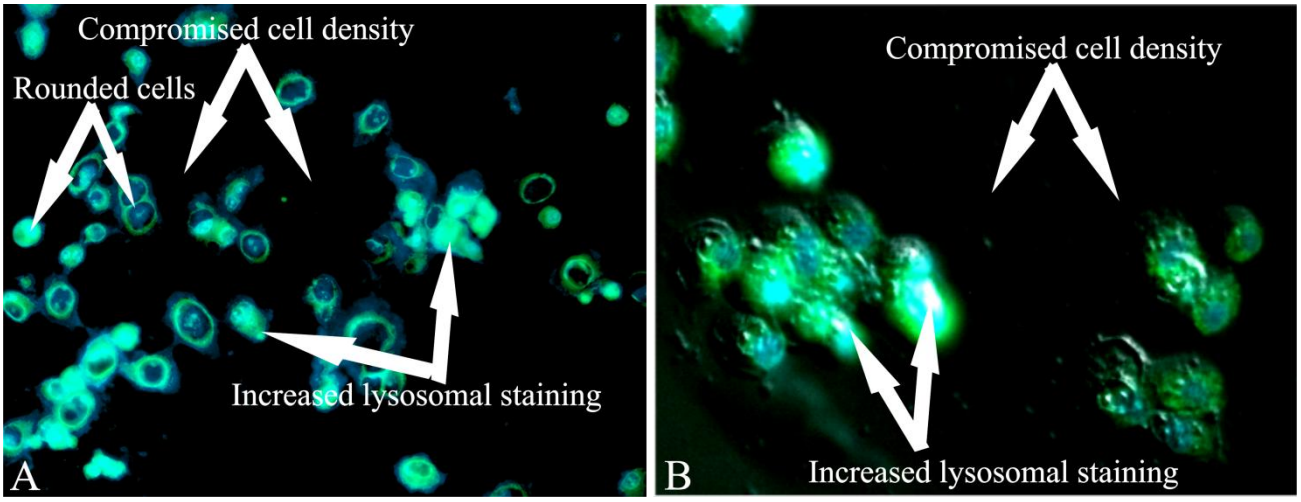

Figure 3.27: 2-MeOE2bisMATE-treated MCF-7 cells (A and B) after 48h of exposure revealed increased lysosomal staining (green), rounded cells accompanied with decreased cell density when compared to the vehicle-treated cells. However, no propidium iodide staining was observed (20X magnification).

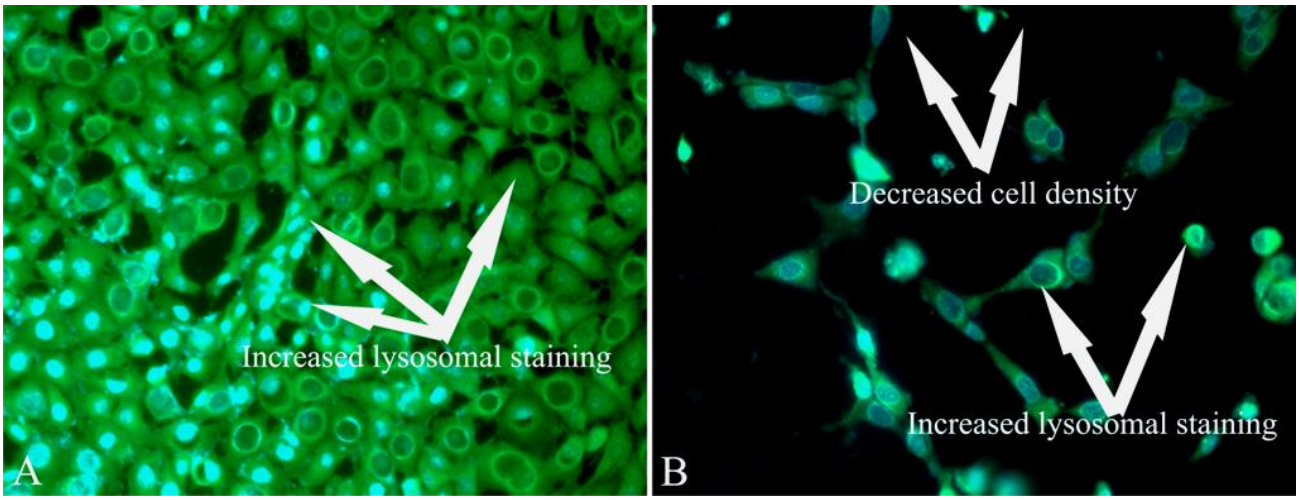

Figure 3.28: MCF-7 cells with induced starvation used as a positive control for autophagy displayed increased lysosomal staining (A) (green). Cells exposed to 0.1µg/ml actinomycin D for 48h revealed a severe decrease in cell density (B) (20X magnification).

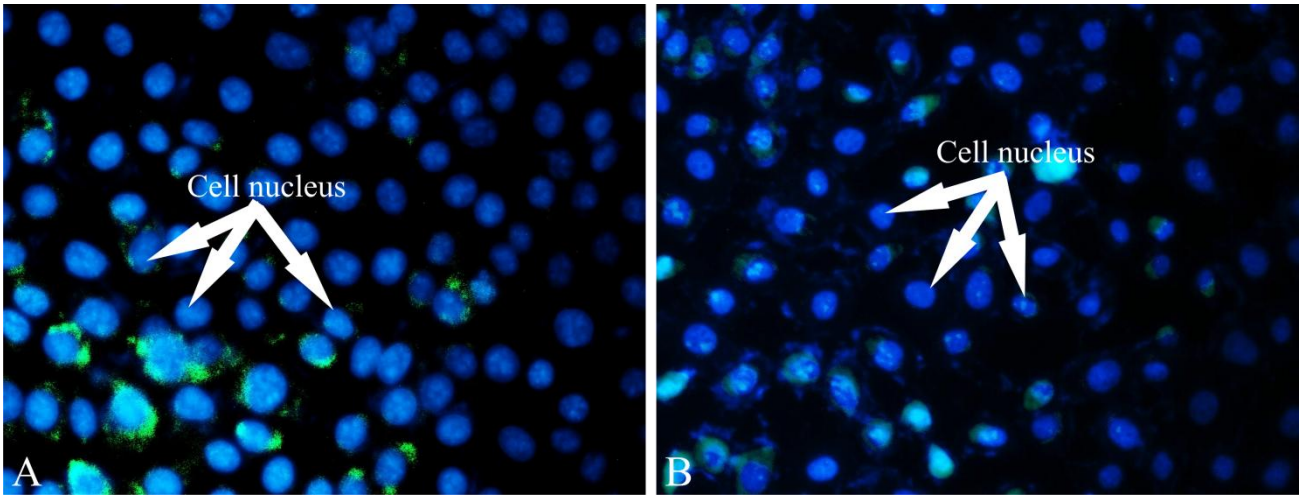

Figure 3.29: MCF-12A cells propagated in growth medium and vehicle-treated control cells were confluent (A and B). The nucleus can be distinguished since Hoechst 33342 stained the DNA blue. Background lysosomal staining (green) was observed (20X magnification).

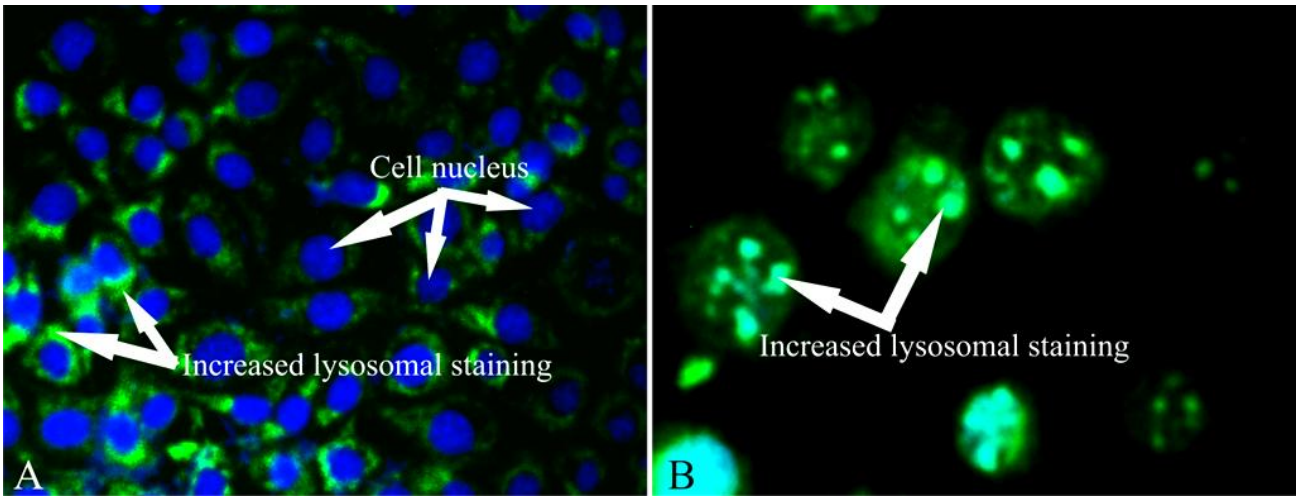

Figure 3.30: 2-MeOE2bisMATE-treated MCF-12A cells after 48h (B) of exposure revealed decreased cell density when compared to vehicle-treated cells. Increased intensity of the lysosomal staining (green) indicates the increased presence of increased acidic vesicles suggesting the presence of autophagy. However, no propidium iodide staining was observed (20X magnification in A and 100X magnification in B).

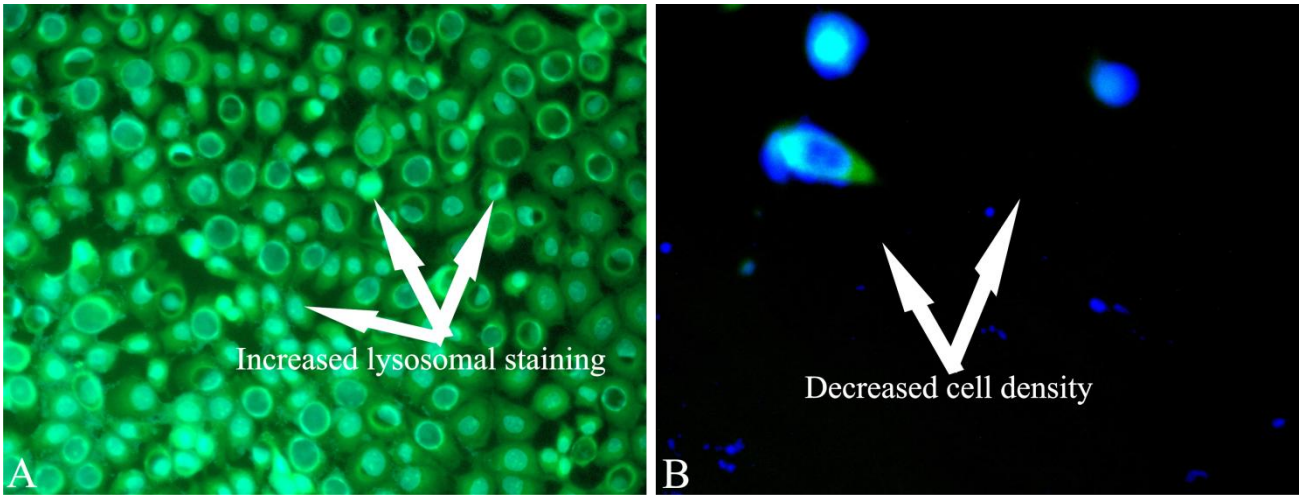

Figure 3.31: MCF-12A cells with induced starvation used as a positive control for autophagy displayed increased lysosomal staining (A) (green). Cells exposed to 0.1µg/ml actinomycin D for 48h revealed a severe decrease in cell density (B) (20X magnification).

3.5 Flow cytometry studies

3.5.1 Cell cycle progression

Propidium iodide staining detected by flow cytometry was utilised to investigate the effects of 2-MeOE2bisMATE on cell cycle progression. The latter allowed for the quantification of DNA content. Cell cycle distribution, a G_2M block and detection of a sub-G_1 apoptotic peak were revealed. Investigation of the *in vitro* effect of 2-MeOE2bisMATE on the MCF-7 cell cycle progression revealed a sub-G_1 apoptotic peak (41%) with no G_2M arrest when compared to cells propagated in growth medium and vehicle-treated cells (Figure 3.32, Figure 3.33 and Table 3.1). The 2-MeOE2bisMATE-treated MCF-12A cells revealed a 12% sub-G_1 peak, but with the absence of a G_2M arrest (Figure 3.34, Figure 3.35 and Table 3.2). The latter suggests that MCF-7 cells are more severely affected when compared to MCF-12A cells.

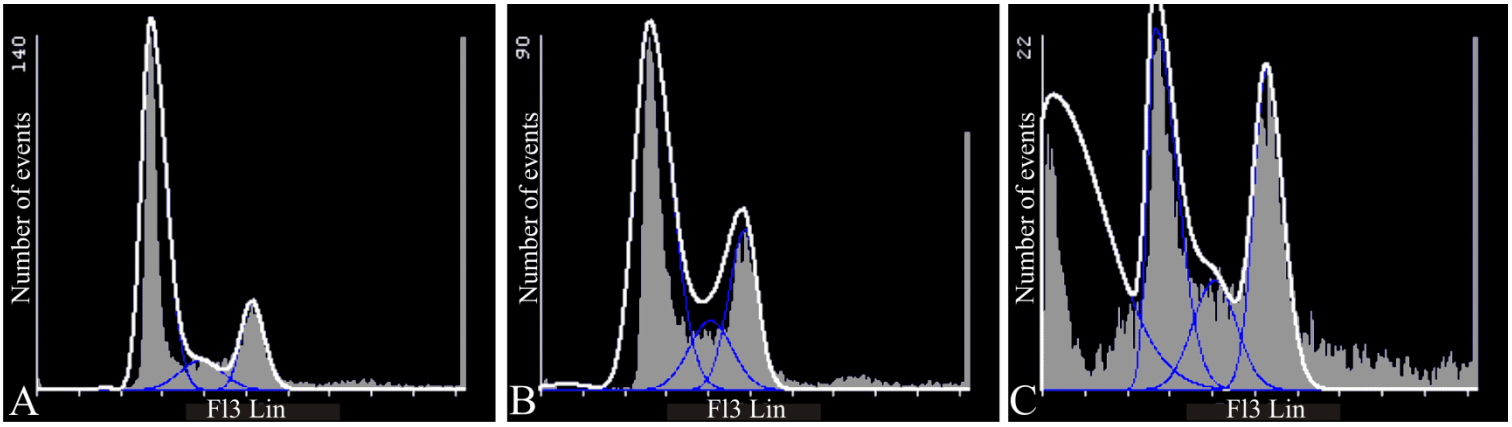

Figure 3.32: Flow cytometry was used to investigate cell cycle progression in MCF-7 cells propagated in growth medium (A) and vehicle-treated MCF-7 cells (B). MCF-7 2-MeOE2bisMATE-treated cells displayed 41% of cells present in apoptosis, 25% in the G_1 phase, 11% in the S phase and 22% in G_2M (C).

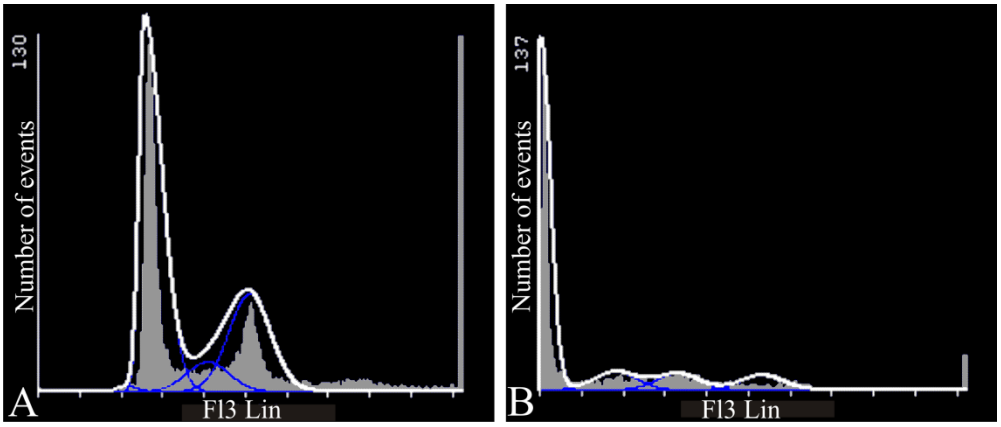

Figure 3.33: Starved MCF-7 cells used as a positive control for autophagy (A) displayed 61% of cells present in G_1, 9% present in the S phase and 29% occupied G_2M with 0,75% cells undergoing apoptosis. Cells treated with actinomycin D used as a positive control for apoptosis (B) showed 63% of cells undergoing apoptosis, 20% in the G_1, 12% occupied the S phase and 11% occupied G_2M.

Table 3.1: MCF-7 cell cycle progression

Percentage	Apoptotic cells	Cells occupying G1 phase	Cells occupying S phase	Cells occupying G2/M phase
Cells propagated in growth medium	0.18%	72.44%	10.23%	17.13%
Vehicle-treated cells	0.33%	62.71%	14.02%	22.3%
2-MeOE2bisMATE-treated cells	41.16%	25.1%	11.18%	22.53%
Control for apoptosis	63.74%	20.26%	12.08%	10.74%
Control for autophagy	O.71%	61.01%	8.91%	29.37%

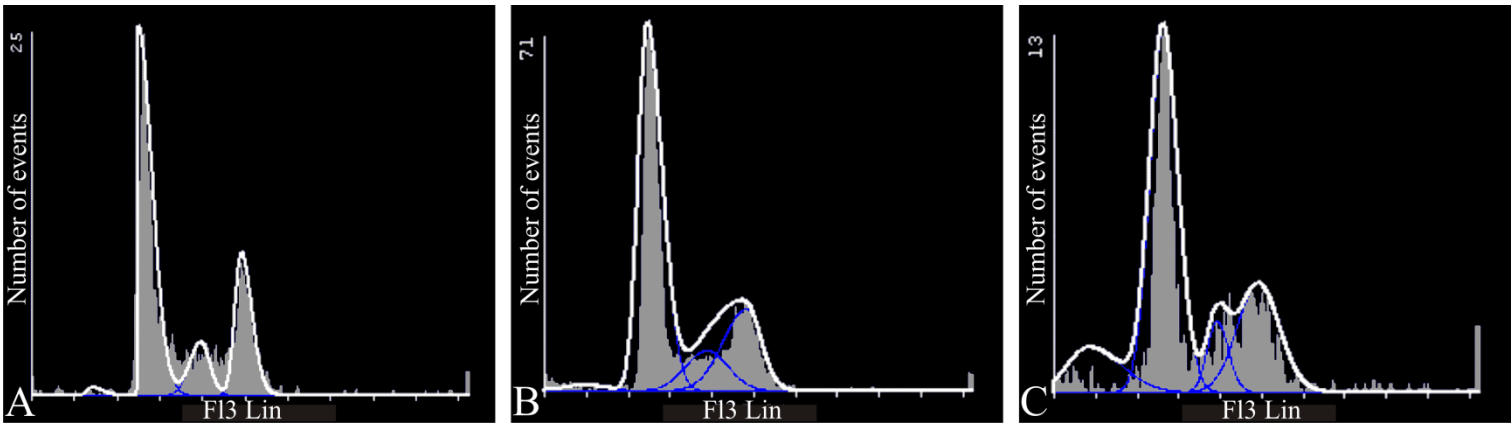

Figure 3.34: Flow cytometry was used to investigate cell cycle progression in MCF-12A cells propagated in growth medium (A), vehicle-treated MCF-12A cells (B) and 2-MeOE2bisMATE-treated MCF-12A cells (C). 2-MeOE2bisMATE had minor effect on the MCF-12A cell cycle progression with 12% of cells present in apoptosis, 55% present in the G_1 phase, 8% in the cells present in the S phase and 25% in G_2M. The *in vitro* effect of 2-MeOE2bisMATE on the MCF-12A cell cycle progression was observed with the occurrence of the sub-G_1 peak, however not as severe when compared to the MCF-7 cells.

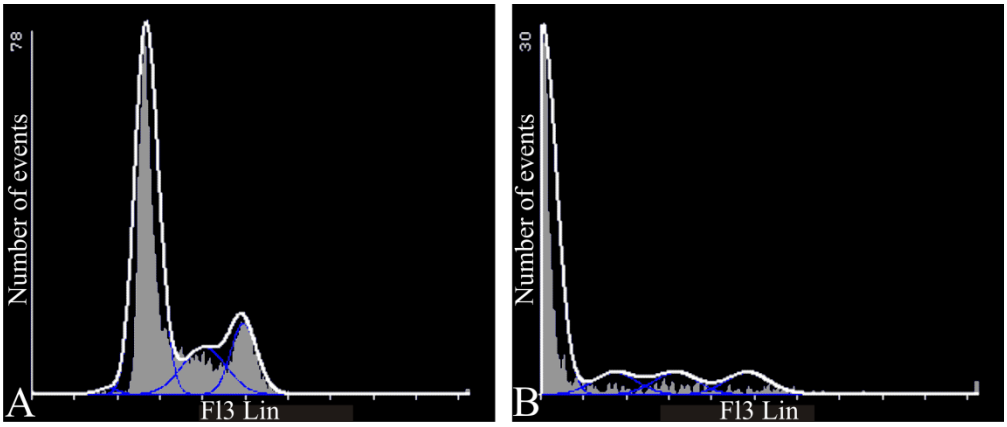

Figure 3.35: Starved MCF-12A cells used as a positive control for autophagy (A) showed 43% of cells present in G_1, 28% present in the S phase and 29% occupied G_2M with 0,77% cells undergoing apoptosis. Cells treated with actinomycin D used as a positive control for apoptosis (B) showed 66% of cells undergoing apoptosis, 11% in the G_1, 11% occupied the S phase and 11% occupied G_2M.

Table 3.2: MCF-12A cell cycle progression

Percentage	Apoptotic cells	Cells occupying G1 phase	Cells occupying S phase	Cells occupying G2M phase
Cells propagated in growth medium	1.35%	59.36%	12.03%	27.25%
Vehicle-treated cells	1.62%	63.27%	12.34%	22.76%
2-MeOE2bisMATE-treated cells	12.22%	55.33%	7.88%	24.56%
Control for apoptosis	66.02%	11.32%	11.32%	11.32%
Control for autophagy	0.77%	42.51%	28.01%	28.69%

3.5.2 Apoptosis detection analysis

Annexin V-FITC

The cell surface expression of phosphatidylserine translocated from the inner cytoplasmic membrane to the outer cytoplasmic membrane is considered an early characteristic of apoptosis. The latter event was investigated by means of fluorescein isiothiocyanate conjugated Annexin V. Annexin V is a 35-36 kDa, Ca^{2+}-dependent, phospholipid binding protein with a high affinity for PS. Propidium iodide was used to investigate necrosis. Propidium iodide is a fluorescent dye that can only enter cells with compromised cell membrane integrity.

The percentage of viable cells decreased to 54% in the MCF-7 2-MeOE2bisMATE-treated cells when compared to cells propagated in growth medium and vehicle-treated cells (Figure 3.36 and Figure 3.37). Furthermore, MCF-7 2-MeOE2bisMATE-treated cells revealed that 26% were found present in early apoptosis, 10% in late apoptosis and 9% in necrosis. 2-MeOE2bisMATE-treated MCF-12A cells revealed a cell viability of 76%, 11% were found present in early apoptosis, 9% in late apoptosis and 4% in necrosis when compared to the MCF-12A cells propagated in growth medium and vehicle-treated cells (Figure 3.38 and Figure 3.39).

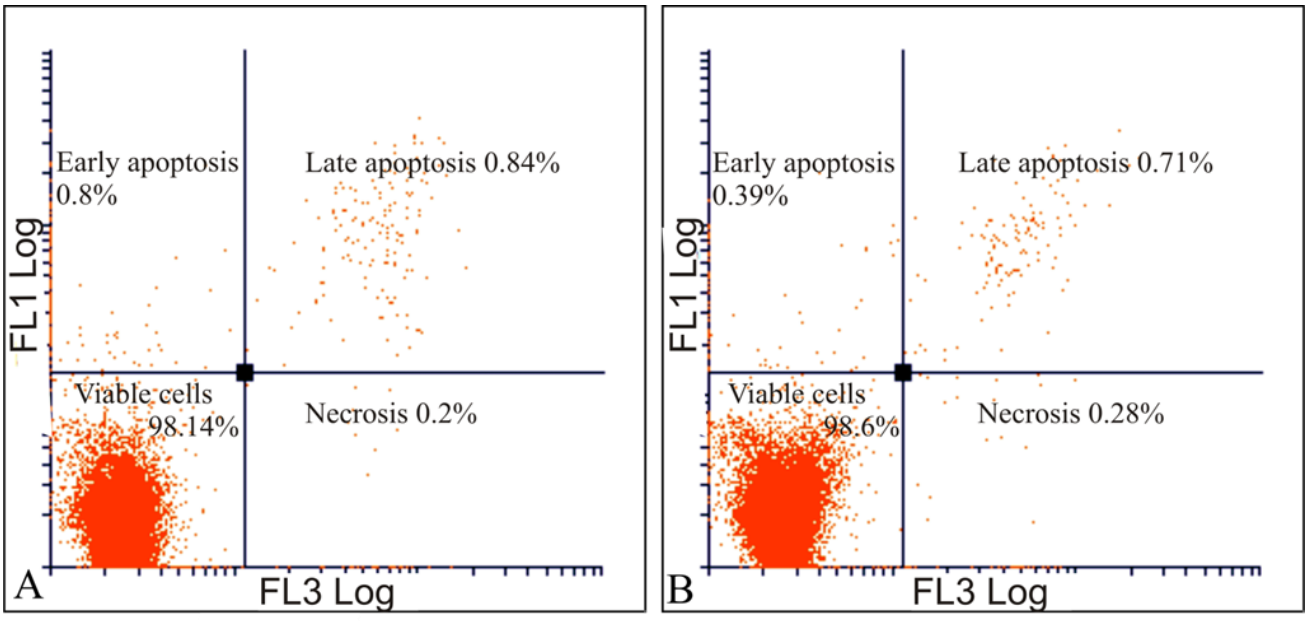

Figure 3.36: Flow cytometry investigation using annexin-V-FITC revealed cell viability of more than 98% for the MCF-7 cells propagated in growth medium (A) and vehicle-treated cells (B).

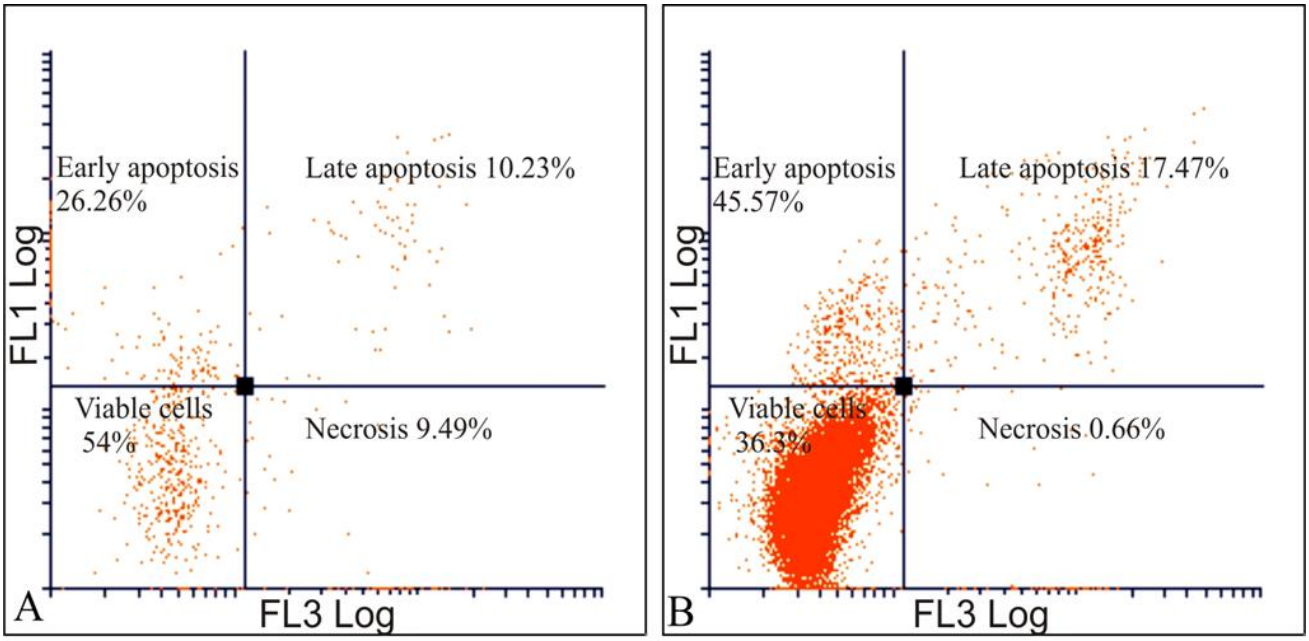

Figure 3.37: Flow cytometric investigation revealed that 54% of the 2-MeOE2bisMATE-treated MCF-7 cells (A) were viable, 26% found were to be in early apoptosis, 10% in late apoptosis and 9% in necrosis. Cells in which apoptosis was induced (B) had severe apoptosis induction where 36% were still viable.

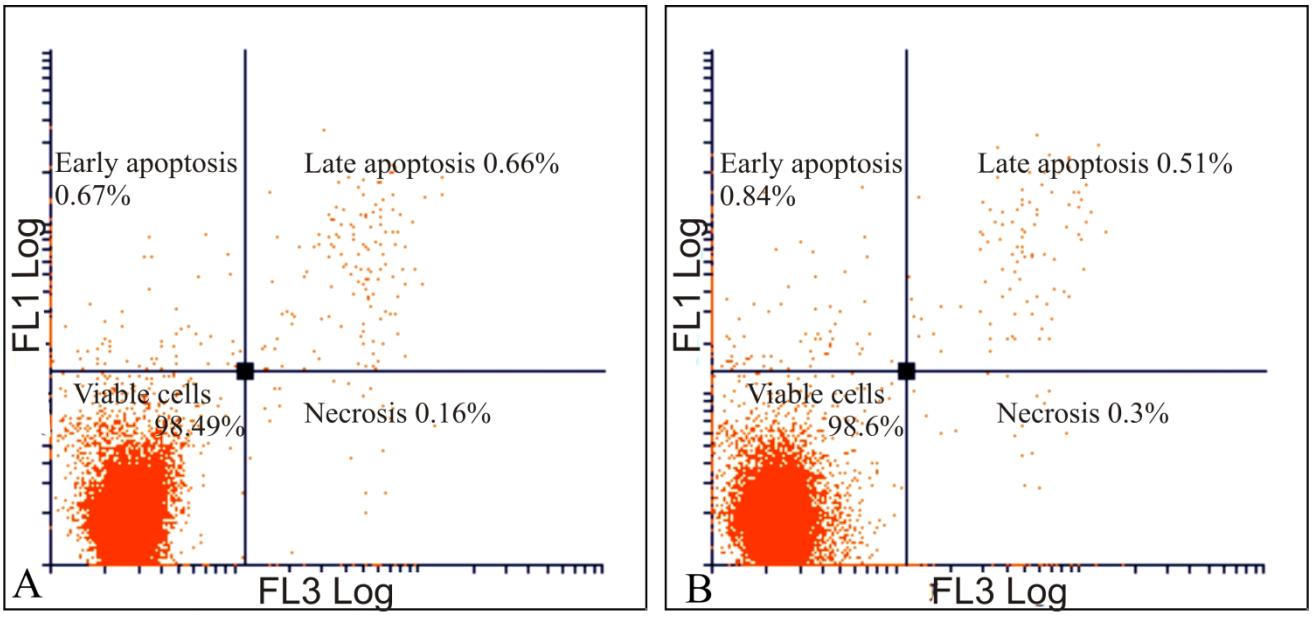

Figure 3.38: MCF-12A cells propagated in growth medium (A) and vehicle-treated cells (B) had cell viability above 98%.

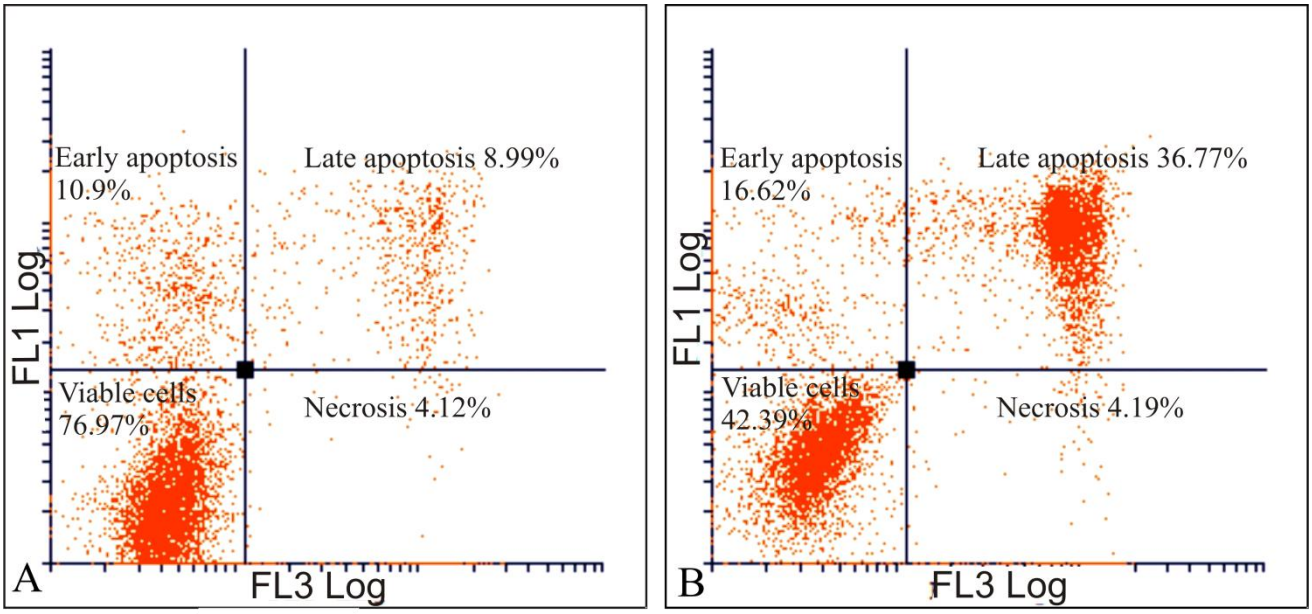

Figure 3.39: Investigation by means of flow cytometry revealed that 2-MeOE2bisMATE-treated MCF-12A cells (A) had decreased cell viability to 76%, 11% were found in early apoptosis, 9% in late apoptosis and 4% in necrosis. Cells treated with actinomycin D (B) resulted in 42% cell viability, 17% cells in early apoptosis, 37% in late apoptosis and 4% in necrosis.

3.5.3 Mitochondrial membrane potential

Mitocapture mitochondrial kit

A reduction in mitochondrial membrane potential is an early characteristic of apoptotic cell death due to loss of the electrochemical gradient across the mitochondrial membrane. Data obtained by means of the mitocapture mitochondrial kit, that uses a cationic dye, 5,5',6,6'-tetrachloro-1,1',3,3' tetraethylbenzimidazolylcarbocyanine iodide provided quantitive apoptosis information. In healthy cells, the dye concentrates in the mitochondrial matrix to form red fluorescent aggregates. In any event that reduces the mitochondrial potential, such as induced apoptosis, the dye remains in the cytoplasm in a green fluorescent monomeric form. Intensity of fluorescence was measured by flow cytometry.

2-MeOE2bisMATE-treated MCF-7 cells had a reduction in mitochondrial membrane potential where 5% were affected when compared to cells propagated in growth medium and vehicle-treated cells (Figure 3.40 and Figure 3.41). 2-MeOE2bisMATE-treated MCF-12A cells had a reduction in the mitochondrial membrane potential where 3% of cells displayed a reduced mitochondrial membrane potential when compared to cells

propagated in growth medium and vehicle-treated cells (Figure 3.42 and Figure 3.43). The latter suggests that MCF-7 cells are more severely affected when treated with 2-MeOE2bisMATE than MCF-12A cells.

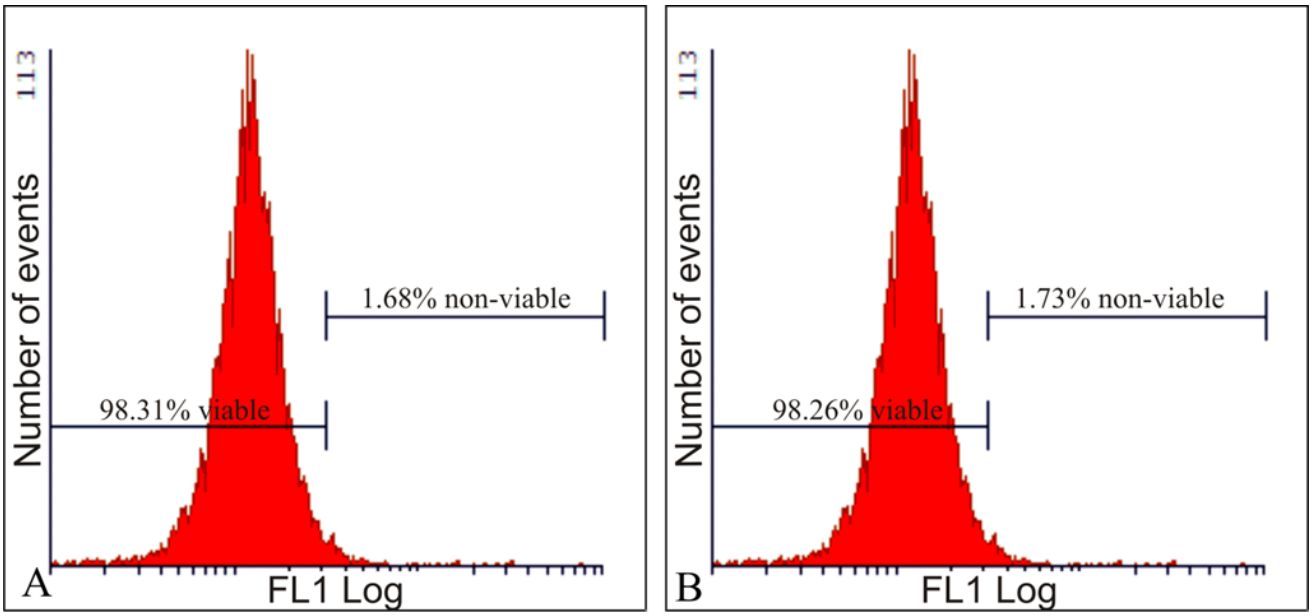

Figure 3.40: Mitochondrial membrane potential of MCF-7 cells propagated in growth medium (A) and vehicle-treated cells (B). Less than 2% of cells had reduced mitochondrial membrane potential accompanied with 98% of vehicle-treated MCF-7 cells still unaffected.

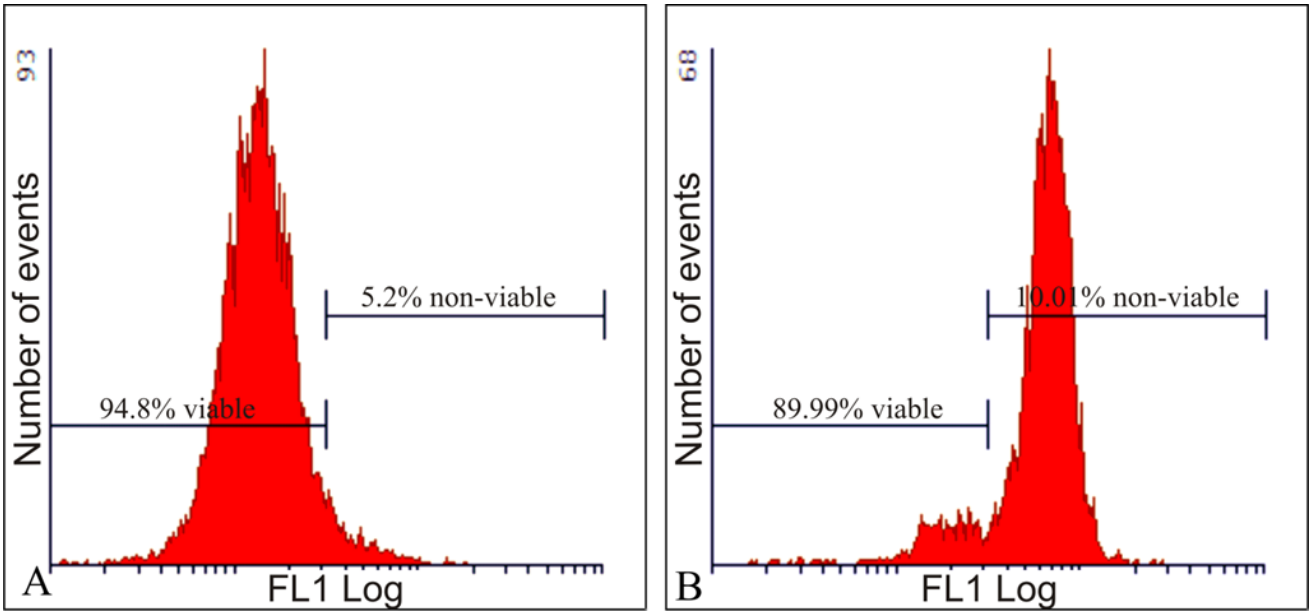

Figure 3.41: 2-MeOE2bisMATE-treated MCF-7 cells (A) revealed 5% of cells had reduced mitochondrial membrane potential. Cells treated with actinomycin D (B) revealed that 10% of cells had a reduction in mitochondrial membrane potential.

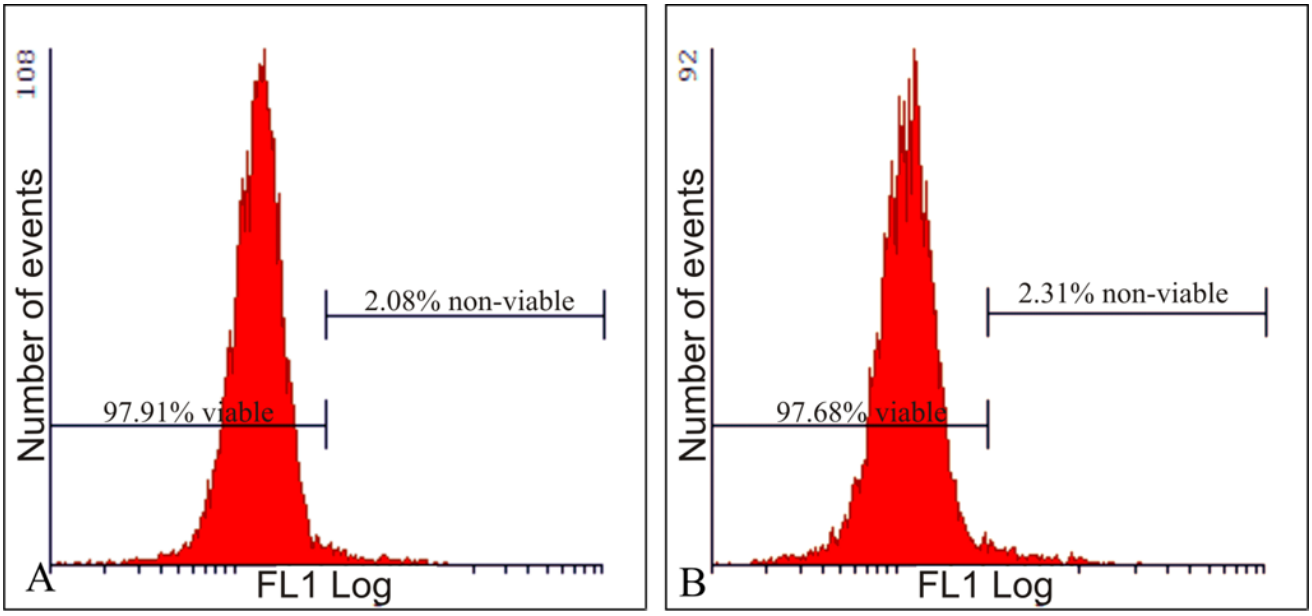

Figure 3.42: Mitochondrial membrane potential of MCF-12A cells propagated in growth medium (A) and vehicle-treated cells (B). Less than 3% of cells had reduced mitochondrial membrane potential accompanied with 97% of vehicle-treated MCF-12A cells still unaffected.

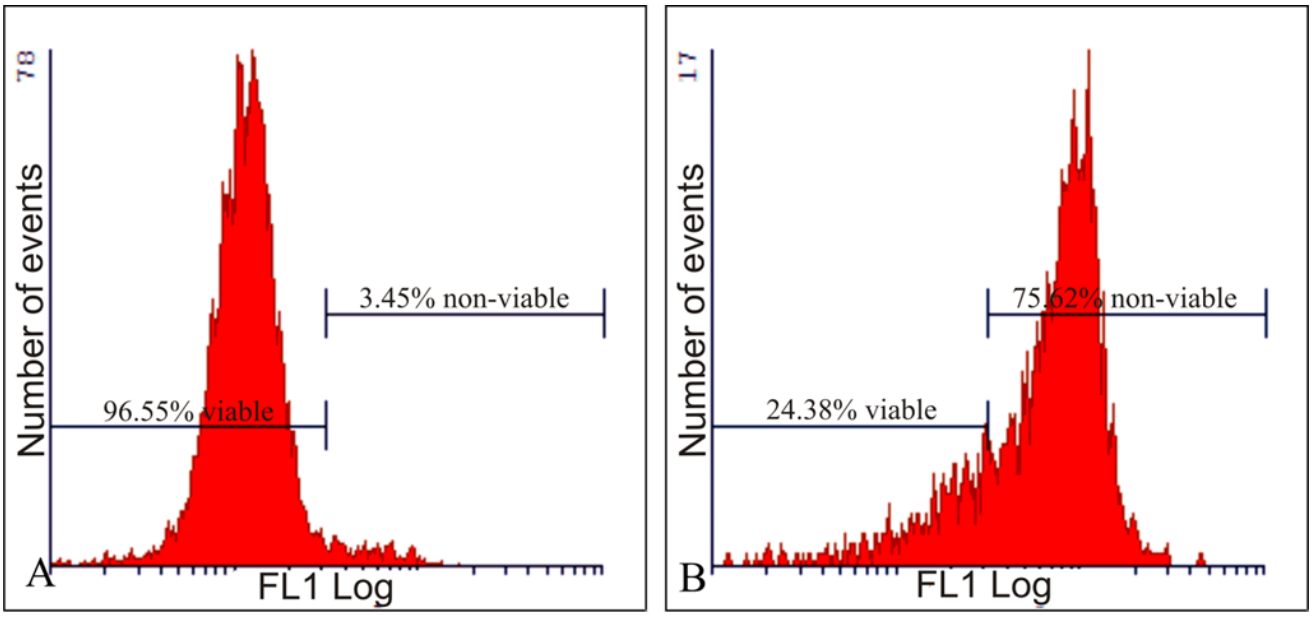

Figure 3.43: 2-MeOE2bisMATE-treated MCF-12A cells (A) revealed 4% of cells possessed reduced mitochondrial membrane potential. Cells treated with actinomycin D (B) revealed that 76% of cells had a reduction in mitochondrial membrane potential.

3.5.4 Autophagy detection

Rabbit polyclonal anti-LC3B conjugated to DyLight 488

The detection of the conversion of LC3-I to LC3-II is a useful and accurate indicator for the detection of autophagy in mammalian cells. The anti-LC3B antibody allowed for autophagy identification and confirmation (results provided by light microscopy and Hoechst 33342, propidium iodide and acridine orange staining) in the breast tumorigenic and non-tumorigenic cell lines during flow cytometry.

Flow cytometry detected increased autophagy induction in the 2-MeOE2bisMATE-treated MCF-7 cells when compared to cells propagated in growth medium and vehicle-treated samples (Figure 3.44 and Figure 3.45). A slight increase of autophagy induction in the 2-MeOE2bisMATE-treated MCF-12A cells was observed when compared to cells propagated in growth medium and vehicle-treated samples (Figure 3.46 and Figure 3.47). However, the autophagic cell death found in the MCF-7 cells was more pronounced.

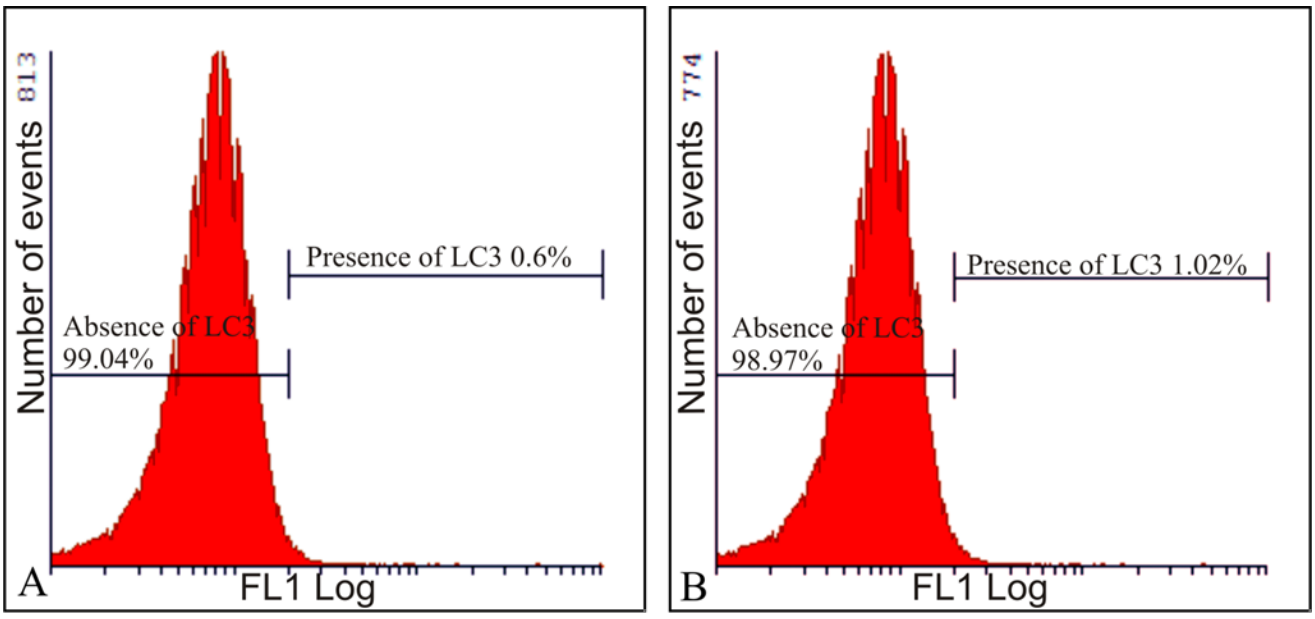

Figure 3.44: MCF-7 cells propagated in growth medium (A) and vehicle-treated cells (B) revealed insignificant induction of autophagic cell death. Cells suspended in growth medium displayed 1% of cells in autophagy and the vehicle-treated cells 0.4% of cells in autophagy.

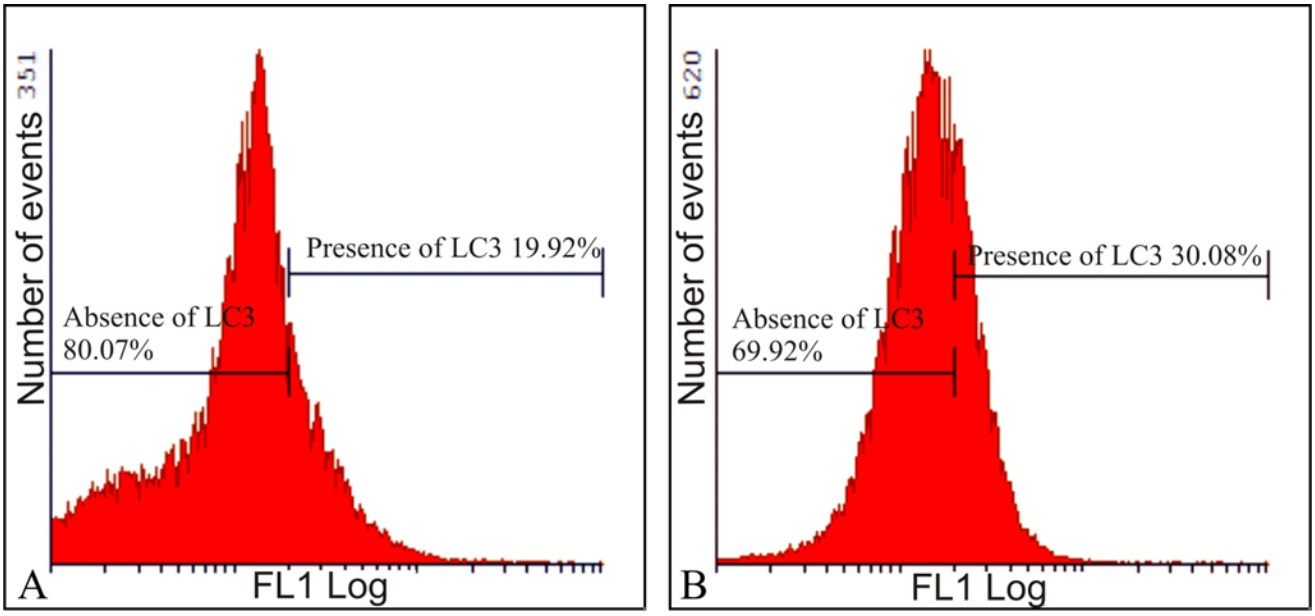

Figure 3.45: Flow cytometry revealed that 20% of 2-MeOE2bisMATE-treated MCF-7 cells (A) were present in autophagy. Starved cells showed 30% of cells present in autophagy.

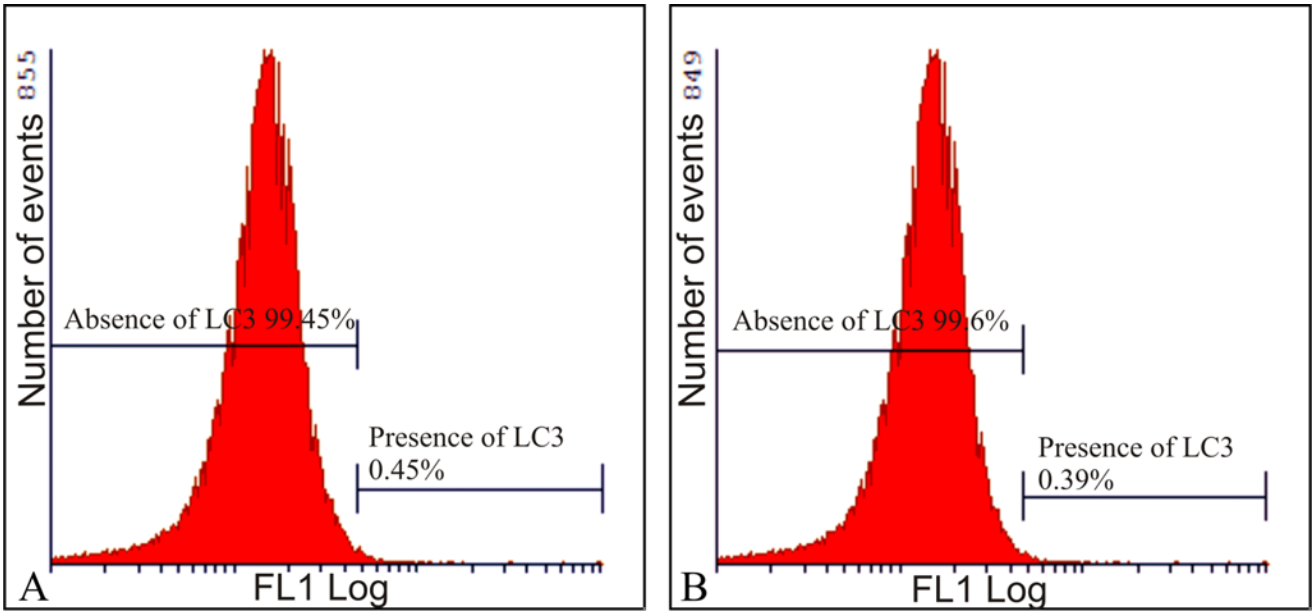

Figure 3.46: MCF-12A cells suspended in growth medium (A) and vehicle-treated cells (B) revealed less than 1% present in autophagic cell death.

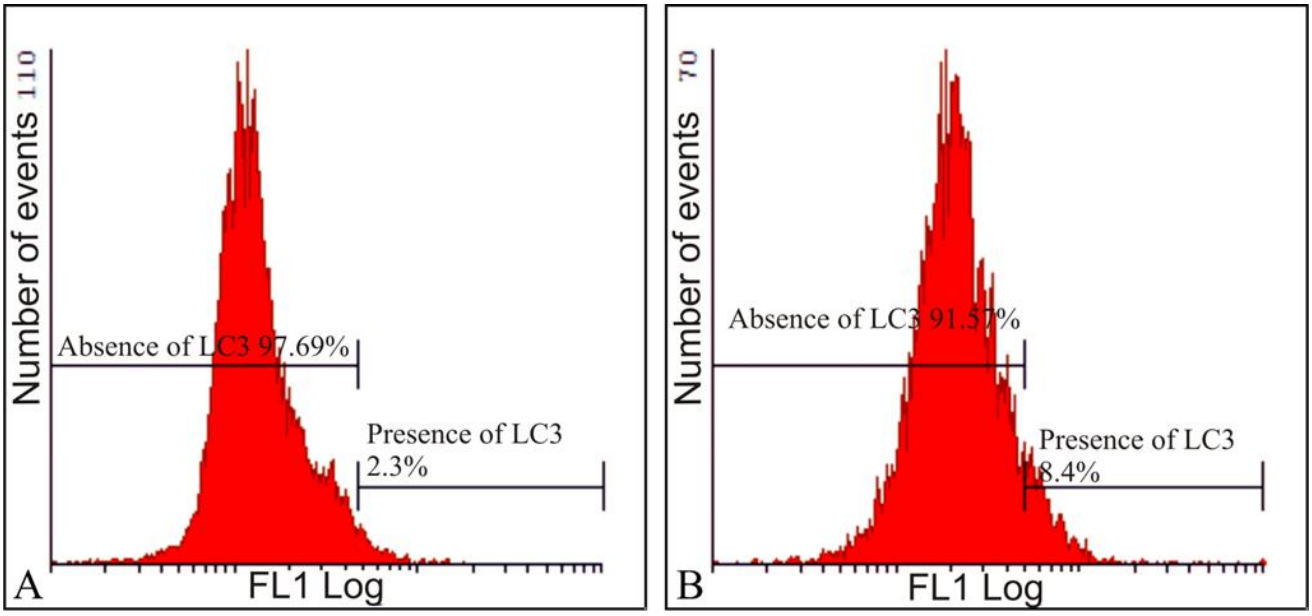

Figure 3.47: Flow cytometry analysis revealed that 2.3% of 2-MeOE2bisMATE-treated MCF-12A cells (A) were present in autophagy. MCF-12A starved cells with the purpose of inducing autophagy resulted in 8.4% of cells present in autophagy.

3.5.5 Reactive oxygen species detection

Hydrogen peroxide measurement

Hydrogen peroxide production was investigated by means of 2,7-dichlorofluorescein diacetate (DCFDA), a non-fluorescent probe, which upon oxidation by ROS and peroxides is converted to the highly fluorescent derivative DCF. Hydrogen peroxide production of 2-MeOE2bisMATE-treated MCF-7 cells increased to 10% compared to vehicle-treated cells and cells treated with hydrogen peroxide (Figure 3.48). 2-MeOE2bisMATE-treated MCF-12A cells revealed 4% hydrogen peroxide production compared to the vehicle-treated cells and cells treated with hydrogen peroxide used as a positive control for the presence of hydrogen peroxide (Figure 3.49).

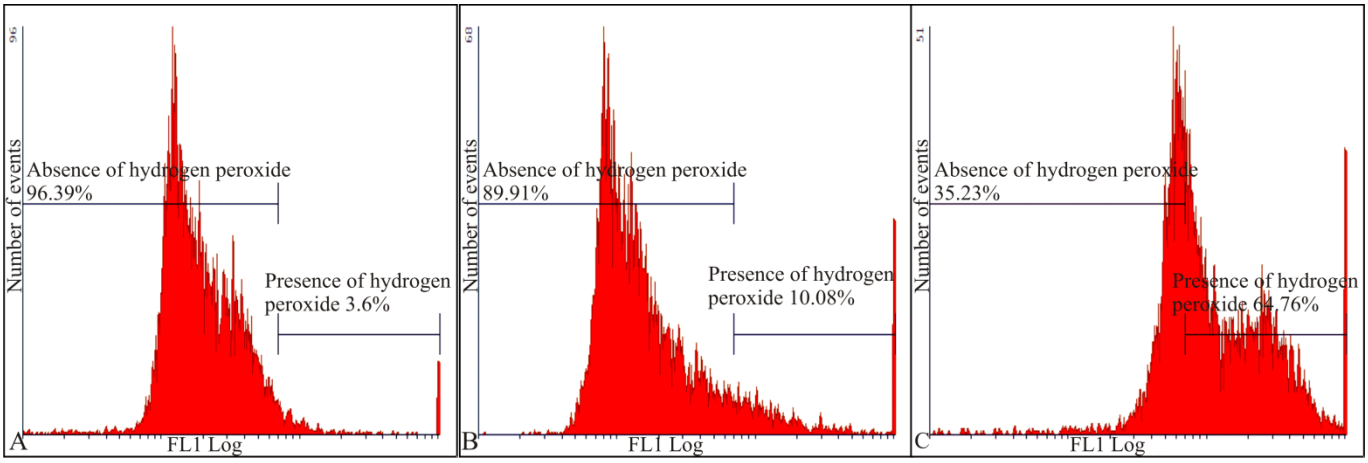

Figure 3.48: Hydrogen peroxide production investigation of vehicle-treated MCF-7 cells (A), 2-MeOE2bisMATE-treated MCF-7 cells (B) and MCF-7 cells treated with hydrogen peroxide (C). 2-MeOE2bisMATE-treated cells resulted in 10% hydrogen peroxide production when compared to vehicle-treated cells. MCF-7 cells treated with hydrogen peroxide (positive control for the presence of hydrogen peroxide) resulted in 65% hydrogen peroxide.

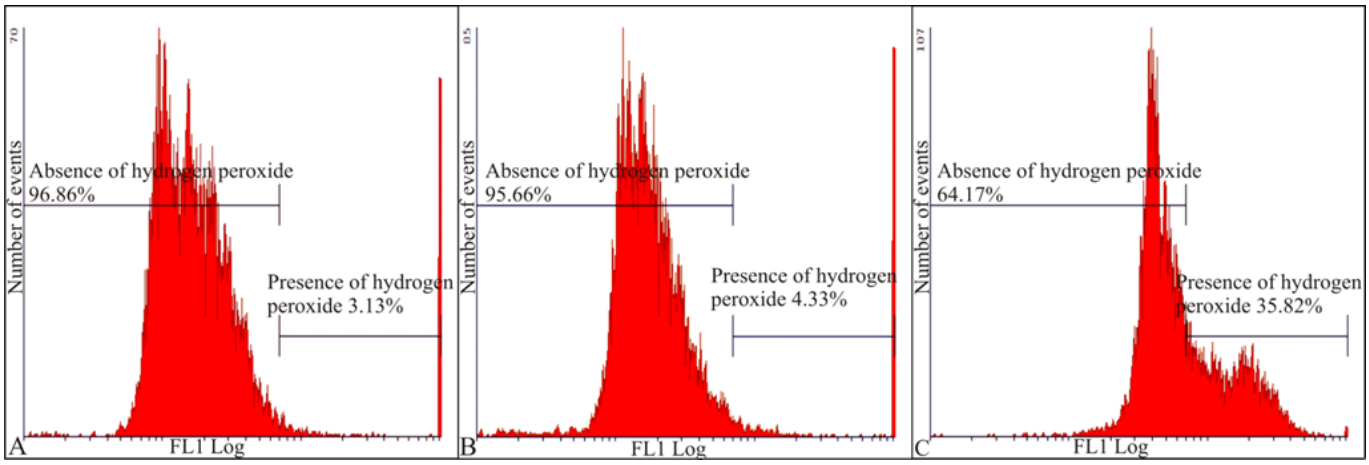

Figure 3.49: Flow cytometry analysis of hydrogen peroxide production of vehicle-treated MCF-12A cells, 2-MeOE2bisMATE-treated MCF-12A cells (B) and MCF-12A cells treated with hydrogen peroxide (C) that were used as a positive control for the presence of hydrogen peroxide. The 2-MeOE2bisMATE-treated cells had 4% hydrogen peroxide production, compared to 3% of the vehicle-treated cells. Thus, there is statistically insignificant difference between the vehicle-treated and the 2-MeOE2bisMATE-treated cells. The MCF-12A cells treated with hydrogen peroxide used as a positive control for the presence of hydrogen peroxide showed an increase to 36%.

Superoxide measurement

Superoxide generation was assessed using hydroethidine (HE) employing flow cytometry. HE is oxidized by superoxide and not by hydroxyl radicals, singlet O_2, H_2O_2 or nitrogen radicals to a red fluorescing compound. Superoxide production was detected at 11% in the 2-MeOE2bisMATE-treated MCF-7 cells when compared to vehicle-treated cells (Figure 3.50). MCF-12A 2-MeOE2bisMATE-treated cells revealed a 3% superoxide production when compared to vehicle-treated cells (Figure 3.51). The latter indicates that MCF-7 cells are more susceptible than the MCF-12A cells.

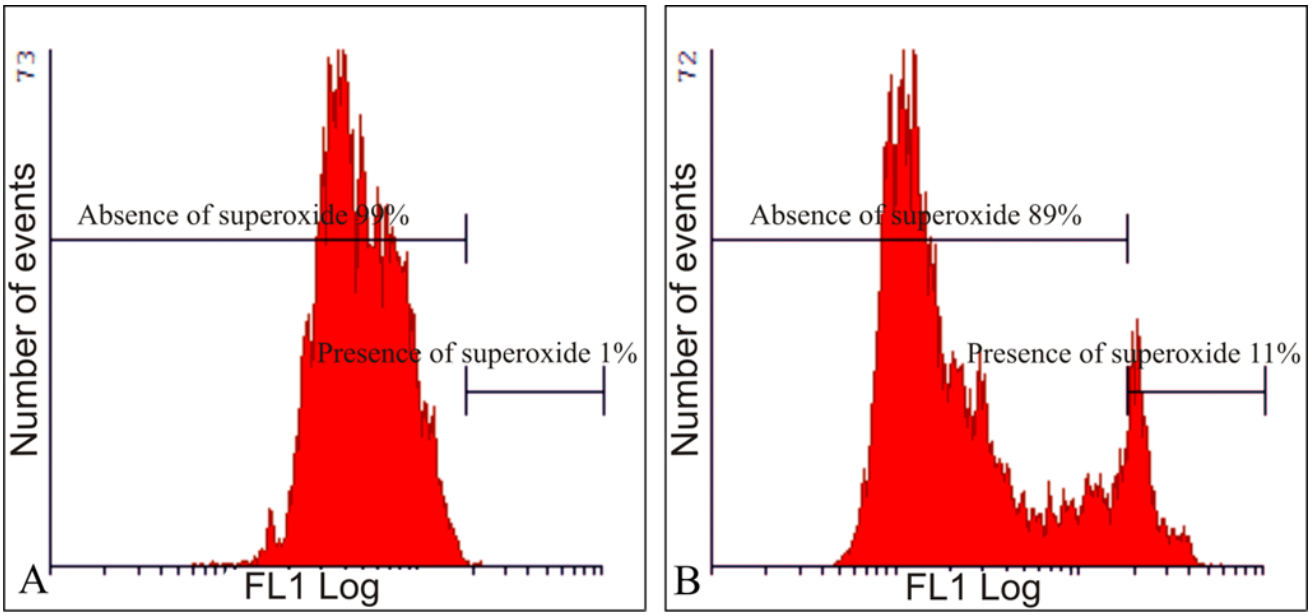

Figure 3.50: The superoxide production of vehicle-treated (A) and 2-MeOE2bisMATE-treated MCF-7 cells (B) was detected by means of flow cytometry. 2-MeOE2bisMATE-treated MCF-7 cells revealed 11% of the cells presented with superoxide production when compared to the vehicle-treated cells.

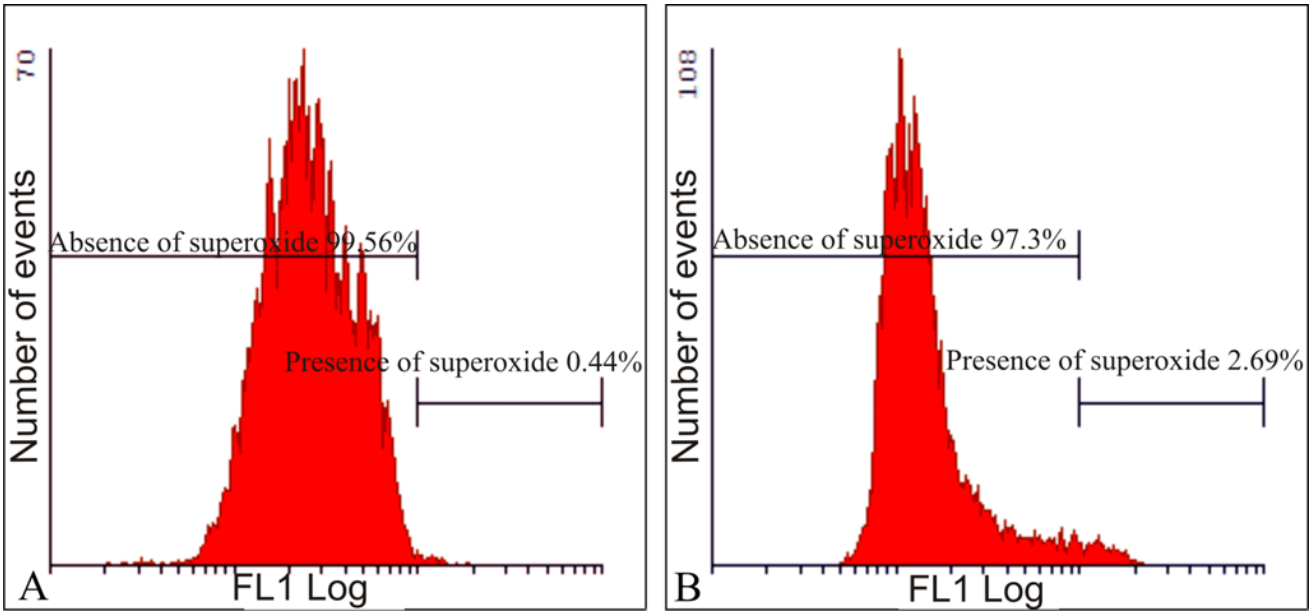

Figure 3.51: Superoxide production of MCF-12A vehicle-treated (A) and 2-MeOE2bisMATE-treated MCF-12A cells (B). Less than 1% superoxide production was detected in vehicle-treated cells, when compared to the 3% detected in MCF-12A 2-MeOE2bisMATE-treated cells.

Chapter 4

Discussion

2-MeOE2bisMATE, a novel antiproliferative analogue of 2ME2 and currently commercially unavailable, was investigated as a possible anticancer agent *in vitro* (199, 200, 201). Its possible *in vitro* differential effects on cell numbers, morphology, cytotoxicity, cell cycle progression, ROS production and induction of possible types of cell death (apoptosis and autophagy) were investigated in the tumorigenic MCF-7 cell line and the non-tumorigenic MCF-12A cell line.

Crystal violet staining revealed that 2-MeOE2bisMATE exerted antipropliferative effects on the MCF-7 cell line and the MCF-12A cell line in a dose- and time dependent manner. However, the tumorigenic MCF-7 cell line was severely affected when compared to the non-tumorigenic MCF-12A cell line after exposure to 2-MeOE2bisMATE. The antiproliferative activity was also reported by Newman *et al*. (2007) with IC_{50} values approximately 10-fold less than 2ME2 (180). In addition, Raobaikady, *et* al (2005) reported that the IC_{50} for 2-MeOE2bisMATE in the MDA-MB-231 is found at 0.33µM and was determined by cell number quantification conducting flow cytometry (201). Cell growth was also inhibited in a dose-dependent manner (0.1-1µM) in the estrogen receptor positive human breast adenocarcinoma cell line (MCF-7), prostate cancer cell line (LNACaP), highly tumorigenic estrogen receptor negative breast adenocarcinoma cell line (MDA-MB-231), human cervical adenocarcinoma cell line (HeLa), human ovarian carcinoma (A2780), androgen-sensitive human prostate adenocarcinoma cells (LNCaP) and the CAL51 human breast carcinoma cell line (14, 174, 175, 199, 200, 201). In CAL51 cells the IC_{50} for 2-MeOE2bisMATE was reported as 0.5µM (178). Newman *et al*. (2007) observed that 2-MeOE2bisMATE inhibited cell growth of human umbilical vein endothelial cells (HUVEC) where the IC_{50} is <50nm and suggested that 2-MeOE2bisMATE may be a potent inhibitor of angiogenesis (180). *In vivo* antipropliferative activity was reported in xenografts derived from estrogen receptor positive human breast adenocarcinoma wild type cell line ($MCF\text{-}7_{WT}$), mitoxantrone resistant breast adenocarcinoma cell line (MCF-7 MR), drug resistant human adenocarcinoma cell line ($MCF\text{-}7\ _{DOX}40$), prostate cancer cell line (LNACaP), MDA-MB-435, human umbilical vein endothelial cells (HUVEC) and prostate hormone independent PC-3 xenograft model (173, 174, 179, 180, 181, 202).

The influence of 2-MeOE2bisMATE on LDH production was investigated by means of a colorimetric assay based on reduction of the tetrazolium salt MTT in a NADH-coupled enzymatic reaction to a reduced form of MTT. Reduced pyridine nucleotide cofactor, NADH, is responsible for MTT reduction and is associated not

only with mitochondria, but also with non-mitochondrial membranes and the cytoplasm. NADH is produced by means of the Krebs cycle and glycolysis in the mitochondria and cytoplasm, respectively. Therefore reduction of MTT is regarded as an indication of metabolic activity (203, 204). LDH is a soluble cytosolic enzyme that catalyzes the interconversion of lactate and pyruvate and contributes to the acification of the cytosol. Cells release LDH during injury or cell damage, following the loss of membrane integrity consequential from either apoptosis or necrosis (205). This study revealed that 2-MeOE2bisMATE did not increase LDH production in a statistically significant manner and the cell membrane was not compromised to allow for acute leakage of LDH in 2-MeOE2bisMATE-treated cells when compared to the vehicle-treated cells. Previous reports indicated that the precursor molecule, 2ME2, increased LDH production in a cell line derived from bone marrow of an individual with myelodysplastic syndrome (MDS-RAEB MUTZ-1 cell line) and the human promyelocytic leukaemia cell line (HL-60 cell line) (206, 207). Nonetheless, the relationship between LDH and apoptosis remains elusive and literature regarding the influence of 2ME2 and 2-MeOE2bisMATE on LDH production is limited.

Qualitative data obtained by means of PlasDIC, light microscopy, transmission electron microscopy and fluorescent microscopy revealed that 2-MeOE2bisMATE exerts differential effects on morphology of MCF-7 and MCF-12A cell lines. PlasDIC demonstrated decreased cell density, shrunken cells and clearly visible apoptotic bodies in the MCF-7 cells. MCF-12A cells displayed rounded cells with the cell density unaffected. Light microscopy revealed hypercondensed chromatin, apoptotic bodies and compromised cell density in the MCF-7 cell line. Hypercondensed chromatin, membrane blebbing, budding and mitochondria migration towards the nucleus were observed in the 2-MeOE2bisMATE MCF-7-treated cells by means of TEM. All of the above-mentioned characteristics observed in the treated-cells are hallmarks of apoptosis. The induction of apoptosis by 2-MeOE2bisMATE is supported in previous data, where 2-MeOE2bisMATE induced this form of cell death in MCF-7, prostate cancer cells (PC-3), human umbilical vein endothelial cells (HUVEC) and the human breast adenocarcinoma CAL51 cell line (179, 180). Wood *et al.* (2004) reported that by using the terminal deoxynucleotidyl transferase nick end labelling (TUNEL) assay, it was revealed that 5µM 2-MeOE2bisMATE induced apoptosis in CAL51 cells (178). In another study using Annexin V-FITC by conducting flow cytometry apoptosis induction was found in PC-3 cells, MCF-7_{WT} cells and MCF-7_{DOX} cells.

TEM also demonstrated several intracellular vacuoles in the 2-MeOE2bisMATE MCF-7-treated cells, but these were absent in the MCF-12A cells. The latter is an indication of cell death also occurring via autophagy. Acridine orange was employed during fluorescent microscopy as a lysosomotropic fluorescent compound that serves as a tracer for acidic vesicular organelles including autophagic vacuoles and lysosomes. Increased

lysosomal staining detected by means of fluorescent microscopy also indicated that 2-MeOE2bisMATE induced autophagy in MCF-7 cells and MCF12A cells. However, lysosomal staining was more prominent in treated-MCF-7 cells when compared to treated-MCF-12A cells, indicating MCF-7 cells are more prone to autophagy induction when treated with 2-MeOE2bisMATE when compared to MCF-12A cells. Since observations of autophagy have not been associated with 2-MeOE2bisMATE-treated cells in previous studies, additional studies where employed in order to investigate whether autophagic activity was present or increased in 2-MeOE2bisMATE-treated cells.

Qualitative data was supplied for the investigation of autophagy induction by 2-MeOE2bisMATE in tumorigenic MCF-7 and non-tumorigenic MCF-12A cell lines by means of flow cytometry employing rabbit polyclonal anti-LC3B conjugated to DyLight 488. The latter confirmed that autophagic cell death was induced in both MCF-7 cells and MCF-12A cell lines when treated with 2-MeOE2bisMATE. However, MCF-12A cells was less prominently affected by 2-MeOE2bisMATE, again indicating that MCF-7 cells are more susceptible to 2-MeOE2bisMATE treatment. As previously mentioned, no literature exists regarding 2-MeOE2bisMATE's capability to induce autophagy. 2ME2, its precursor molecule, induced autophagy in cell lines namely human glioblastoma-astrocytoma epithelial-like cell line (U87), human cervical adenocarcinoma cells (HeLa), transformed human embryonic kidney cells (HEK293), osteosarcoma cells and ewing sarcoma cells (151, 206). 2ME2 induced autophagy in Ewing sarcoma cells by initiating both p53 and JNK pathways. Furthermore, p53 regulates JNK activation which in turn controls autophagy through two different mechanisms. The JNK pathway promotes Bcl-2 phosphorylation resulting in the dissociation of the Beclin-1 Bcl-2 complex and on the other hand it leads to the upregulation of Damage-Regulated Autophagy Modulator (DRAM), a p53 target gene. This indicates that the JNK and p53 pathway is activated by 2-MeOE2bisMATE resulting in Bcl-2 phosphorylation leading to autophagy (208). This is supported by the observation of 2-MeOE2bisMATE exposure results in p53 protein phosphorylation in MCF-7_{WT} cells. Immunoblotting revealed that 2-MeOE2bisMATE exposure resulted in Bcl-2 phosphorylation in MCF-7_{WT} and MCF-7_{DOX} cells (180, 181).

Cell cycle progression revealed a significant apoptotic peak in MCF-7 cells treated with 2-MeOE2bisMATE. MCF-12A cells also demonstrated an apoptotic peak, however, less prominent when compared to MCF-7 cells treated with 2-MeOE2bisMATE. Previous reports conducting flow cytometry indicated that 2-MeOE2bisMATE induces a G_2M arrest followed by induction of apoptosis in cell lines including MCF-7_{DOX}40, MCF-7 MR and MDA-MB-231 (176, 202). Day *et al.* (2009) observed similar results to this project after 24h exposure to 2-MeOE2bisMATE in the human 2-MeOE2bisMATE-resistant cell line (A2780.140) derived from the human ovarian carcinoma cell line (A2780) resulted in G_2M arrest; however, 48h exposure resulted in a sub-G_1 peak accompanied with no changes in the cell cycle distribution (202).

Mitotic indices indicated a statistically insignificant increase in the number of cells with morphological characteristics of metaphase and a decrease in the number of cells with morphological characteristics of prophase, anaphase, telophase and interphase in the MCF-7 and MCF-12A cell lines. The statistically insignificant increase of cells present in metaphase was more prominent in the MCF-7 cell line when compared to MCF-12A cell line.

Data supplied from Annexin V-FITC indicated that 2-MeOE2bisMATE induced apoptosis in both MCF-7 and MCF-12A cells. However, MCF-7 cells were more susceptible to apoptotic cell death induced by 2-MeOE2bisMATE when compared to MCF-12A cells. As previously mentioned, 2-MeOE2bisMATE induces apoptotic cell death in various cell lines, including MCF-7, MDA-MB-321, prostate cancer cells (PC-3), human umbilical vein endothelial cells (HUVEC), human ovarian cancer cell line (A2780), androgen-sensitive human prostate cancer cells (LNCaP) and the human breast adenocarcinoma CAL51 cell line (178, 178, 180, 199). Furthermore, studies have revealed that 2-MeOE2bisMATE exposure to A2780, LNCaP results in the activation of caspase 3 and 7 (199). 2-MeOE2bisMATE exposure in the CAL51 cells resulted in rapid activation of caspase 3 and 9. Interference of FAS- or TRAIL-receptor function did not prevent induction of apoptosis by 2-MeOE2bisMATE in the CAL51 cell line, indicating involvement of the intrinsic apoptosis pathway being activated (178). TRAIL-resistant CAL51 cells treated with TRAIL and 2-MeOE2bisMATE resulted in apoptosis, suggesting that 2-MeOE2bisMATE can overcome TRAIL-resistance by means of activating downstream caspases (178).

Investigation of the possible *in vitro* influence of 2-MeOE2bisMATE on the mitochondrial membrane potential was investigated based on an early event in apoptosis whereby the mitochondrial membrane permeability transition pores (MPT) open (209). Pores open when exposed to high Ca^{2+} content or inorganic phosphate, NAD(P)H, alkaline pH or ROS. The latter allows for the passing of low molecular weight accompanied with water through the mitochondrial membrane, resulting in mitochondrial swelling and release of cytochrome *c* (210). Data revealed a reduction of the mitochondrial membrane potential in both 2-MeOE2bisMATE-treated cell lines. However, the *in vitro* effect was again more severe in the 2-MeOE2bisMATE MCF-7-treated cells when compared to the non-tumorigenic MCF-12A cell line. Although literature addressing effects of 2-MeOE2bisMATE on the mitochondrial membrane potential is limited, 2-MeOE2bisMATE was found to depolarise the mitochondrial membrane potential in A2780, LNCaP and MCF-7 cell lines (199). Nonetheless, the data obtained from this project indicates that 0.4µM 2-MeOE2bisMATE exposure for 48h induces apoptosis more prominently in MCF-7-treated cells when compared to MCF-12A-treated cells. Furthermore, 2-MeOE2bisMATE induced the activation of the mitochondrial (intrinsic) pathway in the MCF-7 cell line with caspase 9 activation (178). Mitochondrial

membrane reduction occurs due to increased ROS levels (211). 2-MeOE2bisMATE increased hydrogen peroxide to 10% in MCF-7 cells and 4% in MCF-12A cells demonstrating the higher susceptibility of 2-MeOE2bisMATE to tumorigenic MCF-7 cells when compared to non-tumorigenic MCF-12A cells. Superoxide production was increased to 11% in the tumorigenic both MCF-7 cell line and 3% in the non-tumorigenic MCF-12A cell line; confirming the heightened susceptibility of the tumorigenic MCF-7 cell line to 2-MeOE2bisMATE when compared to the non-tumorigenic cell line. However, the source and processing of ROS and the role they play in 2-MeOE2bisMATE-induced growth inhibition and cell death remains to be elucidated. The novel discovery regarding the *in vitro* effect of 2-MeOE2bisMATE on ROS production in tumorigenic and non-tumorigenic lines has not been reported previously. However, 2ME2 increased ROS production in ewing sarcoma cells, myeloid leukaemia U937 cells, myeloid leukaemia HL-60 cell line, human acute T cell leukaemia cells (Jurkat cells), HeLa cells and MCF-7 cells (212, 213, 214, 215, 216).

ROS and autophagy are both implicated in cell survival and death pathways. The presence of ROS at high levels is harmful to cells leading to PCD. At low levels, ROS serve as a signaling molecule in various growth and survival pathways (57, 217, 218, 219, 220). Starvation conditions of Chinese Hamster Ovarian cells (CHO) results in ROS formation leading to the induction of autophagy (217). Hydrogen peroxide exposure in HEK293, U87 and HeLa cells results in autophagy induction with the presence of autophagosomes and autolysomes (218). ROS induce autophagy by means of Atg4, catalase and the mitochondrial electron transport chain. Atg4 cleaves LC3 from the autophagosome membrane during autophagy and Atg8 at the C-terminus to facilitate lipidation. ROS oxidizes cellular components namely proteins, lipids and DNA thus compromising cell structures and cellular functions (151). Increased ROS production results in the destabilisation of the lysosomal membrane by means of excessive peroxidation of membrane lipids. The lysosomal membrane destabilisation results in cathepsin release that acts in the signaling pathway of apoptosis. Furthermore, intralysosomal iron generated from degraded metallo proteins reacts with hydrogen peroxide to produce highly reactive hydroxyl radicals that leads to peroxidation of the lysosomal membrane (220). The mitochondrial electron transport chain continuously leaks electrons that generate superoxide and hydrogen peroxide (151). Caspase 8 inhibition resulted in catalase depletion that lead to prolonged hydrogen peroxide signaling and severe increased ROS levels and consequently lipid accumulation, lipid oxidation and ultimately autophagic cell death (57, 151). An acute ROS imbalance leads to significant cellular damage resulting in turnover of the organelles by means of autophagy or the destruction of the entire cell by apoptosis. Various publications have reported that ROS mediates apoptosis and is dependent on p38. Apoptosis signal-regulated kinase 1 (ASK1), an evolutionary conserved mitogen-activated protein 3-kinase activates JNK and

p38 MAPK may also be activated by ROS. In addition, oxidative stress results in a positive feedback loop in the ASK1-p38-TNF-α pathway which enhances ROS-mediated apoptosis (151).

2-MeOE2bisMATE thus induces both autophagy and apoptosis. On molecular levels apoptosis and autophagy share common signaling transduction pathways including PI3K/AKT signal pathways, MAPK/ERK1/2 signal pathways and the mitochondrial pathways (221). PI3K/AKT signal pathways inhibit apoptosis and autophagy (222). PI3K/Akt signal pathways are inhibited by a p53-inducible protein (PH domain) (223). Furthermore, p53 can induce apoptosis by upregulating the expression of a direct p53 target gene known as DRAM. As previously mentioned, beclin-1 is involved in autophagic cell death. Beclin-1 also interacts with major anti-apoptotic Bcl family members (222). The interaction between Bcl-2 and beclin-1 may function as a rheostat that maintains autophagy at levels that are more compatible with cell survival than cell death. Nonetheless, disruption between the beclin-1 BH3 domain and Bcl-2 increases autophagic cell death (223).

Thus, 2-MeOE2bisMATE inhibits cellular growth in tumorigenic MCF-7 and non-tumorigenic MCF-12A cells in a dose- and time-dependent manner with the MCF-7 cell line being the more susceptible of the two lines. Growth inhibition and hallmarks of apoptosis and autophagy were found in the morphological studies. Flow cytometry studies demonstrated a reduction in the mitochondrial membrane potential, reactive oxygen species generation and induction of apoptosis and autophagy in both MCF-7 and MCF-12A cell lines. All of the above-mentioned effects were observed more prominently in the MCF-7 cell line when compared to the MCF-12A cell line.

Chapter 5

Conclusion

In conclusion, 2-MeOE2bisMATE inhibited cellular proliferation in a dose- and time-dependent manner in the MCF-7 and MCF-12A cell lines. However, the anti-proliferative effects in the tumorigenic MCF-7 cell line were more pronounced when compared to the non-tumorigenic MCF-12A cell line. LDH production was not statistically increased by 2-MeOE2bisMATE. Morphological changes was also induced by 2-MeOE2bisMATE in both cell lines indicating the presence of autophagy and apoptosis. The latter morphological changes were more prominent in the tumorigenic MCF-7 cells when compared to the non-tumorigenic MCF-12A cells. Flow cytometrical data demonstrated the presence of a substantial sub-apoptotic peak, reduction in the mitochondrial membrane potential, increased ROS production and the induction of cell death via apoptosis and autophagy. All of the above-mentioned *in vitro* effects of 2-MeOE2bisMATE was observed more prominently in the tumorigenic MCF-7 cell line when compared to the non-tumorigenic MCF-12A cell line.

Future studies will include investigating differential cell signaling events exerted in adenocarcinoma cell lines (MCF-7) and the non-tumorigenic epithelial breast cell line (MCF-12A) respectively by analyzing its influence on adenosine-5-triphosphate generation, intracellular Ca^{2+} mobilization, protein aggregation, caspases 6 and caspase 8 activation, gene expression and protein expression. Gene and protein expression studies will aid in identifying potential targets for further experiments. Furthermore, the *in vitro* signaling events will be investigated of other sulphamoylated 2ME2 analogues in adenocarcinoma cell lines and the non-tumorigenic epithelial breast cell line.

Data obtained from this study contributes the unraveling the signaling mechanism used by 2-MeOE2bisMATE. As 2-MeOE2bisMATE is a potential anticancer agent, it is of vital importance to investigate the effects on tumorigenic and non-tumorigenic cell lines. In addition, this project supports the notion of a crosstalk between different types of cell death including apoptosis and autophagy by way of lysosomes and mitochondria.

References

1. Matatiele PR, Van den Heever WMJ. Breast cancer profiles of women presenting with newly diagnosed breast cancer at Univeritas Hospital (Bloemfontein, South Africa). *SA Fam Prac* 2008; 50(6): 48-49.
2. Emedicine.Medsacape. United States of America. Breast cancer evaluation, reported by Singal H, Cohel MS, Kaur K. C2009 [updated 17 Dec 2009; cited 4 April 2010]. Available from: http://emedicine.medscape.com/article/263733-overview
3. Gerber B, Freund M, Reimer T. Recurrent breast cancer. *Dtsch Arztebl Int* 2010; 107(6): 85-91.
4. Kwan ML, Kushi LH, Weltzien E, Maring B, Kutner SE, Fulton RS, et al. Epidemiology of breast cancer subtypes in two prospective cohort studies of breast cancer survivors. *Breast Cancer Res* 2002; 11(3): R31.
5. Kelsey JL, Berstein L. Epidemiology and prevention of breast cancer. Annu. Rev. *Public Health*. 1996; 17: 47-67.
6. Mayi-Tsong S, Kamga H, Meye JF, Belembaogo E. Risk factors of bilaterazation of breast cancer: description of five cases in Libreville (Gabon) and review of the literature. *Med Trop (Mars)* 2009: 69(9): 583-586.
7. Runnebaum IB, Nagarajan M, Bowman M, Soto D, Sukumar S. Mutations in p53 as a potential molecule marker for human breast cancer. *Proc Natl Acad Sci* U S A 1991; 88(23): 10657-10661.
8. Potter P. "Westernizing" Women's Risks? Breast Cancer in Lower-Income Countries. *N Engl J Med* 2008; 358 (3): 213-216.
9. Kelsey JL, Berkowitz GS. Breast cancer epidemiology. *Cancer Res* 1988; 48(20): 5615-5623.
10. Shapiro CL, Recht A. Side effects of adjuvant treatment of breast cancer. *N Engl J Med* 2001; 344(26): 1997-2008.
11. Evans KD, Weiss B, Knopp M. High-intensity focused ultrasound (HIFU) for specific therapeutic treatments a literature review. *JDMS* 2007 Nov/Dec; 23: 319-327.
12. Popat S, Smith IE. Breast cancer. *Update Cancer Ther* 2009; 1: 187-210.
13. Chen S, Masri S, Wang X, Phung S, Yuan YC, Wu X. What do we know about the mechanism of aromatse inhibitor resiostance. *J Steroid Mol Biol* 2006; 102(1-5): 232-240.
14. Raobaikady B, Purohit A, Chander SK, Woo LWL, Leese MP, Potter BVL, et al. inhibition of MCF-7 breast cancer cell proliferation and in vivo steroid sulphatase activity by 2-methoxyestradiol-bis-sulphamate. *J Steroid Biochem Mol Biol* 2003; 84: 351-358.
15. Jonat W, Howell A, Blomqvist C, Eiermann W, Winbad G, Tyrrell C, et al. A romdomised trail comparing two doses of the new selective aromatase inhibitor anastrozole (arimidex) with megastrol acetate in postmenopausal patients with advanced breast cancer. *Eur J Cancer* 1996; 32A(3): 404-412.
16. Thiery JP, Sastre-Garau X, Vincent-Salomon B, Sigal-Zafrani X, Pierga JY, Decraene C, et al. Challenges in the stratification of breast tumors for tailored therapies. *Bull Cancer* 2006; 93(8): E81-89.

17. Partridge AH, Burstein HJ, Winer EP. Side effects of chemotherapy and combined chemohormonal therapy in women with early stage breast cancer. *J Natl Cancer Inst Monogr* 2001; 30: 135-142.
18. Moy B, Goss PE. Lapatininb: Current status and future directions on breast cancer. *Oncologist* 2006; 11: 1047-1057.
19. Platia MP, Fenci MD, Elkind-Hirsch KE, Canick JA, Tulchinsky D. Estrone sulfatase activity in the human brain and estrone sulfate levels in the normal menstrual cycle. *J Steroid Biochem* 1984; 21(3): 237-241.
20. Utsumi T, Yoshimura N, Takeuchi S, Maruta M, Maeda K, Harada N. Elevated steroid sulfatase expression in breast cancers. *J Steroid Biochem Mol Biol* 2000; 73: 141-145.
21. Duncan L, Purohit A, Howarth M, Potter BVL, Reed MJ. Inhibition of estrogen sulfatase activity by estrone-3-methylthiophosphonate: potential therapeutic agent in breast cancer. *Cancer Res* 1993; 53: 298-303.
22. Evans TR, Rowlands MG, Silva MC, Law M, Coombes RC. Prognostic significance of aromatase and estrone sulfatase enzymes in human breast cancer. *J Steroid Biochem Mol Biol* 1993; 44: 583-587.
23. Billich A, Nussbaumer P, Lehr P. Stimulation of MCF-7 breast cancer cell proliferation by estrone sulphate and dehydroepiandrosterone sulphate: inhibition by novel non-steriodal steroid sulfatase inhibitors. *J Steroid Biochem Mol Biol* 2000; 72: 225-235.
24. Nussbaumer p. Billich A. steroid sulphatase inhibitors: their potential in the therapy of breast cancer. *Curr Med Chem* 2005; 5: 607-528.
25. Raobaikaby B, Purohit A, Chander SK, Woo L, Leese MP, Potter VL, et al. Inhibition of MCF-7 breast cancer cell proliferation and in vivo steroid sulphatase activity by 2-methoxyoestradiol-bis-sulphamate. *J Steroid Biochem Mol Biol* 2003; 84: 351-358.
26. Stanway SJ, Delavault P, Purohit A, Woo LW, Thurieau C, Potter BV, *et al*. Steroid sulfatase: a new target for the endocrine therapy of breast cancer. *Oncologist* 2007; 12: 370-374.
27. Leese MP, Hejaz HA, Mahon MF, Newman SP, Purohit A, *et al*. A-ring-substituted estrogen-3-O-sulphamates: potent multitargeted anticancer agents. *J Med Chem* 2005; 48: 5243-5256.
28. Budirahardja Y, Gönczy P. Coupling the cell cycle to development. *Development* 2009; 136(17): 2861-2872.
29. Sridhar J, Akula N, Pattabiraman N. Selectivity and potency of cyclin-dependent kinase inhibitors. *The AAPS J* 2006; 8(1): E205-E221.
30. Inzé D. Green light for the cell cycle. *The EMBO J* 2005; 24: 657-662.
31. Nigg EA. Cyclin-dependent protein kinases: key regulators of the eukaryotic cell cycle. *Bioassays* 1995; 17(6): 471-480.
32. Miller ME, Cross FR. Cyclin specificity: How many wheels do you need on a unicycle? *J Cell Sci* 2001; 114: 1811-1820.

33. Chivukula RR, Mendell JT. Circular reasoning: microRNAs and cell cycle control. *Trends Biochem Sci* 2008; 33(10): 474-481.
34. Díaz-Martínez LA, Giménez-Abián JF, Clarke DJ. Chromosome cohesion- rings, knots, orcs and fellowship. *J Cell Sci* 2008; 121(13): 2107-2114.
35. Bell SP, Dutta A. DNA replication in eukaryotic cells. *A. Rev. Biochem* 2002; 71: 333-374.
36. Duncker BP, Chesnokov IN, McConkey BJ. The origin recognition complex protein family. *Genome Biol* 2009; 10(3): 214.1-214.8.
37. Sivaprasad U, Machida YJ, Dutta A. APC/C- master controller of origin licensing? *Cell Division* 2007;2(8).
38. Balk SP, Knudsen KE. AR, the cell cycle and prostate cancer. *Nuclear receptor signaling* 2008; 6: 1-12.
39. Kitagawa R., Law E, Tang L, Rose AM. The Cdc20 homolog, FZY-1, and its interacting protein, IFY-1, are required for proper chromosome segregation in *Caenorhabditis elegans*. *Curr Biol* 2002; 12, 2118–2123.
40. Queralt E, Uhlmann F. Cdk-counteracting phosphatases unlock mitotic exit. *Curr Opin Cell Biol* 2008; 20(6): 661-668.
41. Furuta T, Tuck S, Kirchner J, Koch B, Auty R, Kitagawa R, et al (2000). EMB-30: an APC4 homologue required for metaphase-to-anaphase transitions during meiosis and mitosis in *Caenorhabditis elegans*. *Mol. Biol. Cell 11*, 1401–1419.
42. Li M, Zhang P. The function of APC/C^{CDH1} in cell cycle and beyond. *Cell Devision* 2009;4(2).
43. Matyskiela ME, Rodrigo-Brenni MC, Morgan DO. Mechanisms of ubiquintin transfer by the anaphase-promoting complex. *J Biol* 2009; 8: 92.1-92.10.
44. Belizario JE, Alves J, Garay-Malpartida M, Occhiucci JM. *Curr Protein Pept Sci* 2008; 9: 210-220.
45. Fung TK, Siu WY, Yam CH, Lau A, Poon RYC. Cyclin F is degraded during G_2-M by mechanisms fundamentally different from other cyclins. *J Biol Chem* 2002; 277(38): 35140-35149.
46. Thornton TM, Rincon M. Non-classical P38 Map Kinase functions: cell cycle checkpoints and survival. *Int J Bio Sci* 2009; 5: 44-51.
47. Willis N, Rhind N. Regulation of DNA replication by the S-phase DNA damage checkpoint. *Cell Div* 2009; 4(13): 1-10.
48. Pardee AB. G1 events and regulation of cell proliferation. *Science* 1989; 246: 603-508.
49. Weinburg RA. The restinoblastoma protein and cell cycle control. *Cell* 1995; 81: 323-330.
50. Todd R, Hinds PW, Munger K, Rustgi AK, Opitz OG, Suliman Y, Wong DT. Cell cycle dysregulation in oral cancer. *Crit Rev Oral Biol* 2002; 13(1): 51-61.
51. Tyner AL. A new year, a new role for p21. *Cell Cycle* 2009; 8(2): 183-184.
52. Gillis LD, Leidal AM, Hill R, Lee PWK. $P21^{Cip1/WAF1}$ mediates cyclin B1 degradation in response to DAN damage. *Cell Cycle* 2009; 8(2): 253-256.

53. May KM, Hardwick KG. The spindle checkpoint. *J Cell Sci* 2006; 119(20): 4139-4142.
54. Ciliberto A, Shah JV. A quantitative systems view of the spindle assembly checkpoint. *EMBO J* 2009; 28: 2162-2173.
55. Fang G, Yu H, Kirschner MW. Control of mitotic transitions by the anaphase-promoting complex. *Philos Trans R Soc Lond Biol Sci* 1999; 354(1389): 1583-1590.
56. Elmore S. Apoptosis: a Review of programmed cell death. *Toxicol Pathol* 2007; 35: 495-516.
57. Yu L, Wan F, Dutta S, Welsh S, Liu Z, Freundt E, et al. Autophagic programmed cell death by selective catalase degradation. *PNAS* 2006; 103(13): 4952-4957.
58. Kroemer G, Galluzzi L, Van de Nabeele P, Abrams J, Alnemri ES, Baehrecke EH, et al. Classification of cell death: recommendations of the nomenclare committee on cell death 2009. *Cell Death Differ* 2009; 16: 3-11.
59. Taatjes DJ, sobel BE, Budd RC. Morphological and cytochemical determination of cell death by apoptosis. *Histochem Cell Boil* 2008; 129: 33-43.
60. Hergartner MO. The biochemistry of apoptosis. *Nature* 2000; 407: 770-776.
61. Igney, FH, Krammer P H. Death and anti-death: tumour resistance apoptosis. *Nat Rev Cancer (2002)*; 2, 277–88.
62. Balasubramanian K, Mirnikjoo B, Schroit AJ. Regulated externalization of Phosphatidylserine at the Cell Surface: Implications for apoptosis. *Biol Chem* 2007; 22; 282(25): 18357-18364.
63. Kumar S. Caspase function in programmed cell death. *Cell Death Differ* 2007; 14: 32-43.
64. Wolf BB, Green DR. Suicidal tendencies: apoptotic cell death by caspase family proteinases. *J Biol Chem* 1999; 274(29): 20049-20052.
65. Bao Q, Shi Y. Apoptosome: a platform for the activation of initiator caspases. *Cell Death Differ* 2007; 14: 56-65.
66. Sadowski DK, Coy JF, Mier W, Hug H, Los M. Caspases-their role in apoptosis and other physiological processes as revealed by knock out studies. *Arch Immunol Ther Exp* 2002; 50(1): 9-34.
67. Allan LA, Clarke PR. Apoptosis and autophagy: regulation of caspase-9 by phosphorylation. *FEBS* 2009; 276: 6063-6073.
68. Khosravi-Far R, Esposti MD. Death receptor signals to mitochondria. *Cancer Biol Ther* 2004; 3(11): 1051-1057.
69. Peter ME, Krammer PH. The CD95(APO-1/Fas) DISC and beyond. *Cell Death Differ* 2003; 10: 26–35.
70. Jin Z, EL-Deiry WS. Overview of cell death signalling pathways. *Cancer Biol Ther* 2005; 4(2): 139-163.
71. Kim R. Recent advances in understanding the cell death pathways activated by anticancer therapy. *Cancer* 2005; 103(8): 1661-1680.
72. Yang JK. Flip as an anti-cancer therapapeutic target. *Yonsei Med J* 2008; 49(1): 19-27.

73. Fischer U, Jänicke RU, Schulze-Osthoff K. Many cuts to ruin: a comprehensive update of caspase substrates. *Cell Death Differ*. 2003; 10: 76–100.
74. Qiang FX, Guo YJ. Apoptosis in oncology. *Cell Res* 2001; 11(1): 1-7.
75. Pitti RM, Masters SA, Ruppert S, Donahuel CJ, *et al*. Induction of Apoptosis by Apo-2 Ligand, a New Member of the Tumor Necrosis Factor Cytokine Family. *J Biol Chem* 1996; 271(22): 12687-90.
76. Russo A, Terrasi M, Agnese V, Santini D, Bazan V. Apoptosis : a relevant tool for anticancer therapy. *Ann Oncol* 2006; 17(7): vii115-vii123.
77. Gliniak B, Le T. Tumor necrosis factor-related apoptosis-inducing ligand's antitumor activity in vivo is enhanced by the chemotherapeutic agent CPT-11. *Cancer Res* 1999; 59: 6153–6158.
78. Wu XX, Ogawa O, Kakehi Y. TRAIL and chemotherapeutic drugs in cancer therapy. *Vitam Horm* 2004; 67: 365–383.
79. Desagher S, Osen-Sand A, Nichols A, Eskes R, Montessuit S, Lauper S, et al. Bid-induced conformational change of Bax is responsible for mitochondrial cytochrome *C* release during apoptosis. *J. Cell Biol* 1999; 144(5): 891-901.
80. Narita M, Shimizu S, Ito T, Chittenden, T, Lutz RJ, Matsuda H, et al. Bax interacts with the permeability transition pore to induce permeability transition and cytochrome c release in isolated mitochondria. *Proc Natl Acad Sci USA* 1998; 95: 14681-14686.
81. Basanez G, Nechushtan A, Drozhinin O, Chanturiya A, Choe E, Tutt S, et al. Bax, but not Bcl-XL decreases the lifetime of planar phospholipid bilayer membranes at subnanomolar concentrations. *Proc Natl Acad Sci USA* 1999; 96: 5492-5497.
82. Luo X, Budihardio I, Zou H, Slaughter C, Wang X. Bid, a Bcl-2 interacting protein, mediates cytochrome c release from mitochondria in response to activation of cell surface death receptors. *Cell* 1998; 94: 481-490.
83. Green DR, Kroemer G. The pathophysiology of mitochondrial cell death. *Science* 2004; 305: 626-629.
84. Danial NN. BCL-2 family proteins: critical checkpoints of apoptotic cell death. *Clin Cancer Res* 2007; 13(24): 7254-7263.
85. Wang K,Yin XM, Chao DT, Milliman CL, Korsmeyer SJ. BID: a novel BH3 domain-only death agonist. *Genes Dev* 1996; 10: 2859-2869.
86. Solá S, Aranha MM, Steer CJ, Rodrigues CM. Game and Players: Mitochondrial Apoptosis and the Therapeutic Potential of Ursodeoxycholic Acid. *Curr Issues Mol Boil* 2007; 9(2): 123-138.
87. Bayir H, Kagan VE. Bench-to-bedside review: mitochondrial injury, oxidative stress and apoptosis-there is nothing more practical than a good theory. *Crit Care* 2008; 12(1): 1-11.

88. Li P, Nijhawan D, Budihardjo I, Srinivasula SM, Ahmad M, Alnemri ES *et al*. Cytochrome c and dATP-Dependent Formation of Apaf-1/Caspase-9 Complex Initiates an Apoptotic Protease Cascade. *Cell* 1997; 91: 479–489.
89. Qin H, Srinivasula SM, Wu G, Fernandes-Alnemri T, Alnemri ES, Shi Y. Structural basis of procaspase-9 recruitment by the apoptotic protease-activating factor 1. *Nature* 1999; 399: 547–555.
90. Bao Q, Shi Y. apoptosome: a platform for the activation of initiator caspases. *Cell Death Differ* 2007; 14: 56-65.
91. Zimmerman KC, Bonzon C, Green DR. The machinery of programmed cell death. *Pharmacol Ther* 2002; 92: 57-70.
92. Aleo E, Henderson CJ, Fontanini A, Solazzo B. Identification of new compounds that trigger apoptosome independent Caspase activation. *Cancer Res* 2006; 66(18): 9235-9244.
93. Schafer ZT, Parrish AB,Wright KM, *et al*. Enhanced sensitivity to cytochrome c ^ induced apoptosis mediated by PHAP1 in breast cancer cells. *Cancer Res* 2006; 66: 2210-2218.
94. Johnson CE, HuangYY, Parrish AB, *et al*. Differential Apaf-1levels allow cytochrome c to induce apoptosis in brain tumors but not in normal neural tissues. *Proc Natl Acad Sci USA* 2007; 104: 20820-20825.
95. Ledgerwood ED, Morison IM. Targeting the apoptosome for cancer therapy. *Clin Cancer Res* 2009; 15(2): 420-424.
96. Debatin KM, Poncet D, Kroemer G. Chemotherapy: targeting the mitochondria cell death pathways. *Oncogene* 2002; 21: 8786-8803.
97. Rao RV, Ellerby HM, Bredensen DE. Coupling endoplasmic reticulum stress to the cell death program. *Cell Death Differ* 2004; 11: 372-380.
98. Groenedyk J, Mickalak M. endoplasmic reticulum quality control and apoptosis. *Acta Biochimica Polonica* 2005; 52(2): 381-395.
99. Nakagawa T, Zhu H, Morishima N, Li E, Xu J, Yankner BA, *et al*. Caspase-12 mediates endoplasmic-reticulum-specific apoptosis and cytotoxicity by amyloid-beta. Nature 2000; 403: 98-103.
100. Hitomi J, Katayama T, Eguchi Y, Kudo T, Taniguchi M, Koyama Y, *et al*. Involvement of caspase-4 in endoplasmic reticulum. J Cell Biol 2004; 165: 347-356.
101. Ng FW, Nguyen M, Kwan T, Branton PE, Nicholson DW, Cromlish JA, Shore GC. p28 Bap31, a Bcl-2/Bcl-XL- and procaspase-8-associated protein in the endoplasmic reticulum. *J Cell Biol* 1997, 139: 327–338.
102. Jin Z, El-Deiry WS. Overview of cell death signalling pathways. *Cancer Biol Ther* 2005; 4(2): 139-163.
103. Johnson DE. Noncaspase proteases in apoptosis. *Leukemia* 2000; 14: 1695-1703.
104. Low RL. Mitochondrial Endonuclease G function in apoptosis and mtDNA metabolism: a historical perspective. *Mitochondrion*; 2(4): 225-236.

105. Widlak P, Garrard WT. Discovery, regulation, and action of the major apoptotic nucleases DFF40/CAD and endonuclease G. *J Cell Biochem* 2005; 94(6): 1078-1087.

106. Moffitt KL, Martin SL, Walker B. the emerging role of serine proteases in apoptosis. *Biochem Soc Trans* 2007; 35(3): 559-560.

107. Heibein JA, Goping IS, Barry M, Pinkoski MJ, Shore GC, Green DR, *et al.* Granzyme B-mediated cytochrome *C* release is regulated by the Bcl-2 family members bid and Bax. *J Exp Med* 2000; 192(10): 1391-1402.

108. Rosenfeldt MT, Ryan KM. the role of autophagy in tumor development and cancer therapy. *Expert Rev Mol Med* 2009; 11(e36): 1-20.

109. Jaeger PA, Wyss-Coray. All-you-can-eat: autophagy in neurodegeneration and neuroprotection. *Mol Neurodegener* 2009; 4: 16-38.

110. Xie Z, Klionssky DJ. Autophagosome formation: core machinery and adaptions. *Nature Cell Biol* 2007; 9 (10): 1102-1109.

111. Dice JF. Chaperone-mediated autophagy. *Autophagy* 2007; 3(4): 295-299.

112. Zhang C, Cuervo AM. Restoration of chaperone-mediated autophagy in aging liver improves cellular maintenance and hepatic function. *Nat Med* 2008; 14(9): 959-965.

113. Mizushima N, Levine B, Cuervo AM, Klionksy DJ. Autophagy fights disease through cellular self-digestion. *Nature* 2008; 451(7182): 1069-1075.

114. Cuervo AM, Mann L, Bonten EJ, d'Azzo A, Dice JF. Cathepsin A regulates chaperone-mediated autophagy through cleavage of the lysosomal receptor. *EMBO J* 2003; 22(1): 47-59.

115. Jones RG, Thompson CB. Tumor suppressors and cell metabolism: a recipe for cancer growth. *Genes Dev* 2009; 23: 537-548.

116. Tsujimoto Y, Shimizu S. Another way to die: autophagic programmed cell death. *Cell Death Differ* 2005; 12: 1528-1534.

117. Kabeya Y, Mizushima N, Ueno T, Yamamoto A, Kirisako T, Noda T, *et al*. LC3, a mammalian homologue of yeast Apg8p, is localized in autophagosome membranes after processing, *Embo J* 2000; 19: 5720–5728.

118. Mizushima N, Yamamoto A, Hatano M, Kobayashi Y, Kabeya Y, Suzuki K, *et al*. Dissection of autophagosome formation using Apg5-deficient mouse embryonic stem cells. *J Cell Biol* 2001; 152: 657–667.

119. Yoshimori T. Autophagy: a regulated bulk degradation process inside cells. *Biochem Biophys Res Commun* 2004; 313: 453-458.

120. Sinha S, Levine B. The autophagy effector Beclin 1: a novel BH3-only protein. *Oncogene* 2008; 27(1): 137-148.

121. Salvador N, Aguado C, Horst M, Knecht E. Import of a cytosolic protein into lysosomes by chaperone-mediated autophagy depends on its folding state. *Journal Biol Chem* 2000; 275(35): 27447-27456.

122. Klionsky DJ, Cuervo AM, Seglen PO. Methods for monitering autophagy from yeast to human. *Autophagy* 2007; 3(3): 181-206.

123. Dubouloz F, Deloche O, Wanke V, Cameroni E, De Virgilio C. The TOR and EGO protein complexes orchestrate microautophagy in yeast. *Mol Cell* 2005; 19: 15-26.

124. Shoji JY, Arioka M, Kitamoto K. Possible involvement of pleiomorphic vacuolar networks in nutrient recycling in filamentous fungi. *Autophagy* 2006; 2(3): 226-227.

125. Okada H, Mak TW. Pathways of apoptotic and non-apoptotic death in tumor cells. *Nature Rev Cancer* 2004; 4: 592-603.

126. Letai AG. Diagnosing and exploiting cancer's addiction to blocks in apoptosis. *Nature Rev Cancer* 2008; 8: 121-132..

127. Castedo M, Perfettini JL, Roumier T, Kroemer G. Cyclin dependent kinase-1: linking apoptosis to cell cycle and mitotic catastrophe. *Cell Death Differ* 2002; 9: 1287-1293.

128. Vakifahmetoglu H, Olson M, Zhivotovsky B. death through a tragedy: mitotic catastrophe. *Cell Death Differ* 2008; 15: 1153-1162.

129. DeBaradinis RJ, Cheng T. Q's next: the diverse function of glutamine in metabolism, cell biology and cancer. *Oncogene* 2010: 21(3): 313-324.

130. Young CD, Anderson SM. Sugar and fat- that's where it's at: metabolic changes in tumor cells. *Breast Cancer Res* 2008; 10(1): 1-9.

131. Arsham AM, Plas DR, Thompson CB, Simon MC. Akt and hypoxia-1-inducible factor-1 independently enhance tumor growth and angiogenesis. *Cancer Res* 2004; 640: 3500-3507.

132. Rankin EB, Giaccia AJ. The role of hypoxia-inducible factors in tumorigenesis. *Cell Death Differ* 2008; 15: 678-685.

133. Wenger RH. Cellular adaptation to hypoxia: O2-sensing protein hydroxylases, hypoxia-inducible transcription factors, and O2-regulated gene expression. *FASEB J* 2002; 16: 1151-1162.

134. Grabacka M, Reiss K. anticancer properties of PPARα-effects on cellular metabolism and inflammation. *PPAR Res* 2008; 2008: 1-9.

135. Jin S, Dipaola RS, Mathew R, White E. metabolic catastrophe as a means to cancer cell death. *J Cell Sci* 2007; 120(3): 379-383.

136. Majno G and Joris I. Apoptosis, oncosis and necrosis. An overview of cell death. *Am J Pathol* 1995. 146: 3-15.

137. Van Cruchten S, Van den Broeck W. morphological and biochemical aspects of apoptosis, oncosis and necrosis. *Anat Histo Embryol* 2002; 31: 214-223.

138. Mills EM, Xu D, Fergusson MM, Combs CA, Xu Y, Finkel T. regulation of cellular oncosis by uncoupling protein 2. *J Biol Chem* 2002; 277(30): 27385-27392.

139. Shirai T. commentary: oncosis and apoptosis: two faces of necrosis in a new proposal to clear up the confusion regarding cell death. *Toxicol Pathol* 1999; 27: 495-496.

140. Matsouka S. A cell surface receptor defined by a mAB mediates a unique type of cell death similar to apoptosis. *Proc Natl Acad Sci* 1998; 95: 6290-6295.

141. Kanduc K, Mittelman A, Serpico R, Sinigalia E, Sinha AA, Natale C, et al. Cell death: apoptosis versus necrosis. *Int J Oncol* 2002; 21(1): 165-170.

142. Koyama AH, Irie H, Ueno F, Ogawa M, Nomoto A, Adachi A. Suppression of apoptotic and necrotic cell death by poliovirus. *Journal Of General Virology* 2001; 85: 2965-2972.

143. Fischer S, Maclean Aa, Liu M, Cardella JA, Slutsky AS, Suga M, et al. Dynamic changes in apoptotic and necrotic cell death correlate with severity of ischemia-reperfusion injury in lung transplantation. *Am j Respir Crit Care Med* 2000; 162(5): 1932-1939.

144. Holler N, Zaru R, Micheau O, Thome M, Attinger A, Valitutti S, et al. *F*as triggers an alternative, caspase-8-independent cell death pathway using the kinase RIP as effector molecule. *Nat Immunol* 2000; 1: 489–495.

145. Chai H. Hydrogen peroxide regulation of endothelial function: origins, mechanisms, and consequences. *Cardiovasc Res* 2005; 68: 26-36.

146. Bensaad K, Cheung EC, Voudsen KH. Modulation of intracellular ROS levels by TIGAR controls autophagy. *EMBO J* 2009; 28: 3015-3026.

147. Lu W, Ogasawara MA, Huang P. Models of reactive oxygen species in cancer. *Drug Disc Today Dis Models* 2007; 4(2): 67-73.

148. Pan JS, Hong MZ, Ren JL. Reactive oxygen species: a double-edged sword in oncogenesis. *World J Gastroenterol* 2009; 15(14): 1702-1707.

149. Pelicano H, Feng L, Zhou Y, Carew JS, Hileman EO, Plunkett W, et al. Inhibition of mitochondrial respiration. *J Biol Chem* 2003; 278(39): 37832-37839.

150. Huang J, Brumell JH. NADPH oxidases contribute to autophagy regulation. *Autophagy* 2009; 5(6): 887-889.

151. Azad MB, Chen Y, Gibson SB. Regulation of autophagy by reactive oxygen species (ROS): implications for cancer progression and treatment. *Antioxid Redox Signal* 2009; 11(4): 1-14.

152. Pribluda VS, Gubish ER, La Vallee TM, Treston A, Swartz GM, Green SJ. 2-Methoxyestradiol: An endogenous antiangiogenic and antiproliferative drug candidate. *Cancer Metastasis Rev* 2000; 19: 173-179.

153. Azab SS, Salama SA, Hassan MH, Khalifa AE, El-Demerdash E, Fouad H, et al. 2-Methoxyestradiol reverses doxorubicin resistance in human breast tumor xenograft. *Cancer Chemother Pharmacol* 2008; 62(5): 893-902.

154. Fufuki M, Song J, Zhu BT. Mechanism of 2-methoxyesradiol-induced apoptosis and growth arrest in human breast cancer cells. *Mol Carcinog* 2008; 9999: 1-13.

155. Cicek M, Iwaniec UT, Goblirsch MJ, Vrabel A, Ruan M, Clohisy DR, et al. 2-methoxyestradiol suppresses osteolytic breast cancer tumor progression in vivo. *Cancer Res* 2007; 67(21): 10106-10111.

156. Sutherland TE, Anderson RL, Hughes RA, Altmann MS, Ziogas J, Stewart AG. 2-methoxyestradiol-a unique blend of activities generating a new class of anti-tumor/anti-inflammatory agents. *Drug Discov Today* 2007; 12 (13/14): 577-384.

157. Zhu BT, Conney AH. Is 2-methoxyestradiol an endogenous estrogen metabolite that inhibits mammary carcinogenesis. *Cancer Res* 1998; 58: 2269-2277.

158. Bhati R, Gokmen-Polar Y, Sledge GW, Fan C, Nakshatri H, Ketelsen D, et al. 2-Methoxyestradiol inhibits the anaphase-promoting complex and protein translation in human breast cancer cells. *Cancer Res* 2007; 67: 702-708.

159. Kato S, Sadarangani A, Lange S, Delpiano AM, Vargas M, Brañes J, et al. 2-Methoxyestradiol Mediates Apoptosis Through Caspase-Dependent and Independent Mechanisms in Ovarian Cancer Cells But Not in Normal Counterparts. *Reprod Sci* 2008; 15 (9): 878-894.

160. Lavallee, TM; Zhan, XH; Herbstritt, CJ; Kough, EC; Green, SJ; Pribluda, VS. 2-Methoxyestradiol inhibits proliferation and induces apoptosis independently of estrogen receptors alpha and beta. *Cancer Res* 2002; 62: 3691–3697.

161. Banerjeei, SK; Zoubine, MN; Sarkar, DK; Weston, AP; Shah, JH; Campbell, DR. 2-Methoxyestradiol blocks estrogen-induced rat pituitary tumor growth and tumor angiogenesis: possible role of vascular endothelial growth factor. *Anticancer Res* 2000; 20: 2641–2645.

162. Lippert, TH; Adlercreutz, H; Berger, MR; Seeger, H; Elger, W; Mueck, AO. Effect of 2-methoxyestradiol on the growth of methyl-nitroso-urea (MNU)-induced rat mammary carcinoma. *J Steroid Biochem Mol Biol* 2003; 84: 51–56.

163. Check Biotech (Homepage on the internet). United States of America. 2007-2008 Checkbiotech.org [updated 2008/06: cited 2008/09/16]. EntreMed presents phase 2 results for Panzem capsules in multiple myeloma. Available

from:http://rarediseases.checkbiotech.org/news/2007/06/05/EntreMed_presents_phase_2_results_for_Panzem_capsules_in_multiple_myeloma/

164. Medical News today (Homepage on the internet). United Kingdom. 2008 Medilexicon International Ltd. [updated 2006/12/02: cited 2008/09/16}. entremed commences phase 2 clinical trial with panzem(r) ncd in ovarian cancer. Available from: http://www.medicalnewstoday.com/articles/55637.php

165. What's new in pharma (homepage on the internet). Netherlands. CMP inform Ltd 2007. (updated 2007/06/05: cited 2008/09/16). Phase 2 results for entremed's panzem(r) ncd brain cancer study presented at asco. Available from: http://www.whatsnewinpharma.com/Pharma/Articles.aspx/9781

166. Sutherland TE, Anderson RL, Hughes RA, Altmann E, Schuliga M, Ziogas J, et al. 2-Methoxyestradiol-a unique blend of activities generating a new class of anti-tumour/anti-inflammatory agents. *Drug Discov Today* 2007; 12(13/14): 577-584.

167. Lakhani NJ, Lepper ER, Sparreboom A, Dahut WL, Venitz J, Figg WD. Determination of 2-methxyestradiol in human plasma, using liquid chromatography/tandem mass spectrometry. *Rapid Commun Mass Spectrom* 2005; 19: 1176-1182

168. Foster PA, Ho YT, Newman SP, Kasprzyk MP, Leese MP, Potter BVL, et al. 2-MeOE2bisMATE and 2-EtE2bisMATE induce cell cycle arrest and apoptosis in breast cancer xenografts as shown by a novel ex vivo technique. *Breast Cancer Res Treat* 2008; 111: 251-260.

169. Stanway SJ, Delavault P, Purohit A, Woo LWL, Thurieau C, Potter BVL, et al. steroid sulfatase: a new target for the endocrine therapy of breast cancer. *Oncologist* 2007; 12(4): 370-374.

170. Purohit A, Woo LWL, Chander SK, Newman SP, Ireson C, Ho Y, et al. steroid sulphatase inhibitors for breast cancer therapy. *J Steroid Biochem Mol Biol*. 2003; 89(3-5): 423-432.

171. Reed MJ, Purohit A, Woo LWL, Newman SP, Potter BVL. Steroid Salfatase: Molecular Biology, regulation, and inhibition. *Endocr Rev* 2005; 26(2): 71-202.

172. Utsumi T, Leese MP, Chander SK, Gaukroger K, Purohit A, Newman SP, et al. The effects of 2-methoxyoestrogen sulphamates on the in vitro and in vivo proliferation of breast cancer cells. *J Steroid Biochem Mol Biol* 2005; 94: 219-227.

173. Tagg SL, Foster PA, Leese MP, Potter BV, Reed MJ, Purohit A, et al. 2-methoxyoestradiol-3,27-O,O-bis-sulphamate and 2-deoxy-D-glucose in combination: a potential treatment for breast and prostate cancer. *Br J Cancer* 2008; 99(11): 1842-1848.

174. Ireson CR, Chander SK, Purohit A, Perera S, Newman SP, Parish D, et al. Pharmacokinetics and efficacy of 2-methoxyoestradiol and 2-methoxyoestradiol-bis-sulphamate in vivo in rodents. *Br J Cancer* 2004; 90: 932-937.

175. Raobaikaby B, Purohit A, Chander SK, Woo L, Leese MP, Potter VL, et al. Inhibition of MCF-7 breast cancer cell proliferation and in vivo steroid sulphatase activity by 2-methoxyoestradiol-bis-sulphamate. *J Steroid Biochem Mol Biol* 2003; 84: 351-358.

176. Suzuki RN, Newman SP, Purohit A, Leese MP, Potter BV, Reed MJ. Growth inhibition of multi-drug-resistant breast cancer cells by 2-methoxyoestradiol-bis-sulphamate and 2-ethyloestradiol-bis-sulphamate. *J Steroid Biochem Mol Biol* 2003; 84: 269-278.

177. Foster PA, Newman SP, Leese MP, Bernetiere S, Diolez C, Camara J, et al. A new micronized formulation of 2-methoxyestradiol-bis-sulfamate (STX140) is therapeutically potent against breast cancer. *Anticancer Res* 2008; 28: 577-581.

178. Wood L, Leese MP, Mouzakiti A, Purohit A, Potter BV, Reed MJ, et al. 2-MeOE2bisMATE induces caspase-dependent apoptosis in CAL51 breast cancer cells and overcomes resistance to TRAIL via cooperative activation of caspases. *Apoptosis* 2004; 9: 323-332.

179. Newman SP, Leese MP, Purohit A, James DRC, Rennie CE, Potter BVL. Inhibition of in vitro angiogenesis by 2-Methoxy- and 2-ethyl-estrogen sulfamates. *Int J Cancer* 2004; 109: 533-540.

180. Newman SP, Foster PA, Ho YT, Day JM, Raibaikady B, Kasprzyk PG, et al. The therapeutic potential of a series of bioavailable anti-angiogenic microtubule disruptors as therapy for hormone-independent prostate and breast cancers. *Br J Cancer* 2007; 97: 1673-1682.

181. Newman SP, Foster PA, Stengel C, Day JM, HO YT, Judde JG, et al. STX140 is efficacious in vitro and in vivo taxane-resistant breast carcinoma cells. *Clin Cancer Res* 2008; 14(2): 597-606.

182. Ho YT, Newman SP, Purohit A, Leese MP, Potter BVL, Reed MJ. The effects of 2-methoxy oestrogens and their sulphomoylated derivatives in comjunction with TNF-α on endothelial and fibroblast cell growth, morphology and apoptosis. *J Steroid Biochem Mol Biol* 2003; 86: 189-196.

183. Nussbaumer P, Billich A. Steriod sulphatase inhibitors: their potential in the therapy of breast cancer. *Curr Med Chem- Anti-cancer agents* 2005; 5: 207-528.

184. Freshney RI. Animal cell cultures. 3rd ed. Oxford: URL Press; 1995.

185. R. Danz, A. Vogelgsang, and R. Kathner. PlasDIC - a useful modification of the differential interference contrast according to Smith/Nomarski in transmitted light arrangement (monograph on Photonik; 2004 [cited 2009 March 23]. Available from: www.zeiss.com/C1256F8500454979/0/366354E1E8BA8703C1256F8E003BBCB9/$file/plasdic

186. Gillies RJ, Didier N, Denton M. Determination of cell number in monolayer cultures. *Anal Biochem* 1986; 159(1): 109-113.

187. Kueng W. Silber E. Eppenberger U. Quantification of cells cultured on 96-well plates. *Anal Biochem* 1989; 182(1): 16-19.

188. Berry JM, Huebner E, Butler M. The crystal violet nuclei staining technique leads to anomalous results in monitoring mammalian cell cultures. *Cytotechnology* 1996; 21(1): 73-80.

189. American Type Culture Collection [www.ATCC.org]. Manassas, USA; [updated
    a. 2007 April 31; cited 2007 November 14]. Available from:http://www.atcc.org/common/catalog/numSearch/numResults.cfm?atccNum=HTB-22

190. American Type Culture Collection [www.ATCC.org]. Manassas, USA; [updated
    a. 2007 April 31; cited 2007 November 14]. Available from:
    b. http://www.atcc.org/common/catalog/numSearch/numResults.cfm?atccNum=CRL-10782

191. Grever MR, Schepartz SA, Chabner BA. The National Cancer Institute: cancer drug discovery and development program. *Semin Oncol* 1992; 19(6): 622-638.

192. Thompson, SW. Selected Histochemical and histopathological methods. Springfield, C.C. Thomas Publications 1966, p.377-378.

193. Burge RE. Contrast and image formation of biological specimens. *Princ Tech Elec Microsc* 1976; 6: 85-116.

194. Klionsky DJ, Cuervo AM, Seglen PO. Methods for monitoring autophagy from yeast to human. *Autophagy* 2007; 3(3): 181-206.

195. Mehta SB, Sheppard CJR. Partially coherent image formation in differential interference contrast (DIC) microscrope. *Optics express* 2008; 16(24): 19462-19479.

196. Solomon EP, Berg LR, Martin DW. Biology. 6th ed. United States of America: Thomson Brooks/cole; 2002. P. 72-102

197. Kroemer G, El-Deiry WS, Golstein P, Peter ME, Vaux D, Vandenabeele P, et al. Classification of cell death: recommendations of the nomenclature committee on cell death. *Cell differ* 2005; 12: 1463-1467.

198. Kusuzaki K, Murata H, Takeshita H, Hashiguchi S, Nozaki T, Emoto K, et al. Intracellular binding sites of acridine orange in living osteosarcoma cells. *Anticancer Res* 2000; 20(2A): 971-975.

199. Foster PA, Ho Y, Newman SP, Leese MP, Potter BV, Reed MJ, et al. STX 140 and STX 641 cause apoptosis via the intrinsic mitochondrial pathway and downregulate survivan and XIAP expression in ovarian and prostate cancer cells. *Anticancer Res* 2009; 29(10): 3751-3757.

200. Foster PA, Stengel C, Ali T, Leese MP, Potter BV, Reed MJ, et al. A comparison of two orally bioavailable anti-cancer angents, IRC-110160 and STX140. *Anticancer Res* 2008; 28(3A): 1483-1491.

201. Raobaikady B, Reed MJ, Leese MP, Potter BVL, Purohit A. Inhibition of MDA-MB-231 cell cycle progression and cell proliferation by C-2-substituted oestradiol *mono*- and *bis*-3-O-sulphamates. Int J Cancer 2005 ;117: 150-159.

202. Day JM, Foster PA, Tutill HJ, Newman SP, Ho YT, Leese MP, et al. BCRP expression does not result in resistance to STX140 in vivo, despite the increased expression of BCRP in A2780 cells in vitro after long-term STX140 exposure. *Br J Cancer* 2009; 100: 476-486.

203. Vistica DT, Skehan P, Scudiero D, Monks A, Pittman A, Boyd MR. Tetrazolium-based assays for cellular viability: a critical examination of selected parameters affecting formazan production. *Cancer Res* 1991; 51(10): 2515-2520.

204. Liu Y, Peterson DA, Kimura H, Schubert D. Mechanism of cellular 3-(4,5-dimethylthiazol-2-yl)-2,5-diphenyltetrazolium bromide (MTT) reduction. *J Neurochem* 1997; 69(2): 581-593.

205. Jeong D, Kim TS, Lee JW, Kim KT, Kim HJ, Kim IH, et al. Blocking of acidosis-mediated apoptosis by a reduction of lactate dehydrogenase activity through antisense mRNA expression. *Biochem Biophys Res Commun* 2001; 289(5): 1141-1149.

206. Xia GH, Chen BA, Shao ZY, Lu HX, Konstanze D, Hartmut D. Mechanism of 2-methoxyestradiol-induced apoptosis in myelodysplastic syndrome MUTZ-1 cell line. *Zhongguo Shi Yan Xue Ye Xue Za Zhi* 2007; 15(2): 296-301.

207. Kachadourian R, Liochev SI, Cabelli DE, Patel MN, Fridovich I, Day BJ. 2-Methoxyestradiol does not inhibit superoxide dismutase. *Arch. Biochem. Biophys***.** 2001**;** 392(2): 349-353.

208. Lorin S, Borges A, Dos Santos LR, Souquere S, Pierron G, Ryan KM, Codogno P, Djavaheri-Mergny M. C-Jun NH_2-terminal kinase activation is essential for DRAM induction of autophagy and apoptosis in 2-Methoxyestradiol-treated ewing sarcoma cells. *Cancer Res* 2009; 69: 6924-6931.

209. Li P, Dietz R, von Harsdorf R. p53 regulates mitochondrial membrane potential through reactive oxygen species and induces cytochrome c-independent apoptosis blocked by Bcl-2. *EMBO J* 1999; 18(21): 6027-6037.

210. Scatena R, Bottoni P, Botta G, Martorana GE, Giardina B. The role of mitochondria in pharmacotoxicology: a reevaluation of old, newly emerging topic. *Am J Physiol* 2007; 293: 12-21.

211. Brookes PS, Yoon Y, Robotham JL, Andres MW, Sheu SS. Calcium, ATP, and ROS: a mitochondrial love-hate triangle. *Am J Physiol* 2004; 287: C817-C833.

212. Djavaheri-Mergny M, Wietzerbin J, Besancon F. 2-methoxyestradiol in apoptosis in Ewing sarcoma cells through mitochondrial hydrogen peroxide production. *Oncologist* 2003; 22: 2558-2567.

213. Gao N, Ranhmani M, Dent P, Grant S. 2-Methoxyestradiol-induced apoptosis in human leukemia cells proceeds through a reactive oxygen species and Akt-dependent process. *Oncogene* 2005, 24: 3797-3809.

214. She MR, Li JG, Guo KY, Lin W, Du X, Niu, XQ. Requirement of reactive oxygen species generation in apoptosis of leukemia cells induced by 2-methoxyestradiol. *Acta. Pharmacol. Sin.* 2007, 28(7): 1037-1044.

215. Simizu S, Takada M, Umezawa K, Imoto M. Requirement of caspase-3 (like) protease-mediated hydrogen peroxide production for apoptosis induced by various anticancer drugs. *J. Biol. Chem.*1998, 273: 26900–26907.

216. Stander BA, Marais S, Vorster CJ, Joubert AM. *In Vitro* effects of 2-methoxyestradiol on morphology, cell cycle progression, cell death and gene expression changes in the tumorigenic MCF-7 breast epithelial cell line. *J. Steroid. Mol. Biol.* 2010; In Press

217. Scherz-Shouval R, Shvets E, Fass E, Shorer H, Gil L, Elazar Z. Reactive oxygen species are essential for autophagy and regulate the activity of Atg4. *EMBO J* 2007; 26: 1749-1760.

218. Chen Y, Bibson SB. Is mitochondrial generation of reactive oxygen species a trigger for autophagy? *Autophagy* 2008; 4(2): 246-248.

219. Chen, Y., McMillan-Ward, E., Kong, J., Israels, S.J. and Gibson, S.B., Oxidative stress induces autophagic cell death independent of apoptosis transformed and cancer cells. *Cell Death Differ* 2008, 15(1): 171-182.

220. Johansson AC, Appelqvist H, Nillson C, Kagedal K, Roberg K, Öllinger K. Regulation of apoptosis-associated lysosomal membrane permeabilization. *Apoptosis* 2010; 15: 527-540.

221. Duan W, Jin X, Li Q, Tahiro SI, Onodera S, Ikejima T. Silibinin induced Autophagic and apoptotic cell death in HT1080 cells through a reactive oxygen species pathway. *J pharmacol* 2010; 133: 48-56.

222. Thorburn A. Apoptosis and autophagy: regulatory connections between two supposedly different processes. *Apoptosis* 2008; 13(1): 1-9.

223. Bras M, Queenan B, Susin SA. Programmed cell death via mitochondria : different modes of dying. *Biochemistry (Mosc)* 2005; 70(2): 231-239.

224. Nishida K, Yamaguchi O, Otsu K. Crosstalk between autophagy and apoptosis in heart disease. *Circ Res* 2008; 103: 343-351.